Online ISSN 2716-9650
Print ISSN 2676-5837

Volume 2, Jun. 30, 2020

# *Journal of*
# Composites and Compounds

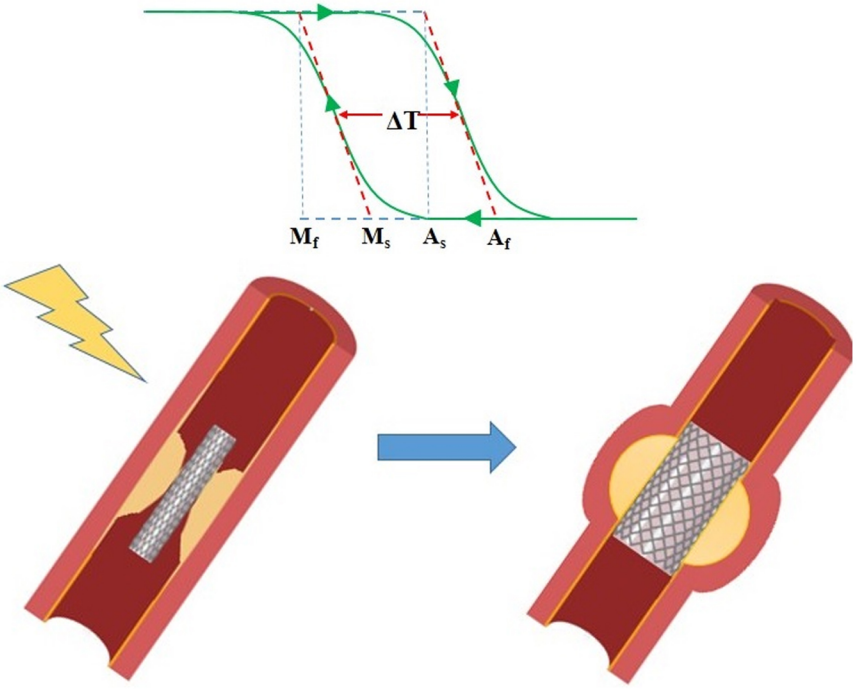


**Editor In Chief: F. Sharifianjazi**

www.JOURCC.com

*Journal of*
**Composites and Compounds**

Online ISSN 2716-9650
Print ISSN 2676-5837
Jun. 30, 2020
Volume 2
No. 3



**Available online at www.jourcc.com**

**Janatabad St., Tehran, Iran**

**+982144437782**

*Journal of*
**Composites and Compounds**

Online ISSN 2716-9650
Print ISSN 2676-5837
Jun. 30, 2020
Volume 2
No. 3

## Table of contents



**Available online at www.jourcc.com**

**Janatabad St., Tehran, Iran**
**+982144437782**

Available online at www.jourcc.com

Journal homepage: www.JOURCC.com

Journal of Composites and Compounds

# TZNT alloy for surgical implant applications: A systematic review

*Shima Nasibi[a], Kiana Alimohammadi[b], Leila Bazli[c]*, Sara Eskandarinezhad[d], Ali Mohammadi[e], Niloufar Sheysi[e]*

[a] *Materials Science and Engineering Department, School of Engineering, Shiraz University, Shiraz, Iran*
[b] *Khajeh Nasir Toosi University of Technology (KNTU), Tehran, Iran*
[c] *School of Metallurgy and Materials Engineering, Iran University of Science and Technology, Tehran, Iran*
[d] *Department of Mining and Metallurgical Engineering, Yazd University, Yazd, Iran*
[e] *Department of Pharmaceutical Chemistry, Tehran Medical Sciences, Islamic Azad University, Tehran ,Iran*

A B S T R A C T

Owing to its good mechanical properties, enhanced wear resistance, good biological properties, biocompatibility, low cytotoxicity, and great corrosion behavior, Ti-Nb-Ta-Zr (TZNT) alloy, as new β titanium alloy, has attracted considerable attention for surgical implant applications. The need for the improvement of the implant properties in the physiological environment can be fulfilled by using the β titanium alloy with low elastic modulus. Additionally, this alloy can inhibit the surgical implant fracture, infection, inflammation, and the reaction of soft tissue with particulate debris. Therefore, the aim of this paper is to review the properties and applications of TZNT alloy as a promising choice for surgical implant applications.



Peer review under responsibility of jourcc

A R T I C L E I N F O R M A T I O N

*Article history:*
Received 31 May 2020
Received in revised form 8 June 2020
Accepted 23 June 2020

*Keywords:*
TZNT alloy
Surgical implant
β-titanium alloy
Biomedical applications

Table of contents



## 1. Introduction

Given the good performance including good biocompatibility, lower elastic modulus, excellent corrosion resistance, and high specific strength, Ti and its alloys are considered as the optimum materials for surgical implants [1]. With scientific advances, the third generation of titanium alloys as the new type of β alloys for biomedical applications has been developed such as Al-free Ti-Zr-Ta-Nb- and Ti-Zr-Mo-based alloys. The newly developed β titanium alloys have more advantages over conventional Ti alloys and are considered as more suitable materials for human-implant applications [2].

In the past few decades, Ti alloys, especially, Ti-6Al-4V alloy and commercially pure (cp) Ti, have been widely utilized in orthopedic implants due to their desirable biocompatibility, excellent corrosion properties, and promising mechanical performance. Based on the history of thermo-mechanical processing and material composition, titanium alloys have been divided into α, near-α, metastable β, stable β or α + β categories. Zr is a neutral stabilizer while elements such as Ta and Nb are isomorphs of β-stabilizers. Compared to cp titanium (α-Ti) and Ti-6Al-4V (α + β Ti), β-Ti alloys exhibit some enhanced characteristics [3].

* *Corresponding author: Leila Bazli; E-mail: leilabazli64@gmail.com*
https://doi.org/10.29252/jcc.2.2.1 

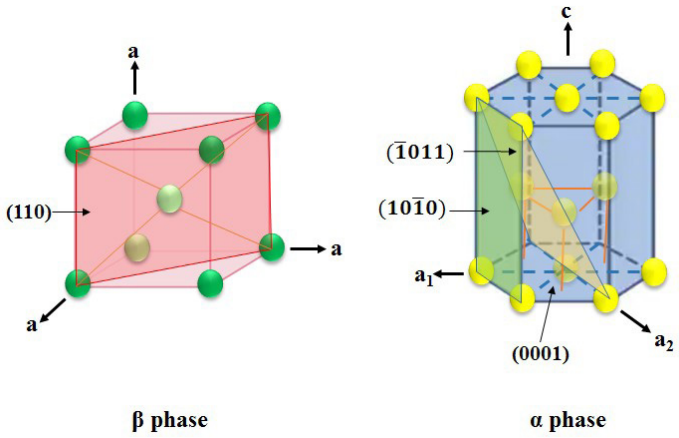


**Fig. 1.** Crystal structure of the α and β phases.

TNZT is a β-titanium quaternary alloy developed in recent years for orthopedic applications [4]. This alloy exhibits some promising properties including superior low elastic modulus [5-11] biocompatibility [12-16], good resistance to corrosion as well as the absence of toxic elements like vanadium and aluminum. The adverse tissue reaction and cytotoxicity resulting from V and Al have been extensively reported in the literature [3]. Complications caused by inflammation can be severe enough to make revision surgery necessary. Therefore, biomaterials and surface modification methods are required for the provision of the optimal infection resistance. In this regard, a comprehensive understating of the complicated interactions that occur at the interface of bone-implant is required. Two-thirds of implant-associated infections and revision surgeries have been reported to be due to the interaction of biomaterial with Staphylococcus and Staphylococcus aureus epidermis [17, 18]. Thus, investigations on the novel TNZT alloy with promising characteristics for surgical implant applications have attracted the attention of researchers.

## 2. Processing of β-titanium alloys

β alloys usually undergo a hot working process and the subsequent heat treatment. In the leaner β alloys, the α+β field is where the final hot working operation is conducted, while in the richer β alloys, it is preferentially performed in the β field. The heat treatment includes three steps: solution, quenching, and aging. If the solution treatment is performed above the temperature of β transus, the formed β grains will be coarse. On the other hand, the precipitation of the primary $\alpha_p$ phase occurrs when the solution treatment is performed just below the β transus. The crystal structure of the α and β phases are illustrated in Fig.1. The $\alpha_p$ volume fraction and shape is controlled by the heat treatment temperature and forging/rolling deformation, respectively. A needle-like $\alpha_p$ is formed when no working is done and by increasing the time of hot working the shape moves toward a spherical $\alpha_p$ shape [19].

An appropriate selection of deformation and temperatures initiating from the breakdown of ingot could control the size distribution and grain size of the β phase. It is possible to obtain small grain sizes by several deformation and recrystallization cycles [20].

A film-like α phase is preferentially precipitated in grain boundaries during the forging process, cooling process from β-forging, and final heat treatment. The suppression of the harmful precipitation of α in grain boundaries is possible by the high cooling rate from the beta phase region. If the cross-section is large, the grain boundary film can be broken by subsequent α/β-processing.

The secondary $\alpha_s$ precipitation with fine distribution occurs at lower temperatures between 400 ˚C to 600 ˚C. Aging time and temperature besides the temperature of solution treatment could control the volume and size of the phase. Depending on the volume fraction of the precipitates and their size, a remarkable strengthening effect can be achieved. In richer beta alloys, inhomogeneous precipitation of $\alpha_s$ can be conducted, while in lean beta alloys it is homogeneous. In the case of rich beta alloys, grain boundaries are the first sites for precipitation and then the precipitates are formed in the grain leading to the creation of some local unaged areas. Generally, a more homogenous distribution of the $\alpha_s$ precipitates and an enhanced aging response can be obtained by cold work. To summarize, the control of the beta titanium alloys properties are influenced by β grain size, grain boundary α, the size, shape, and volume fraction of $\alpha_p$ and $\alpha_s$ [21, 22]. $\alpha_p$, $\alpha_s$, and grain boundary α are schematically illustrated in Fig. 2.

## 3. Mechanical properties

### *3.1. Tensile strength*

Yield stresses in the range of 900 to 1400 MPa can be obtained by the aging of β titanium alloys. However, by increased aging, a significant reduction in ductility is observed in all β alloys. This is due to the larger difference between the yield stress of the aged β matrix soft and primary α as well as the increase of strain localization in the aged matrix that results in early crack nucleation [23]. Duplex aging processes have been used to improve the fatigue and toughness resistance in more highly β-stabilized alloys, which have inhomogeneous $\alpha_s$ precipitations. The duplex aging consists of “low/high” - or “high/low” aging steps, which allow obtaining higher strength in shorter time, compared to aging in just one step [24, 25].

The ductility of the alloys can also be influenced by primary $\alpha_p$.

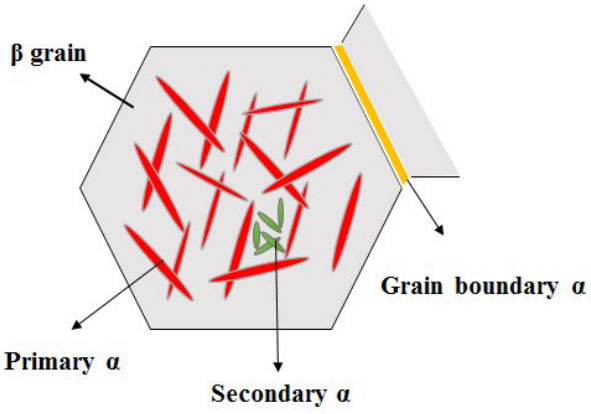


**Fig. 2.** Primary, secondary and grain boundary α.

The change from globular to acicular shape in primary $\alpha_p$ and also its coarsening, resulting from the processing, leads to the ductility reduction. This is due to the increased slip length or effective size of the soft primary $\alpha_p$ resulting in early crack nucleation [26]. Lower temperatures of solution heat treatment lead to the increase in the volume fraction of primary $\alpha_p$ and the reduction of ductility at a constant yield strength. For obtaining desirable yield stress, higher aging of the β phase with a larger volume fraction of soft $\alpha_p$ is required; however, this is in favor of crack nucleation. In other words, increased ductility and reduced yield strength is the consequence of the increased volume fraction of $\alpha_p$ at a constant aging treatment [27]. There is a correlation between the effects of grain boundary and grain size. Strength is not affected by these parameters; however, they can influence ductility. Because of the localized strain in the soft α film in the grain boundary, ductility is reduced resulting in the occurrence of crack nucleation and subsequent fracture in grain boundaries [28, 29]. In the case of intergranular crack nucleation, no conclusive explanation existed for the effect of the grain size on ductility.

### *3.2. Fracture Toughness*

Fracture toughness is significantly reduced by increased aging. According to fractography analyses for ductility, the reason for this trend is an increase in localized strain and the strength difference between the aged matrix and the soft $\alpha_p$ [30]. Single-step aging has been replaced by duplex aging to improve toughness and strength [24]. Studies indicated that a combination of fine secondary α (resulting from low aging) and long, coarse primary α (resulting from high aging) forms a tortuous crack path leading to the increase in the toughness. Moreover, toughness will decrease when the shape of $\alpha_p$ phase transforms from elongated to globular shape [31]. Based on fractographic studies, a more pronounced crack deviation occurs when elongated $\alpha_p$ existed [32]. Increasing the volume fraction of $\alpha_p$ can also decrease toughness drastically at constant yield strength. An increase in the degree of matrix aging compensates for the higher volume fraction of soft $\alpha_p$. The increased $\alpha_p$ volume fraction leads to an increase in toughness at constant aging [19].

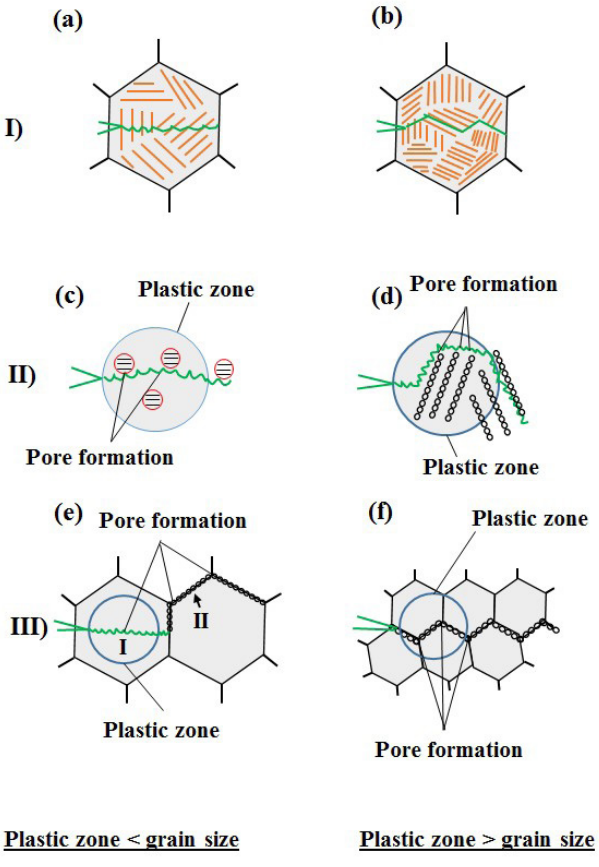


**Fig. 3.** Crack initiation and growth in β alloys.

Several authors [33, 34] have studied the role of grain boundary α and grain size. For instance, the fracture toughness of Ti-15-3 has been found to be reduced by beta grain refinement [35, 36]; while no effect was found for Ti-10-2-3 and Beta C [37]. It has been indicated that grain boundary α could lead to increase or decrease in fracture toughness, or it may has no effect on it. It has been reported that microstructures with very fine, recrystallized grains, and primary $\alpha_p$ decorated with grain boundary α show a drastic drop in fracture toughness in comparison with the microstructure with large grains [38].

To explain contradictory observations, one should consider different parameters including grain boundary, grain size, stress state, plastic zone size, and degree of aging [39]. In the following conclusions, the plastic zone is confined to the grain boundary α which acts as a low energy fracture path (Fig. 3).

The transgranular pre-fatigue crack will be the initiation of the fracture if the grain size is much larger than the plastic zone (large grain, high strength) [40]. Fracture toughness is not affected by grain boundary α in this fracture mode, because it is influenced by the intrinsic toughness of the aged matrix.

(II) The low energy path of soft grain boundary α can be the initiation site of cracks and its propagation when the beta grain size is much smaller than the size of plastic zone (low strength, small grain). For the transgranular fracture, smaller fracture toughness is obtained at constant yield stress. In the case of active grain boundary fracture mechanism, the increase in grain size results in more tortuosity in the crack path and the subsequent enhancement of toughness. When a broken up grain boundary α, called necklace, is formed instead of a continuous film, the cracks are still deflected; however, a higher energy path is provided and ductility is not reduced. Additionally, the plastic zone will be more confined to the grain boundary α film with an increase in matrix aging in the case of intergranular fracture, which will result in a lower toughness. Anisotropy in fracture toughness could be observed in stretched grains produced by forging due to the crack deviation effect and intergranular fracture.

(III) In the absence of grain boundary α, beta grain size does not influence toughness fracture due to transgranular fracture [19].

To sum up, a combination of maximum crack deviation and high-energy crack paths could result in an optimum toughness. This could be the combination of an aged matrix with acicular primary $\alpha_p$ or a large grain size with a broken up grain boundary α.

### *3.3. Fatigue*

Beta alloys have good fatigue potential; for example, a cycle fatigue strength (HCF) of Ti-10-2-3 with large cross-section has been reported to be 700 MPa (R= –1, $K_t$= 1), which cannot be achieved for any other titanium alloys [41]. HCF strength can be increased by the increase in 0.2 % yield strength or aging. Some studies have also shown that the richer beta alloys exhibit a lower fatigue strength compared to leaner alloys. This is because $\alpha_s$ is heterogeneously precipitated in the richer beta alloys. Because of using a duplex aging, an increase in fatigue strength was obtained due to a more homogeneous $\alpha_s$ precipitation. Moreover, the results indicated that HCF strength could not exceed the upper limit by further aging. It can be concluded that at a higher strength, the soft regions such as primary $\alpha_p$, zones without precipitates, or grain boundary α, which are fatigue cracks initiation sites, become more dominant. This is because the difference of strength between the aged matrix and these soft zones becomes higher. Additionally, the higher fatigue strength can

be due to the localized slip in the aged matrix [42, 43].

It has been also shown that the fatigue strength of beta titanium alloys is enhanced by grain size reduction. It has been discussed that grain boundary α is the crack nucleation site. Similar to static properties, delayed crack nucleation occurs due to the reduction of the slip length of grain boundary alpha in smaller grain sizes. The studies on the effect of α/β deformation on fatigue strength after β-forging indicated that a higher ratio of high cycle fatigue strength to yield strength was observed in the purely β-forged condition in comparison with the beta+ alpha/beta-forged material with alpha/beta deformation higher than 30%. By an α/β deformation higher than 30%, high amounts of α grain boundary that were produced in the purely β-processed condition were effectively removed. This is also the reason why no further improvement of fatigue strength is observed in more than 30% α/β deformation. HCF strength is independent of the grain size effect in the case of grain boundary α suppression and the initiation of cracks from the aged matrix [19, 44, 45].

There is still a lack of data to understand and optimize the fatigue behavior; however, the obtained results already shed light on the fatigue resistance improvement approaches including homogeneous dispersion of secondary α, suppression, or reduction of grain boundary α, small grain size, and aging to an optimum level.

## 4. Properties of TZNT alloys

As mentioned, Ti alloys with metastable β structure, are good candidates for orthopedic applications due to high ductility, low elastic modulus, and the good corrosion resistance in the body environment [46, 47]. To avoid problems such as the stress shielding and the consequent osteoporosis, the difference between Young's moduli of bone and biomaterial should be reduced. Therefore, orthopedic materials are needed to have low Young's modulus. In general, Young's modulus of metastable β-Ti alloys is almost half of the Ti-6Al-4V alloy. By employing different methods such as conventional aging treatment [48, 49], severe plastic deformation [50], and the addition of alloying elements like Fe [23, 51], the strength of these alloys can be increased.

Zareidoost et al. [6] investigated the properties of different TZNT alloys by adding Ag (TZNT-Ag), Sn (TZNT-Sn), and Fe (TZNT-Fe) alloying elements. After suction casting, dendritic morphology was formed in the designed alloys; however, a more homogenous microstructure was obtained for the TZNT-Ag alloy. TZNT, TZNT-Ag, and TZNT-Fe consisted of the β phase, while TZNT-Sn showed separation of β-lean and β-rich regions in the alloy. Moreover, upon cold compressive deformation, very high ductility was obtained for the new TZNT alloys and TZNT-Ag showed the lowest Young's modulus around 65 GPa. Moreover, the ratio of compressive yield stress to Young's modulus was obtained in the range of 0.92-1.08% for all the prepared alloys. TZNT-Ag revealed the highest corrosion resistance in Ringer's solution.

In another study also conducted by Zareidoost et al. [52], as-cast $(Ti_{55}Zr_{25}Nb_{10}Ta_{10})_{99.5}$-$Fe_{0.5}$ alloy was cold-rolled and its effect on texture evolution and microstructure of the alloy was investigated. They reported that after different cold-rolling stages, hardness increased which was proposed to be related to grain refinement, the increase of microstrain, and the decrease of crystallite size. Additionally, it was indicated that the reduction of elastic modulus with the cold deformation increase was related to the texture evolution. Cold rolling up to 90% resulted in the increase in the intensity of α-fiber texture and the consequent increase in hardness and decrease in Young's modulus.

Li et al. [53] compared the corrosion behaviors of Ti12.5Zr2.5Nb2.5Ta, Ti6Al7Nb, TA2, and Ti6Al4V in Ringer's solution using the potentiodynamic technique. According to the results, the corrosion resistance of TZNT was higher than that of TA2, Ti6Al7Nb, and Ti6Al4V. $Ta_2O_5$, $Nb_2O_5$, $ZrO_2$, and $TiO_2$ were the constituents of the passive film on the TZNT's surface. These oxides with the nobler equilibrium constants improve the stability of the passive film. Additionally, adding elements with low electrochemical reaction potentials, such as Ta, Nb, and Zr could lead to the reduction of the anode activity and improvement of passive properties.

## 5. TZNT alloys for biomedical applications

### *5.1 Application in orthopedic implants*

One of the promising candidates for applications in the orthopedic field is titanium alloys containing Ta, Zr, and Nb with metastable β phase [54-59]. This is because of their high corrosion resistance in biological environments, high ductility, low elastic modulus, and excellent biocompatibility [60]. However, due to their relatively low strength, the use of these alloys for orthopedic implants is limited [51, 52, 59, 61].

Approximately one million hip replacements has been recorded since 2003 in Northern Ireland, Wales, and England according to the National Joint Registry (NJR) report. Ti alloys, mainly Ti6Al-4V, have been utilized for decades in implant applications where load-bearing properties are required. However, they have some limitations including corrosion, wear [62], infection, aseptic loosening, and adverse soft tissue reaction to debris particles resulting in implant failure and the need for revision surgeries [18, 62]. In terms of mechanical properties, low fracture toughness and low strength can result in implant fracture. The main reason for failure is the difference between the elastic modulus of implant and bone, which results in stress shielding and resorption of bone. Using materials with a modulus close to the human bone, such as TNZT, is a sensible solution to this problem. These β-Ti alloys contain no toxic elements and have lowest elastic modulus among the β-Ti family. On the other hand, the poor wear behavior of TNZT limits its application as a load-bearing part of hip implants [63]. Therefore, the improvement of the implant properties is required.

Laser surface nitriding of TNZT is a way to improve its biological response and mechanical properties. Titanium nitride has remarkable antibacterial properties and good biocompatibility. In this regard, Donaghy et al. [18] used laser nitriding to apply an antibacterial surface on TNZT alloys for hip implant applications. They used incremental laser power to prepare laser-nitrided surfaces on TNZT. According to the results, rougher surfaces with distinctive features were formed by laser nitriding. Regardless of laser power, the surface of implants could be tailored to become hydrophilic after laser nitriding. It was proposed that fiber laser nitriding in a high power regime could be employed for the formation of antibacterial surface patterns on TNZT. It was observed that the most effective laser power was 45W, which created an overlapping crescent shape. With increasing power, the overlapping crescent shape becomes more obvious. Accordingly, laser-nitrided surfaces provided the implant with a remarkable antibacterial effect while showing no special advantage to mesenchymal stem cell response.

The micro-scale abrasive wear property of Ti-35Nb-7Zr-6Ta alloy, as human-implant materials, in terms of load and sliding distance was studied by Zheng et al. [2]. The evaluation of micro-scale abrasive wear behavior of the alloy was carried out in distilled water and Hank's solution and the influence of sliding and load distance was studied. According to the results, the increase in the distance led to the increase in the wear volume of the TZNT alloy due to the greater damage, however, the same regularity was not seen in the wear volume with the increase in load. At different simulated body fluids, the wear occurred under the same sliding distance. The wear mechanism affected the wear appearance. In the wastage map, minor areas of low wastage were observed and the rest was medium wastage, and no high wastage was resent. The wastage map was attributed to the alloy wear volume under different

conditions.

Acharya et al. [59] investigated the effect of the Zr addition to a Ti-Nb-Ta-O alloy in terms of the functional response and mechanical properties for orthopedic applications. By varying the processing technique, different crystallographic textures were observed in Ti-Nb-Ta-Zr-O and Ti-Nb-Ta-O. It was found that both alloys possessed low elastic modulus because they have beta microstructures, however, the lower elastic modulus belonged to the Ti-Nb-Ta-O alloy. This is due to its favorable orientation of crystals resulting from the absence of Zr in the structure. Because of the presence of oxygen atoms in interstitial sites, the values of tensile strength were noticeably high for both alloys. In comparison with Ti-Nb-Ta-O alloy, Ti-Nb-Ta-Zr-O showed higher strength revealing the hardening effect of Zr. Both alloys exhibited the satisfactory in vitro biological behavior and corrosion resistance. Additionally, improved osteoblast attachment and lower corrosion rate were observed in the Ti-Nb-Ta-Zr-O alloy. It was concluded that the functional response and mechanical properties of both alloys were promising, and marginal improvement in the performance of Ti-Nb-Ta-Zr-O alloy for orthopedic applications was shown due to the presence of Zr.

*5.2 Application in dental implant*

Dental implantology was first emerged in 1957 by Per-Ingvar Brånemark, a Swedish orthopedic surgeon [64]. He found that bone continued to grow adjacent to Ti, which could provide bone with the capability to adhere to the Ti metal effectively without rejection. The adherence of bone to implant is called “osseointegration” and it is an important indicator of success rates in dental implantology [65, 66]. In 1982, the United States Food and Drug Administration recommended Ti as a dental implant material. Since then, dental implant manufacturing companies have widely investigated the development of modern materials and the surface treatments to improve osseointegration and consequently, enhance the overall implant success [67-71].

A new binary alloy with the formulation of 13-17% zirconium and 83-87% titanium has recently been introduced in dentistry for producing narrow-diameter implants. It has been claimed that better mechanical characteristics (40% higher fatigue strength and tensile strength of 953 MPa) could be achieved by the application of this alloy in comparison with Ti-6Al-4V and cp Ti [72, 73]. Improved osseointegration can be obtained by adding Zr to Ti [65], and enhanced biocompatibility is shown compared to pure titanium [74].

TZNT is considered as another new promising Ti alloy for surgical implants. This alloy benefits from the unique advantage of the elasticity modulus closer to the human bone than that of conventional Ti alloys as well as admission strain (0.65%) near to human bones (0.67%). The incorporation of alloying elements such as Ta, Nb, and Zr enhances the alloy corrosion resistance and no adverse tissue reactions or toxicity is observed [74-76].

Wang et al. [77] conducted osseointegration studies on Ti–Nb–Zr–Ta–Si titanium alloy for dental implant materials. For the preparation of the alloy, high-energy ball milling was used and subsequently, reactive sintering was performed. Based on the results, compared to cp Ti implants, the prepared Ti alloy implants exhibited a higher rate of mineral apposition after four weeks of healing. It was suggested that the prepared alloy implants showed osseointegration comparable to cp Ti implants. Additionally, a more favorable rate of mineral apposition was promoted by the Ti alloy implants compared to cp Ti implants. It was concluded that the prepared TZNT alloy could be considered as an alternative material for dental implants due to improved mineral matrix apposition rate and establishment of a close direct contact compared to cp Ti implants.

The corrosion resistance of Ti−Nb−Ta−Zr−Fe (TNTZF) alloy, which is currently utilized as replacement materials for dental implants, artificial hip joints, and other hard tissues, was studied by Xu et al. [78]. Compared to Ti–6Al–4V ELI alloy, TNTZF alloy showed wider passive region, passive current density with more stability, lower corrosion current density, and higher corrosion potential indicating its better corrosion resistance. Additionally, in contrast to Ti–6Al–4V ELI alloy, pitting corrosion was not indicated on its surface passive film. The surface passive film on TNTZF alloy was found to be composed of TiO, $ZrO_2$, $Ta_2O_5$, $NbO_2$, $Nb_2O_5$, and $Ti_2O_3$ oxides in the $TiO_2$ matrix. These oxides provide the passive film of TNTZF with more stability and protective ability compared to Ti−6Al−4V ELI alloy leading to its superior corrosion resistance.

## 6. Conclusions and future insights

As elements such as titanium, niobium, zirconium, and tantalum exhibit good corrosion resistance and excellent biocompatibility in the physiological environments, they are incorporated in the initial Ti alloy (e.g., TZNT). Nb and Ta are also β-stabilizing alloying elements. Moreover, Zr plays a β-stabilizer role in titanium alloys containing Nb and/or Ta. Owing to their excellent physicochemical properties, low density, high corrosion resistance, and good biocompatibility, TZNT alloy have been used as a surgical implant material. Additionally, the low elastic modulus of TZNT alloy can provide protection from adverse soft tissue reaction to debris, inflammation, infection, and consequent implant failure. In conclusion, the development of TZNT alloy can lead to the achievement of a more promising candidate for application in surgical implants.

It has been found that improvement of properties, particularly in surgical implants, can be achieved by using TZNT alloy. Additionally, there is the possibility to fabricate special implant material and enhance the properties of these alloys to promote the surgical implants’ advantages and reduce the risk factors, and consequently, the surgical implant failure. Thus, it is expected that this novel implant material should be improved owing to the optimal properties offered by TZNT implants. Meanwhile, these implants will be considered as alternatives to Ti-based and Zr-based implants in dental and orthopedic implantology.

REFERENCES

[1] E. Sharifi Sedeh, S. Mirdamadi, F. Sharifianjazi, M. Tahriri, Synthesis and Evaluation of Mechanical and Biological Properties of Scaffold Prepared From Ti and Mg With Different Volume Percent, Synthesis and Reactivity in Inorganic, Metal-Organic, and Nano-Metal Chemistry 45(7) (2015) 1087-1091.

[2] Z. Zheng, Z. Wang, W. Huang, Influence of load and sliding distance on the micro-scale abrasive wear behavior of TZNT alloy, Journal of the Chinese Advanced Materials Society 4(1) (2016) 82-90.

[3] L.C. Donaghy, R. McFadden, C.G. Smith, S. Kelaini, L. Carson, S. Malinov, A. Margariti, C.-W. Chan, Fibre Laser Treatment of Beta TNZT Titanium Alloys for Load-Bearing Implant Applications: Effects of Surface Physical and Chemical Features on Mesenchymal Stem Cell Response and Staphylococcus aureus Bacterial Attachment, Coatings 9(3) (2019).

[4] L. Zhou, T. Yuan, J. Tang, J. He, R. Li, Mechanical and corrosion behavior of titanium alloys additively manufactured by selective laser melting – A comparison between nearly β titanium, α titanium and α + β titanium, Optics & Laser Technology 119 (2019) 105625.

[5] M. Sowa, M. Parafiniuk, C.M.S. Mouzêlo, A. Kazek-Kęsik, I.S. Zhidkov, A.I. Kukharenko, S.O. Cholakh, E.Z. Kurmaev, W. Simka, DC plasma electrolytic oxidation treatment of gum metal for dental implants, Electrochimica Acta 302 (2019) 10-20.

[6] A. Zareidoost, M. Yousefpour, A study on the mechanical properties and corrosion behavior of the new as-cast TZNT alloys for biomedical applications, Materials Science and Engineering: C 110 (2020) 110725.

[7] S. Li, T.-h. Nam, Superelasticity and tensile strength of Ti-Zr-Nb-Sn alloys with high Zr content for biomedical applications, Intermetallics 112 (2019) 106545.

[8] S.F. Jawed, C.D. Rabadia, Y.J. Liu, L.Q. Wang, P. Qin, Y.H. Li, X.H. Zhang, L.C. Zhang, Strengthening mechanism and corrosion resistance of beta-type Ti-

Nb-Zr-Mn alloys, Materials Science and Engineering: C 110 (2020) 110728.
[9] Y.P. Sharkeev, V.A. Skripnyak, V.P. Vavilov, E.V. Legostaeva, A.A. Kozulin, A.O. Chulkov, A.Y. Eroshenko, O.A. Belyavskaya, V.V. Skripnyak, I.A. Glukhov, Special Aspects of Microstructure, Deformation and Fracture of Bioinert Zirconium and Titanium-Niobium Alloys in Different Structural States, Russian Physics Journal 61(9) (2019) 1718-1725.
[10] T. Kokubo, S. Yamaguchi, Simulated body fluid and the novel bioactive materials derived from it, Journal of Biomedical Materials Research Part A 107(5) (2019) 968-977.
[11] A. Vladescu, M. Badea, S.C. Padmanabhan, G. Paraschiv, L. Floroian, L. Gaman, M.A. Morris, J.-L. Marty, C.M. Cotrut, Chapter 15 - Nanomaterials for medical applications and their antimicrobial advantages, in: A.-M. Holban, A.M. Grumezescu (Eds.), Materials for Biomedical Engineering, Elsevier2019, pp. 409-431.
[12] A.S. Konopatsky, S.M. Dubinskiy, Y.S. Zhukova, V. Sheremetyev, V. Brailovski, S.D. Prokoshkin, M.R. Filonov, Ternary Ti-Zr-Nb and quaternary Ti-Zr-Nb-Ta shape memory alloys for biomedical applications: Structural features and cyclic mechanical properties, Materials Science and Engineering: A 702 (2017) 301-311.
[13] V.T. Nguyen, M. Qian, Z. Shi, T. Song, L. Huang, J. Zou, A novel quaternary equiatomic Ti-Zr-Nb-Ta medium entropy alloy (MEA), Intermetallics 101 (2018) 39-43.
[14] X. Meng, X. Wang, Y. Guo, S. Ma, W. Luo, X. Xiang, J. Zhao, Y. Zhou, Biocompatibility Evaluation of a Newly Developed Ti-Nb-Zr-Ta-Si Alloy Implant, Journal of Biomaterials and Tissue Engineering 6(11) (2016) 861-869.
[15] T. Nagase, M. Todai, T. Hori, T. Nakano, Microstructure of equiatomic and non-equiatomic Ti-Nb-Ta-Zr-Mo high-entropy alloys for metallic biomaterials, Journal of Alloys and Compounds 753 (2018) 412-421.
[16] X. Song, C. Xiong, F. Zhang, Y. Nie, Y. Li, Strain induced martensite stabilization in β Ti-Zr-Nb shape memory alloy, Materials Letters 259 (2020) 126914.
[17] W.F. Oliveira, P.M.S. Silva, R.C.S. Silva, G.M.M. Silva, G. Machado, L.C.B.B. Coelho, M.T.S. Correia, Staphylococcus aureus and Staphylococcus epidermidis infections on implants, Journal of Hospital Infection 98(2) (2018) 111-117.
[18] C. Lubov Donaghy, R. McFadden, S. Kelaini, L. Carson, A. Margariti, C.-W. Chan, Creating an antibacterial surface on beta TNZT alloys for hip implant applications by laser nitriding, Optics & Laser Technology 121 (2020) 105793.
[19] C. Leyens, M. Peters, Titanium and Titanium Alloys: Fundamentals and Applications, Wiley2006.
[20] G. Welsch, R. Boyer, E.W. Collings, Materials Properties Handbook: Titanium Alloys, ASM International1993.
[21] A.P. Mouritz, Introduction to Aerospace Materials, Elsevier Science2012.
[22] I. Polmear, D. StJohn, J.-F. Nie, M. Qian, 7 - Titanium Alloys, in: I. Polmear, D. StJohn, J.-F. Nie, M. Qian (Eds.), Light Alloys (Fifth Edition), Butterworth-Heinemann, Boston, 2017, pp. 369-460.
[23] I. Kopova, J. Stráský, P. Harcuba, M. Landa, M. Janeček, L. Bačákova, Newly developed Ti–Nb–Zr–Ta–Si–Fe biomedical beta titanium alloys with increased strength and enhanced biocompatibility, Materials Science and Engineering: C 60 (2016) 230-238.
[24] R. Santhosh, M. Geetha, V. Saxena, M.N. Rao, Effect of duplex aging on microstructure and mechanical behavior of beta titanium alloy Ti–15V–3Cr–3Al–3Sn under unidirectional and cyclic loading conditions, International Journal of Fatigue 73 (2015) 88-97.
[25] A.E. Chaikh, P. Schmidt, H.J. Christ, Fatigue properties of duplex-aged Ti 38-644 metastable beta titanium alloy, Procedia Engineering 2(1) (2010) 1973-1982.
[26] M.J. Donachie, Titanium: A Technical Guide, 2nd Edition, ASM International2000.
[27] Y. Ren, S. Zhou, W. Luo, Z. Xue, Y. Zhang, Influence of primary α-phase volume fraction on the mechanical properties of Ti-6Al-4V alloy at different strain rates and temperatures, IOP Conference Series: Materials Science and Engineering, IOP Publishing, 2018, p. 022022.
[28] Y. Chen, Z. Du, S. Xiao, L. Xu, J. Tian, Effect of aging heat treatment on microstructure and tensile properties of a new β high strength titanium alloy, Journal of alloys and compounds 586 (2014) 588-592.
[29] C. Bo, S. Bing, L. Dong, Effect of heat treatment on microstructure and mechanical properties of laser melting deposited TC17 titanium alloy, Chinese J Lasers 41(4) (2014) 0403001.
[30] G. Srinivasu, Y. Natraj, A. Bhattacharjee, T. Nandy, G.N. Rao, Tensile and fracture toughness of high strength β Titanium alloy, Ti–10V–2Fe–3Al, as a function of rolling and solution treatment temperatures, Materials & Design 47 (2013) 323-330.
[31] S. Sadeghpour, S. Abbasi, M. Morakabati, S. Bruschi, Correlation between alpha phase morphology and tensile properties of a new beta titanium alloy, Materials & Design 121 (2017) 24-35.
[32] V.K. Saxena, V. Radhakrishnan, Effect of phase morphology on fatigue crack growth behavior of α-β titanium alloy—A crack closure rationale, Metallurgical and materials transactions A 29(1) (1998) 245-261.
[33] S. Ankem, C. Greene, Recent developments in microstructure/property relationships of beta titanium alloys, Materials Science and Engineering: A 263(2) (1999) 127-131.
[34] J. Tiley, T. Searles, E. Lee, S. Kar, R. Banerjee, J. Russ, H. Fraser, Quantification of microstructural features in α/β titanium alloys, Materials Science and Engineering: A 372(1-2) (2004) 191-198.
[35] Y. Kawabe, S. Muneki, Strengthening capability of beta titanium alloys, Beta Titanium Alloys in the 1990's1993.
[36] E. Breslauer, A. Rosen, Relationship between microstructure and mechanical properties in metastable β titanium 15–3 alloy, Materials science and technology 7(5) (1991) 441-446.
[37] J. Ferrero, J. Wood, P. Russo, Microstructure/Mechanical property relationships in bar products of Beta-C trademark (Ti-3Al-8V-6Cr-4Mo-4Zr), Beta Titanium Alloys in the 1990's1993.
[38] C. Sauer, G. Lütjering, Influence of α layers at β grain boundaries on mechanical properties of Ti-alloys, Materials Science and Engineering: A 319 (2001) 393-397.
[39] J.W. Foltz, B. Welk, P.C. Collins, H.L. Fraser, J.C. Williams, Formation of grain boundary α in β Ti alloys: its role in deformation and fracture behavior of these alloys, Metallurgical and Materials Transactions A 42(3) (2011) 645-650.
[40] C.M. Branco, L.G. Rosa, Advances in Fatigue Science and Technology, Springer Netherlands2012.
[41] R. Boyer, Applications of beta titanium alloys in airframes, The Minerals, Metal & Materials Society(USA) (1993) 335-346.
[42] G. Lütjering, J. Albrecht, C. Sauer, T. Krull, The influence of soft, precipitate-free zones at grain boundaries in Ti and Al alloys on their fatigue and fracture behavior, Materials Science and Engineering: A 468 (2007) 201-209.
[43] M. Niinomi, Mechanical biocompatibilities of titanium alloys for biomedical applications, Journal of the mechanical behavior of biomedical materials 1(1) (2008) 30-42.
[44] S. Shekhar, R. Sarkar, S.K. Kar, A. Bhattacharjee, Effect of solution treatment and aging on microstructure and tensile properties of high strength β titanium alloy, Ti–5Al–5V–5Mo–3Cr, Materials & Design 66 (2015) 596-610.
[45] C. Tan, X. Li, Q. Sun, L. Xiao, Y. Zhao, J. Sun, Effect of α-phase morphology on low-cycle fatigue behavior of TC21 alloy, International Journal of Fatigue 75 (2015) 1-9.
[46] J. Gao, Y. Huang, D. Guan, A.J. Knowles, L. Ma, D. Dye, W.M. Rainforth, Deformation mechanisms in a metastable beta titanium twinning induced plasticity alloy with high yield strength and high strain hardening rate, Acta Materialia 152 (2018) 301-314.
[47] M.A.-H. Gepreel, Improved elasticity of new Ti-alloys for biomedical applications, Materials Today: Proceedings 2 (2015) S979-S982.
[48] S. Bahl, A.S. Krishnamurthy, S. Suwas, K. Chatterjee, Controlled nanoscale precipitation to enhance the mechanical and biological performances of a metastable β Ti-Nb-Sn alloy for orthopedic applications, Materials & Design 126 (2017) 226-237.
[49] C. Xiong, P. Xue, B. Sun, Y. Li, Effect of annealing temperature on the microstructure and superelasticity of Ti-19Zr-10Nb-1Fe alloy, Materials Science and Engineering: A 688 (2017) 464-469.
[50] V. Cojocaru, D. Raducanu, T. Gloriant, D. Gordin, I. Cinca, Effects of cold-rolling deformation on texture evolution and mechanical properties of Ti–29Nb–9Ta–10Zr alloy, Materials Science and Engineering: A 586 (2013) 1-10.
[51] J. Stráský, P. Harcuba, K. Václavová, K. Horváth, M. Landa, O. Srba, M. Janeček, Increasing strength of a biomedical Ti-Nb-Ta-Zr alloy by alloying with Fe, Si and O, Journal of the Mechanical Behavior of Biomedical Materials 71 (2017) 329-336.
[52] A. Zareidoost, M. Yousefpour, Effect of cold rolling on the microstructure and texture evolution of as-cast $(Ti_{55}Zr_{25}Nb_{10}Ta_{10})_{99.5}$-$Fe_{0.5}$ alloy, Materials Letters 259 (2020) 126876.
[53] J. Li, L. Zhou, Z. Li, Corrosion behaviors of a new titanium alloy TZNT for surgical implant application in Ringer's solution, Rare Metals 29(1) (2010) 37-44.
[54] W. Weng, A. Biesiekierski, Y. Li, C. Wen, Effects of selected metallic and interstitial elements on the microstructure and mechanical properties of beta titanium alloys for orthopedic applications, Materialia 6 (2019) 100323.
[55] W. Weng, A. Biesiekierski, J. Lin, S. Ozan, Y. Li, C. Wen, Impact of the rare earth elements scandium and yttrium on beta-type Ti-24Nb-38Zr-2Mo-base alloys for orthopedic applications, Materialia 9 (2020) 100586.

[56] S. Acharya, A.G. Panicker, V. Gopal, S.S. Dabas, G. Manivasagam, S. Suwas, K. Chatterjee, Surface mechanical attrition treatment of low modulus Ti-Nb-Ta-O alloy for orthopedic applications, Materials Science and Engineering: C 110 (2020) 110729.

[57] W. Xu, X. Lu, J. Tian, C. Huang, M. Chen, Y. Yan, L. Wang, X. Qu, C. Wen, Microstructure, wear resistance, and corrosion performance of $Ti_{35}Zr_{28}Nb$ alloy fabricated by powder metallurgy for orthopedic applications, Journal of Materials Science & Technology 41 (2020) 191-198.

[58] J. Ureña, E. Tabares, S. Tsipas, A. Jiménez-Morales, E. Gordo, Dry sliding wear behaviour of β-type Ti-Nb and Ti-Mo surfaces designed by diffusion treatments for biomedical applications, Journal of the Mechanical Behavior of Biomedical Materials 91 (2019) 335-344.

[59] S. Acharya, A.G. Panicker, D.V. Laxmi, S. Suwas, K. Chatterjee, Study of the influence of Zr on the mechanical properties and functional response of Ti-Nb-Ta-Zr-O alloy for orthopedic applications, Materials & Design 164 (2019) 107555.

[60] I. Çaha, A.C. Alves, P.A.B. Kuroda, C.R. Grandini, A.M.P. Pinto, L.A. Rocha, F. Toptan, Degradation behavior of Ti-Nb alloys: Corrosion behavior through 21 days of immersion and tribocorrosion behavior against alumina, Corrosion Science 167 (2020) 108488.

[61] S. Ozan, J. Lin, Y. Li, Y. Zhang, K. Munir, H. Jiang, C. Wen, Deformation mechanism and mechanical properties of a thermomechanically processed β Ti–28Nb–35.4Zr alloy, Journal of the Mechanical Behavior of Biomedical Materials 78 (2018) 224-234.

[62] S.K. Kolawole, W. Hai, S. Zhang, Z. Sun, M.A. Siddiqui, I. Ullah, W. Song, F. Witte, K. Yang, Preliminary study of microstructure, mechanical properties and corrosion resistance of antibacterial Ti-15Zr-xCu alloy for dental application, Journal of Materials Science & Technology 50 (2020) 31-43.

[63] C.L. Donaghy, R. McFadden, G.C. Smith, S. Kelaini, L. Carson, S. Malinov, A. Margariti, C.-W. Chan, Fibre laser treatment of beta TNZT titanium alloys for load-bearing implant applications: Effects of surface physical and chemical features on mesenchymal stem cell response and Staphylococcus aureus bacterial attachment, Coatings 9(3) (2019) 186.

[64] K. Zhang, Q. Van Le, Bioactive Glass Coated Zirconia for Dental Implants: a review, Composites and Compounds 2(1) (2020).

[65] L. Bazli, H. Nargesi khoramabadi, A. Modarresi Chahardehi, H. Arsad, B. Malekpouri, M. Asgari Jazi, N. Azizabadi, Factors influencing the failure of dental implants: A Systematic Review, Composites and Compounds 2(1) (2020).

[66] F. Sharifianjazi, A.H. Pakseresht, M. Shahedi Asl, A. Esmaeilkhanian, H. Nargesi khoramabadi, H.W. Jang, M. Shokouhimehr, Hydroxyapatite Consolidated by Zirconia: Applications for Dental Implant, Composites and Compounds 2(1) (2020).

[67] J. Diaz-Marcos, 9 - Bone response to decontamination treatments for dental biomaterials, in: A. Piattelli (Ed.), Bone Response to Dental Implant Materials, Woodhead Publishing2017, pp. 163-184.

[68] L. Gaviria, J.P. Salcido, T. Guda, J.L. Ong, Current trends in dental implants, J Korean Assoc Oral Maxillofac Surg 40(2) (2014) 50-60.

[69] S. Rahimi, F. SharifianJazi, A. Esmaeilkhanian, M. Moradi, A.H. Safi Samghabadi, Effect of SiO2 content on Y-TZP/$Al_2O_3$ ceramic-nanocomposite properties as potential dental applications, Ceramics International 46(8, Part A) (2020) 10910-10916.

[70] M. Nejati, M.R. Rahimipour, I. Mobasherpour, A.H. Pakseresht, Microstructural analysis and thermal shock behavior of plasma sprayed ceria-stabilized zirconia thermal barrier coatings with micro and nano $Al_2O_3$ as a third layer, Surface and Coatings Technology 282 (2015) 129-138.

[71] A.H. Pakseresht, A.H. Javadi, E. Ghasali, A. Shahbazkhan, S. Shakhesi, Evaluation of hot corrosion behavior of plasma sprayed thermal barrier coatings with graded intermediate layer and double ceramic top layer, Surface and Coatings Technology 288 (2016) 36-45.

[72] E.H. Jazi, R. Esalmi-Farsani, G. Borhani, F.S. Jazi, Synthesis and Characterization of In Situ Al-$Al_{13}Fe_4$-$Al_2O_3$-$TiB_2$ Nanocomposite Powder by Mechanical Alloying and Subsequent Heat Treatment, Synthesis and Reactivity in Inorganic, Metal-Organic, and Nano-Metal Chemistry 44(2) (2014) 177-184.

[73] A. Esmaeilkhanian, F. Sharifianjazi, A. Abouchenari, A. Rouhani, N. Parvin, M. Irani, Synthesis and Characterization of Natural Nano-hydroxyapatite Derived from Turkey Femur-Bone Waste, Applied Biochemistry and Biotechnology 189(3) (2019) 919-932.

[74] S. Bhasin, E. Perwez, S. Sachdeva, R. Mallick, Trends in prosthetic biomaterials in implant dentistry, Journal of the International Clinical Dental Research Organization 7(3) (2015) 148-159.

[75] A. Brizuela, M. Herrero-Climent, E. Rios-Carrasco, V.J. Rios-Santos, A.R. Pérez, M.J. Manero, J. Gil Mur, Influence of the Elastic Modulus on the Osseointegration of Dental Implants, Materials 12(6) (2019).

[76] Y. Kirmanidou, M. Sidira, M.-E. Drosou, V. Bennani, A. Bakopoulou, A. Tsouknidas, N. Michailidis, K. Michalakis, New Ti-Alloys and Surface Modifications to Improve the Mechanical Properties and the Biological Response to Orthopedic and Dental Implants: A Review, BioMed Research International 2016 (2016) 2908570.

[77] X. Wang, X. Meng, S. Chu, X. Xiang, Z. Liu, J. Zhao, Y. Zhou, Osseointegration behavior of novel Ti–Nb–Zr–Ta–Si alloy for dental implants: an in vivo study, Journal of Materials Science: Materials in Medicine 27(9) (2016) 139.

[78] Y.-f. Xu, Y.-f. Xiao, D.-q. Yi, H.-q. Liu, L. Wu, J. Wen, Corrosion behavior of Ti–Nb–Ta–Zr–Fe alloy for biomedical applications in Ringer's solution, Transactions of Nonferrous Metals Society of China 25(8) (2015) 2556-2563.

Available online at www.jourcc.com

Journal homepage: www.JOURCC.com

Journal of Composites and Compounds

# A review of polyvinyl alcohol/carboxymethyl cellulose (PVA/CMC) composites for various applications

*Hiva Nargesi Khoramabadi[a]*, Mehrnoosh Arefian[b], Mahsa Hojjati[c], Iman Tajzad[d], Ali Mokhtarzade[e], Majid Mazhar[f], Ata Jamavari[g]*

[a] *Department of medical enginnering, Payame Noor University (PNU),19395-3697 Alborz, Iran*
[b] *Department of Biochemistry, Islamic Azad University, Falavarjan Branch, Isfahan, Iran*
[c] *Faculty of Chemistry, Shahrood University of Technology, Shahrood, Semnan, Iran*
[d] *Department of Mechanical Engineering, Islamic Azad University, Majlesi Branch, Isfahan, Iran*
[e] *Department of Biomedical Engineering, Amirkabir University of Technology, Tehran, Iran*
[f] *Chemistry department, basic science faculty, Azarbaijan Shahid Madani University, Tabriz, Iran*
[g] *Department of material science and engineering, Iran University of Science and Technology, Tehran, Iran*

A B S T R A C T

Polyvinyl alcohol/carboxymethyl cellulose (PVA/CMC) composites have attracted considerable attention due to the synergic relation between the two polymers and developing novel blends with improved properties. On one hand, PVA is a versatile polymer with higher mechanical properties compared to CMC. On the other hand, CMC has high biodegradability and biocompatibility, while suffering from poor mechanical properties. Therefore, the blending of the two polymers can help to benefit from the individual component properties. This paper has reviewed the properties and potential applications (e.g. drug delivery, food packaging, and agriculture) of the PVA/CMC composites.



Peer review under responsibility of jourcc

A R T I C L E I N F O R M A T I O N

*Article history:*
Received 1 June 2020
Received in revised form 18 June 2020
Accepted 28 June 2020

*Keywords:*
PVA
CMC
Drug delivery
Food packaging
Agriculture

Table of contents



## 1. Introduction

Blending of polymers can often produce materials with enhanced characteristics more rapidly compared to developing new polymer chemistry [1, 2]. Extensive studies have been conducted on copolymers due to their high application potential [3-8] and their importance in basic science [9]. Developing new polymer blends with improved properties by mixing two or more polymers is usually a less time-consuming process than new polymer development with desired properties. Therefore, their technological applications are broadening faster than their constituents[10] [11-15].

Polyvinyl alcohol (PVA) is the first synthetic colloid that was first developed by Haehnel and Herrmann in 1924 [16-20]. It was supported by a paper in Hangzhou City, China [21]. Because of its strong nonirritant [22, 23], harmlessness, and hydrophilicity [24, 25], PVA had been selected for gel preparation among other water-soluble polymers [24, 26-29]. The PVA gel offers some advantages including easy machinabil-

* *Corresponding author: Hiva Nargesi Khoramabadi; E-mail: Hiva.nargesi@yahoo.com*
https://doi.org/10.29252/jcc.2.2.2 

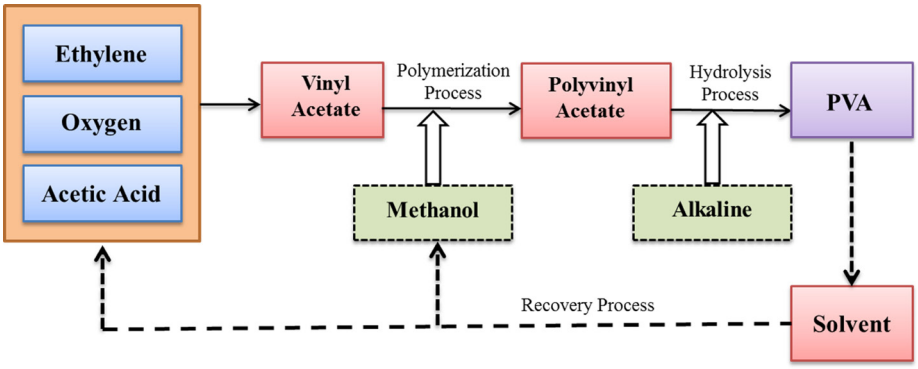


**Fig. 1.** Production outline of PVA.

ity [30], low toxicity [24, 31-33], good strength [34, 35], and high water content [36-38]. Currently, the PVA- based materials are extensively utilized in the medical, industrial, and agricultural industries [39].

Basically, manufacturing of PVA consists of the of vinyl acetate monomer polymerization into polyvinyl acetate (PVAc), and the subsequent acetate groups hydrolysis to produce PVA [1,2]. Based on the used catalyst, three hydrolysis methods are applicable in the PVA preparation. They include acidolysis, aminolysis, and alkaline hydrolysis [1]. On industrial scales, the PVAc to PVA conversion is usually carried on by alkaline alcohol. In this hydrolysis method ester interchanged with methanol, in the presence of sodium hydroxide, to hydrolyze the acetate groups [16]. The production outline of PVA is illustrated in Fig. 1.

PVA is a hydrophilic synthetic polymer with semi-crystalline, planar zigzag structure, and sound mechanical properties [40-43]. PVA is chemically and thermally stable [44] and is resistant to degradation under most physiological environments [41]. Moreover, it is water-soluble due to its elevated polarity, non-toxicity [45], and high biocompatibility [46, 47] and it can be processed easily [48]. PVA has also promising potential for producing biodegradable films [49].

One of the important derivatives of cellulose is CMC, in which carboxylic groups (-$CH_2$-COOH) are bound to some OH groups of natural cellulose [50, 51]. According to the literature, the introduction of CMC into the PVA matrix results in the improvement of this polymer properties [52]. Therefore, this paper aims to review the properties of PVA/CMC composites as well as their applications in the field of drug delivery, food packaging, and agriculture.

## 2. Carboxymethyl cellulose (CMC)

The most important classification of polysaccharides is carboxymethyl cellulose. CMC is a semi-crystalline, water-soluble, non-toxic [53, 54], low-cost [55-57], and biodegradable material [58-60] with excellent film-forming ability; however, it suffers from low conductivity [61, 62] and the lack of strength [63]. Extensive studies have been conducted on the CMC application in single polymer electrolyte systems, however, some problems limit its application in this field due to small elongation at break, exceptionally stiff behavior, (less than 8%), and losing the electrochemical stability required for electrochemical devices. Additionally, outstanding chemical, mechanical, and physical properties cannot be offered by a single polymer for wide range applications, particularly in energy storage devices [7]. CMC exhibits several desirable characteristics including emulsification, thermal filming, gelation, and inspissation [9].

Due to its biodegradability and biocompatibility, CMC can be employed for biotechnological and pharmaceutical applications [3]. For the production of CMC, chloroacetic acid is reacted with OH groups on hydroglucose units (AGU) of cellulose. In the cosmetics and food industries, CMC has been utilized as a water-retention agent and stabilizer [9].

CMC, as a highly hydrophilic derivate of cellulose, is extensively

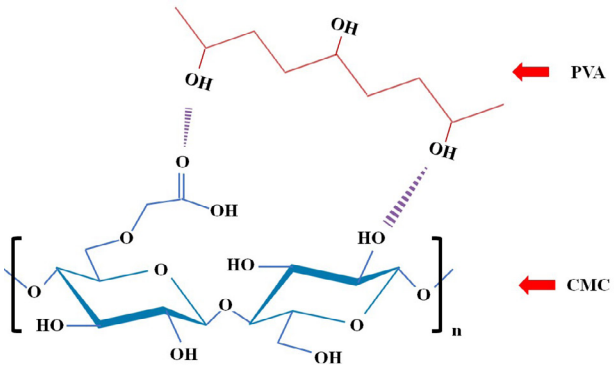


**Fig. 2.** Molecular interaction of PVA and CMC.

used as a suspending and thickening agent in the pharmaceutical and food industry. Because of good modifiability, non-toxicity, and swellability, CMC has attracted the attention of scientists in the field of hydrogels for drug delivery applications. Numerous investigations have reported the development of hydrogels based on CMC as carriers for water-soluble drugs [8]. CMC-based hydrogels have the potential to be used in absorbents, drug delivery, wound healing, and enzyme immobilization owing to their biodegradation, biocompatibility, and solubility [64].

## 3. Synthesis of PVA/CMC composites

Grafting, crosslinking, and degradation are ways to improve or modify polymer materials [9]. PVA can be modified by CMC due to their compatibility and such characteristic is the result of the hydrogen bonding between the OH groups in PVA and the carboxymethyl groups on CMC [9]. The chemical structure of PVA and CMC and their interaction is illustrated in Fig. 2. Fig. 3 also presents the crosslinking of PVA and CMC by cellulose acetate (CA).

Zhang et al. [4] prepared a potential coating material based on CMC/PLA blend film. The biodegradable CMC/PVA blend film was successfully prepared by intra- and inter-molecular cross-linking reaction. According to the obtained favorable biodegradability, the prepared blend film showed environmentally friendly characteristic which can be offered as potential materials for control-release fertilizer's coatings.

Sayed et al. [15] incorporated copper oxide and PVA nanoparticles in CMC films using a solution casting method and investigated their electrical, optical, and structural properties. At low temperature, Schottky emission was the conduction mechanism in the PVA/CMC blend. After the addition of PVA, the transparency of the CMC film increased from

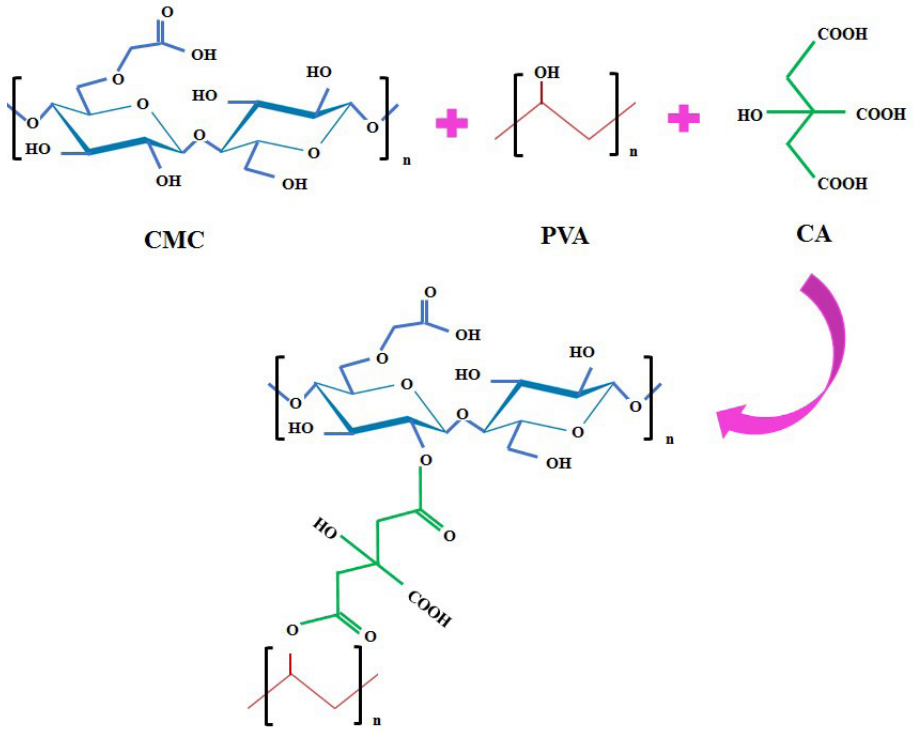


**Fig. 3.** Crosslinking of PVA and CMC by CA .

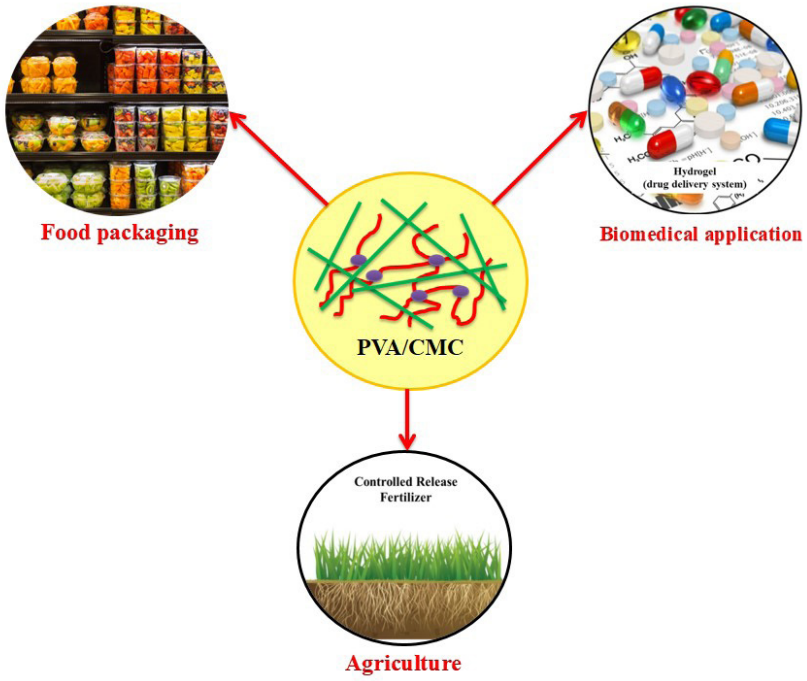


**Fig. 4.** Applications of CMC/PVA composites.

87 to 89 %. The results showed controlled optical constants, refractive index, and insulating properties of CMC by blending with PVA. Additionally, a non-ohmic behavior was observed in the current-voltage characteristics of the blend.

Saadieh et al. [65] developed biopolymer blend electrolytes based on PVA/CMC using the casting solution method. The highest ionic conductivity ($9.12 \times 10^{-6}$ S/cm) was reported for the blend electrolytes with the CMC to PVA ratio of 80:20 at room temperature. According to the results, the reduction of dielectric loss and dielectric constant were observed with an increase in frequency. This was reported to be the result of the ions accumulation contributed by the electrode, ionic polarization, and molecular polarization.

Sayed et al. [9] synthesized the CMC/PVA blend using the solution casting method and subsequent ɣ-rays irradiation. They proposed that ɣ-rays irradiation had the capability for controlling the physical properties of this copolymer. Therefore, they suggested the CMC/PVA blend for several electronic and industrial devices due to improved charge storage capacity and dielectric strength [55].

## 4. Properties of PVA/CMC composites

The physical and chemical properties of polymers are influenced by the chemical structure of polymers. The flow and morphology of polymers depend on their chemical structures, which leads to different physical properties [66]. Taghizade et al. [67] developed PVA/starch (S)/CMC) composite films using the casting method in the presence of glycerol-containing plasticizer. According to the results, PVA/S/CMC blends showed higher thermal stability compared to PVA/S. This was reported to be due to the addition of CMC resulting in the improvement of the thermal stability of the PVA/S blend.

Miao et al. [68] prepared a negatively charged nanofiltration membrane based on PVA/CMC-Na composite produced by interfacial polymerization. The resultant composite membrane exhibited high stability in long-term use. According to this study, the cross-linked PVA-based composite could provide a good balance between the salt rejection and the permeate flux under lower operating pressure. Tajeddin et al. [69] also reported the water absorption of 22.03 percent for PVA/CMC blend film prepared by the casting method after 24 h. Zhu et al. [70] stated that the pure PVA film had low water sorption and it enhanced by adding CMC to the composite film. This was reported to be due to the blending of two different molecule types resulting in the structure deformation and making more hydrophilic networks. Furthermore, the solubility of the composite was around 70 % after 24 h.

Polymer blend films are widely used for metal ions adsorption [71]. Wang et al. [72] prepared PVA/CMC hydrogels using the freeze-thaw process for heavy metal ions adsorption. The formation of crystallites occurred due to the separation of phases in polymer solutions during freezing stages leading to insoluble hydrogels (71% of insoluble gels). The swelling ratio for pure PVA hydrogels was obtained to be 416%, while a higher swelling ratio of 1437% was obtained for the PVA/CMC hydrogel containing one-third of CMC and two-thirds of PVA. This hydrogel had the adsorption capacity of 8.4 mg per gram of hydrogel toward $Ag^{+}$. The prepared hydrogels exhibited potential applications for wastewater treatment and removing heavy metal ions.

Many investigations have been carried out on the electrical and optical properties of polymers for potential applications in optical and electronic devices. The aim of electric properties investigation is to understand the charge transport mechanisms in those materials, which can be certainly changed by different techniques including plasticization, mixing, copolymerization, and the addition of ceramic filers or salts [73].

Abutalib et al. [73] studied dielectric and electrical characteristics of PVA/CMC/ZnO nanorods prepared by the casting method. The results showed that dc conductivity revealed Arrhenius behavior that was enhanced with temperature, whereas the ac conductivity followed Jonscher's law. These nanocomposites have been offered as potential candidates for applications such as electrochemical devices due to their significant improvement in ac and dc conductivities.

In a research conducted by Goswami et al. [74], bionanocomposite films of CMC/PVA/$V_2O_5$ prepared by solution casting of the CMC/PVA thin film, and subsequently impregnation of $V_2O_5$ into the film. The differential scanning calorimetry (DSC) results showed lower transition temperature for CMC/PVA/$V_2O_5$ nanocomposite compared to the CMC/PVA film making it suitable for smart windows. The total conductivity results demonstrated good electrical behavior of the prepared bionanocomposite. Therefore, electrical and optical properties of CMC films were reported to be significantly enhanced in the form of CMC/PVA-$V_2O_5$ nanocomposites enabling them to be used in applications such as storage devices and smart windows.

According to Zhu et al. [70], pure PVA exhibited low dielectric constant, and the increase in the dielectric constant was observed for PVA/CMC composite film.

The addition of PVA can enhance the mechanical properties of CMC [48]. According to Tajeddin et al. [69], the mechanical properties of PVA/CMC composite film (obtained by 10%v of PVA and CMC dissolved in 60 mL of distilled water) including tensile strength, elongation at break, and modulus were reported to be 11.54 MPa, 24.55 %, and 36.2 MPa, respectively.

El-Newehy et al. [48] used the electrospinning technique to prepare CMC/PVA nanofibers for the controlled release of diclofenac sodium (DS). The study showed that the CMC/PVA nanofibers blend exhibited good mechanical properties. Additionally, the in vitro release study showed that the presence of CMC led to the sustained controlled of the DS release from the nanofibers mats. The CMC/PVA nanofibers system could be offered as a promising material for drug delivery applications due to the low cost and biocompatibility of the blend. General applications of PVA/CMC composites are shown in Fig. 4.

## 5. Applications of PVA/CMC composites

### *5.1. Application in food packaging*

An innovative food packaging is active packaging in which the advances in material sciences, packaging, food safety, and food technology are combined for satisfying consumer demand for safe and fresh-like products [49]. Because of environmental considerations over the past few years, using synthetic polymers is restricted. There has been ever-increasing attention in biopolymers including proteins, lipids, and polysaccharides [75]. Active agents can be incorporated into the polymer structure in active packaging leading to a low diffusion rate of active compounds and the maintenance of active agents with high concentrations in the surface of packaging materials during the shelf life [76]. In the cosmetics and food industries, CMC has been utilized as a water-retention agent and stabilizer. PVA has also been incorporated to improve the mechanical properties [77].

Muppalla et al. [49] fabricated PVA/CMC films with clove oil by the casting method as active packaging for ground chicken meat. The results demonstrated an increase in the tensile strength and puncture force of the CMC film and the reduction of water vapor transmission rate with the increase in the PVA concentration. A negligible oxygen transmission rate was observed in all the samples. During refrigerated storage, control samples spoiled in 4 days, while packing of meat samples in the prepared films resulted in lower total viable counts and shelf life of 12 days. The efficacy of the CMC–PVA–clove oil films was also studied against Bacillus cereus and Staphylococcus aureus in ground chicken meat. It was proposed that the prepared films have great potential for the active packaging of meat products.

Fasihi et al. [76] produced biodegradable active films based on CMC/PVA/oleic acid (OL) containing rosemary essential oil (REO) via Pickering emulsions. The results demonstrated that the films containing REO showed considerable antimicrobial and antioxidant properties. In the films with 3% REO, the fungal inhibition against Penicillium digitatum was 100%. In bread slices that were packed with the active films containing 3% REO, no fungal growth was observed at 25 ºC after 60 days of storage. This might be due to the regular, slow release of REO resulting from Pickering emulsions.

Villarruel et al. [78] developed blend films based on CMC and PVA and modified it with UV radiation in the presence of sodium benzoate (SB). According to the result, the newly developed materials showed different chemical and thermal stability compared to single components. Both blend films and UV-induced ones revealed the very low value of oxygen barrier properties making them suitable materials for packaging applications with selective oxygen permeability. Moreover, the UV treatment in the films containing SB inhibited the growth of a wide spectrum of microorganisms and increased their insolubility in water making them potential materials to be used as food packaging emulsion.

### *5.2. Application in biomedical*

There has been a considerable effort in the improvement of drug delivery efficacy by the investigation of new materials [79-82]. In this regard, natural polymers play a substantial role in biomedical applications [83, 84]. Recently, drug delivery systems based on natural polymers hydrogel have attracted the attention of researchers [85]. CMC is a cellulose derivate with high hydrophilicity and is widely applied as a suspending and thickening agent in the pharmaceutical industry [86]. The desired properties of CMC hydrogels such as modifiability, non-toxicity,

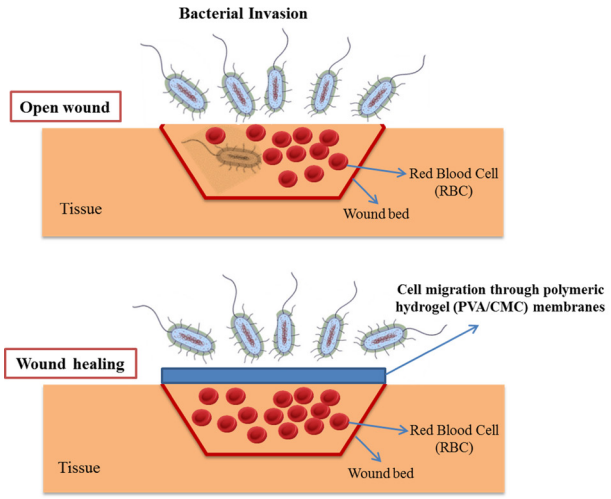


**Fig. 5.** Role of hydrogel membranes in accelerating and enhancing the wound healing phases.

and good swellability encourage scientists to use this material for drug delivery [87].

One of the pressing public health issues is burns treatment. Despite efforts made for its prevention, such as public campaigns, its worldwide incidence is high. Dressings are usually required for the treatment of second-degree burns. Cell hydration through keeping a moisturized environment and promotion of necrotic tissue debridement are of important properties of an ideal dressing. It should also be able to successfully remodel tissue and have transparency to monitor healing. Other characteristics include infection inhibition, pain reduction, non-toxicity, and vapor and oxygen transmittance. Most of these properties are offered by hydrogels; therefore, they have been utilized as biomedical devices for wound treatment. They can be permeable to oxygen, while act as barriers to microorganisms [88]. Hence, hydrogels are considered as patient-friendly systems for drug delivery [77, 89]. Many wound dressing materials belongs to hydrogel dressings because their advantages outweigh their disadvantages. Fig. 5 schematically shows the role of hydrogel membranes in wound healing phases.

Hydrogels are hydrophilic polymers that are cross-linked and undergo swelling in aqueous media while their structural integrity is maintained [88]. However, hydrophobic drugs can be loaded in low amounts due to the hydrophilic network of hydrogels. To overcome this restriction, polymer chemistry investigations have focused on the development of a variety of network structures. As a result of biodegradability and biocompatibility, CMC can be utilized in biotechnological and pharmaceutical applications [77]. Another option for the production of biocompatible hydrogels is PVA, which has a semi-crystalline structure. PVA hydrogels are able to deliver moisture and absorb exudate from the wound site. PVA gels can be cross-linked physically or chemically (with chemical agents via radiation techniques) [88]. Fig. 6 shows the synthesis of PVA/CMC hydrogel.

Ghorpade et al. [86] developed polymeric blend films for the extended release of water-soluble drugs based on citric acid cross-linked CMC/PVA. The model drug of Gentamicin sulfate (GTM) was used. The incorporation of PVA enhanced the mechanical strength of the CMC/PVA hydrogel films. The swellability of the hydrogels was improved by an increase in the PVA content in the hydrogel films. Thus, the developed hydrogel films were considered as promising biomaterials for the delivery of basic drugs soluble in water.

Membranes of PVA/Polyethylene Oxide/CMC were developed by Agarwal et al. [87] by freeze-drying and solvent casting for the drug delivery application. The results demonstrated enough swelling in PBS in the membranes, which can recommend them for exudative wounds.

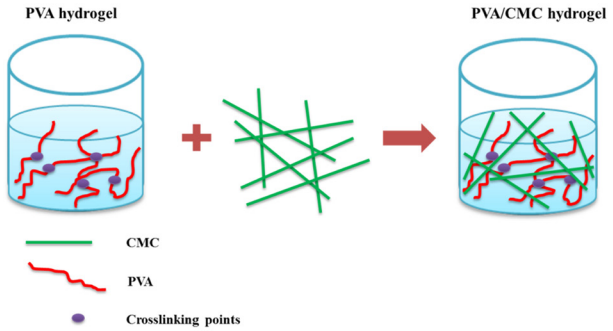


**Fig. 6.** Synthesis of PVA/CMC hydrogels.

Due to the continued drug release up to 10 h, the prepared dressing can inhibit the wound site from infection until complete wound healing. Additionally, the inhibition zone of membranes with the loaded drug revealed the effective release of the drug in the medium and inhibition of the growth of the microorganisms. Therefore, this dressing system could be employed for developing antibacterial wound dressing.

*5.3. Application in agriculture*

Blend films have the potential to be utilized as coating materials for controlling the fertilizer release. However, due to nonbiodegradability and high poison content, some blend films might produce serious soil pollution. Therefore, development of films with biodegradability, innocuity, and low price is critical for the production of coated fertilizers [39].

CMC/PVA blend films were produced by a cross-linking reaction between CMC and PVA for the potential application as coating materials. The results indicated that the prepared CMC/PVA films possessed a smooth surface. The reduction of water permeability and absorbency of the blend films was observed by the increment of the PVA content. As a result of the good biodegradability of the CMC/PVA blend films, they can be considered as potential coating materials for the control-release fertilizer [39].

For efficient fertilizer and water management, Ozen et al. [90] coated nonwoven fabrics with potassium nitrate/CMC. The fabrics were pre-coated with PVA and the cross-linking with CMC was carried out using citric acid. According to the results, the PVA pre-coating and the subsequent cross-linking of CMC led to the provision of a synergistic effect for a considerable enhancement of fertilizer release management and moisture. Obtaining a controlled release of fertilizer with an improvement in water absorption/retention behavior is an outstanding step forward in the efficient sustainable agriculture field.

## 6. Conclusions and future insights

In this study, the recent findings of the properties and applications of PVA/CMC composites and blends including drug delivery, food packaging, and agriculture were reviewed. These novel composites have great potential for the active packaging of food products. Moreover, they show enhanced water solubility leading to improved bioavailability and dissolution for wound healing. These properties make them the promising materials for hydrogel production to deliver drug and moisture to the wound site. In addition, these composites can be utilized in agriculture for the controlled release of fertilizer.

PVA/CMC composites are gaining great attention in biomedical applications due to offering various advantages in different fields. Their properties can be tailored by controlling their structures to enhance their properties for various applications. The PVA/CMC hydrogels as wound dressings act as barriers to microorganisms while retaining their permea-

bility to oxygen. Thus, these attractive composites can be promising materials for drug delivery and wound dressing application and the incorporation of other reinforcement or components might be investigated for the improvement of the properties as well as new production methods. They can also be useful for producing masks to protect against coronavirus. Therefore, further well-designed studies will be required for the development and enhancement of these effective materials.

REFERENCES

[1] L. Bazli, A. Khavandi, M.A. Boutorabi, M. Karrabi, Correlation between viscoelastic behavior and morphology of nanocomposites based on SR/EPDM blends compatibilized by maleic anhydride, Polymer 113 (2017) 156-166.
[2] L. Bazli, A. Khavandi, M.A. Boutorabi, M. Karrabi, Morphology and viscoelastic behavior of silicone rubber/EPDM/Cloisite 15A nanocomposites based on Maxwell model, Iranian Polymer Journal 25(11) (2016) 907-918.
[3] X. Dang, H. Yuan, Z. Shan, An eco-friendly material based on graft copolymer of gelatin extracted from leather solid waste for potential application in chemical sand-fixation, Journal of Cleaner Production 188 (2018) 416-424.
[4] X. Li, S. Cai, X. Hu, X. He, Thermosensitive self-assembled behavior of poly (acrylamide-co-acrylonitrile)/polystyrene triblock copolymer and application in drug loading, International Journal of Polymeric Materials and Polymeric Biomaterials (2020) 1-10.
[5] P. Li, Z. Luo, X. Li, R. Wang, H. Chen, Y. Zhao, J. Wang, N. Huang, Preparation, evaluation and functionalization of biomimetic block copolymer coatings for potential applications in cardiovascular implants, Applied Surface Science 502 (2020) 144085.
[6] Z. Wang, J. Li, Y. Liu, J. Luo, Synthesis and characterizations of zwitterionic copolymer hydrogels with excellent lubrication behavior, Tribology International 143 (2020) 106026.
[7] R. Liu, Y. Sun, H. Gu, X. Zhou, Synthesis and application of acrylate copolymer as high ink-absorption and fast drying coating agent for polyester fabric, Progress in Organic Coatings 136 (2019) 105298.
[8] C.G. Park, S.H. Park, Y. Kim, T.L. Nguyen, H.Y. Woo, H. Kang, H.J. Yoon, S. Park, M.J. Cho, D.H. Choi, Facile one-pot polymerization of a fully conjugated donor–acceptor block copolymer and its application in efficient single component polymer solar cells, Journal of Materials Chemistry A 7(37) (2019) 21280-21289.
[9] A.M. El Sayed, Synthesis and controlling the optical and dielectric properties of CMC/PVA blend via γ-rays irradiation, Nuclear Instruments and Methods in Physics Research Section B: Beam Interactions with Materials and Atoms 321 (2014) 41-48.
[10] L. Bazli, M.H. Bagherian, M. Karrabi, F. Abbassi-Sourki, H. Azizi, Effect of starch ratio and compatibilization on the viscoelastic behavior of POE/starch blends, Journal of Applied Polymer Science 137(29) (2020) 48877.
[11] S. Rahimi, F. SharifianJazi, A. Esmaeilkhanian, M. Moradi, A.H. Safi Samghabadi, Effect of $SiO_2$ content on Y-TZP/$Al_2O_3$ ceramic-nanocomposite properties as potential dental applications, Ceramics International 46(8, Part A) (2020) 10910-10916.
[12] M. Alizadeh, M.H. Paydar, F. Sharifian Jazi, Structural evaluation and mechanical properties of nanostructured Al/$B_4C$ composite fabricated by ARB process, Composites Part B: Engineering 44(1) (2013) 339-343.
[13] E. Sharifi Sedeh, S. Mirdamadi, F. Sharifianjazi, M. Tahriri, Synthesis and Evaluation of Mechanical and Biological Properties of Scaffold Prepared From Ti and Mg With Different Volume Percent, Synthesis and Reactivity in Inorganic, Metal-Organic, and Nano-Metal Chemistry 45(7) (2015) 1087-1091.
[14] H. Ashrafi, M. Bazli, A. Vatani Oskouei, L. Bazli, Effect of Sequential Exposure to UV Radiation and Water Vapor Condensation and Extreme Temperatures on the Mechanical Properties of GFRP Bars, Journal of Composites for Construction 22(1) (2018) 04017047.
[15] A.M. El Sayed, S. El-Gamal, W.M. Morsi, G. Mohammed, Effect of PVA and copper oxide nanoparticles on the structural, optical, and electrical properties of carboxymethyl cellulose films, Journal of Materials Science 50(13) (2015) 4717-4728.
[16] C.C. Thong, D.C.L. Teo, C.K. Ng, Application of polyvinyl alcohol (PVA) in cement-based composite materials: A review of its engineering properties and microstructure behavior, Construction and Building Materials 107 (2016) 172-180.
[17] A. Nawaz, I.A. Hümmelgen, Poly(vinyl alcohol) gate dielectric in organic field-effect transistors, Journal of Materials Science: Materials in Electronics 30(6) (2019) 5299-5326.
[18] M. Said, A.A. Abd El-Azim, M.M. Ali, H. El-Ghazaly, I. Shaaban, Effect of elevated temperature on axially and eccentrically loaded columns containing Polyvinyl Alcohol (PVA) fibers, Engineering Structures 204 (2020) 110065.
[19] A. Krainiukov, J. Liu, E. Kravchenko, D. Chang, Performance of silty sand reinforced with aqueous solution of polyvinyl alcohol subjected to freeze-thaw cycles, Cold Regions Science and Technology 174 (2020) 103054.
[20] S. Xu, M.A. Malik, Z. Qi, B. Huang, Q. Li, M. Sarkar, Influence of the PVA fibers and $SiO_2$ NPs on the structural properties of fly ash based sustainable geopolymer, Construction and Building Materials 164 (2018) 238-245.
[21] Y. Tang, D. Zhou, J. Zhang, Novel polyvinyl alcohol/styrene butadiene rubber latex/carboxymethyl cellulose nanocomposites reinforced with modified halloysite nanotubes, Journal of Nanomaterials 2013 (2013).
[22] X. Tong, J. Huang, J. Mei, J. Ge, L. Han, G. Huang, Characterization of Controlled Release Fertilizer by Infrared Microspectroscopy, Analytical Letters 51(14) (2018) 2252-2270.
[23] L. Yi, Y. Zhang, X. Shi, X. Du, X. Wang, A. Yu, G. Zhai, Recent progress of functionalised graphene oxide in cancer therapy, Journal of Drug Targeting 27(2) (2019) 125-144.
[24] O.M. Abdallah, K.Z. El-Baghdady, M.M.H. Khalil, M.I. El Borhamy, G.A. Meligi, Antibacterial, antibiofilm and cytotoxic activities of biogenic polyvinyl alcohol-silver and chitosan-silver nanocomposites, Journal of Polymer Research 27(3) (2020) 74.
[25] W. Ma, T. Li, Q. Zhang, J. Zhong, H. Matsuyama, Preparation of hybrid membranes by incorporating hydrophilic UiO-66 nanoparticles for high-performance pervaporation dehydration of aprotic solvents, Journal of Nanoparticle Research 22(3) (2020) 64.
[26] Y. Yang, Y. Zhao, J. Liu, Z. Nie, J. Ma, M. Hua, Y. Zhang, X. Cai, X. He, Flexible and Transparent High-Dielectric-Constant Polymer Films Based on Molecular Ferroelectric-Modified Poly(Vinyl Alcohol), ACS Materials Letters (2020) 453-460.
[27] Y. Xie, X. Lin, H. Li, T. Ji, Effect of polyvinyl alcohol powder on the bonding mechanism of a new magnesium phosphate cement mortar, Construction and Building Materials 239 (2020) 117871.
[28] Reena, A. Kumar, V. Mahto, A.K. Choubey, Synthesis and characterization of cross-linked hydrogels using polyvinyl alcohol and polyvinyl pyrrolidone and their blend for water shut-off treatments, Journal of Molecular Liquids 301 (2020) 112472.
[29] M. Hashmi, S. Ullah, I.S. Kim, Electrospun Momordica Charantia Incorporated Polyvinyl Alcohol (PVA) Nanofibers for Antibacterial Applications, Materials Today Communications (2020) 101161.
[30] S. Liu, L. Wang, X. Wang, L. Liu, A. Zhou, X. Cao, Preparation, mechanical and thermal characteristics of d-$Ti_3C_2$/PVA film, Materials Today Communications 22 (2020) 100799.
[31] E. Yan, J. Jiang, X. Yang, L. Fan, Y. Wang, Q. An, Z. Zhang, B. Lu, D. Wang, D. Zhang, pH-sensitive core-shell electrospun nanofibers based on polyvinyl alcohol/polycaprolactone as a potential drug delivery system for the chemotherapy against cervical cancer, Journal of Drug Delivery Science and Technology 55 (2020) 101455.
[32] A. Kumar, H. Kaur, Sprayed in-situ synthesis of polyvinyl alcohol/chitosan loaded silver nanocomposite hydrogel for improved antibacterial effects, International Journal of Biological Macromolecules 145 (2020) 950-964.
[33] R. Ahmed, A. Ibrahim, E. El-Said, Enhancing the Optical Properties of Polyvinyl Alcohol by Blending It with Polyethylene Glycol, Acta Physica Polonica, A. 137(3) (2020).
[34] K. Prusty, S.K. Swain, Nano $ZrO_2$ reinforced cellulose incorporated polyethylmethacrylate/polyvinyl alcohol composite films as semiconducting packaging materials, Journal of Applied Polymer Science n/a(n/a) (2020) 49284.
[35] R.S. Rana, S. Rana, A. Nigrawal, B. kumar, A. kumar, Preparation and mechanical properties evaluation of polyvinyl alcohol and banana fibres composite, Materials Today: Proceedings (2020).
[36] B. Merz, C. Capello, G.C. Leandro, D.E. Moritz, A.R. Monteiro, G.A. Valencia, A novel colorimetric indicator film based on chitosan, polyvinyl alcohol and anthocyanins from jambolan (Syzygium cumini) fruit for monitoring shrimp freshness, International Journal of Biological Macromolecules 153 (2020) 625-632.
[37] M. Afshar, G. Dini, S. Vaezifar, M. Mehdikhani, B. Movahedi, Preparation and characterization of sodium alginate/polyvinyl alcohol hydrogel containing drug-loaded chitosan nanoparticles as a drug delivery system, Journal of Drug Delivery Science and Technology 56 (2020) 101530.
[38] N. Hendrawati, K. Sa'diyah, E. Novika, A.A. Wibowo, The effect of polyvinyl alcohol (PVOH) addition on biodegradable foam production from sago starch, AIP Conference Proceedings 2197(1) (2020) 050008.
[39] L. Zhang, G. Zhang, J. Lu, H. Liang, Preparation and Characterization of Carboxymethyl Cellulose/Polyvinyl Alcohol Blend Film as a Potential Coating Material, Polymer-Plastics Technology and Engineering 52(2) (2013) 163-167.
[40] H. Zhang, J. Zhang, The preparation of novel polyvinyl alcohol (PVA)-based

nanoparticle/carbon nanotubes (PNP/CNTs) aerogel for solvents adsorption application, Journal of Colloid and Interface Science 569 (2020) 254-266.
[41] O.F. Nwabor, S. Sudarshan, S. Paosen, K. Vongkamjan, S.P. Voravuthikunchai, Enhancing food shelf life with polyvinyl alcohol-chitosan polymer nanocomposite films from bioactive Eucalyptus leaf extracts, Food Bioscience (2020) 100609.
[42] F. Reguieg, L. Ricci, N. Bouyacoub, M. Belbachir, M. Bertoldo, Thermal characterization by DSC and TGA analyses of PVA hydrogels with organic and sodium MMT, Polymer Bulletin 77(2) (2020) 929-948.
[43] H.Q. Li, X.J. Liu, H. Wang, H. Yang, Z. Wang, J. He, Proton exchange membranes with cross-linked interpenetrating network of sulfonated polyvinyl alcohol and poly(2-acrylamido-2-methyl-1-propanesulfonic acid): Excellent relative selectivity, Journal of Membrane Science 595 (2020) 117511.
[44] B.H. Musa, N.J. Hameed, Study of the mechanical properties of polyvinyl alcohol/starch blends, Materials Today: Proceedings 20 (2020) 439-442.
[45] D.N. Iqbal, M. Tariq, S.M. Khan, N. Gull, S. Sagar Iqbal, A. Aziz, A. Nazir, M. Iqbal, Synthesis and characterization of chitosan and guar gum based ternary blends with polyvinyl alcohol, International Journal of Biological Macromolecules 143 (2020) 546-554.
[46] D. Nataraj, R. Reddy, N. Reddy, Crosslinking electrospun poly (vinyl) alcohol fibers with citric acid to impart aqueous stability for medical applications, European Polymer Journal 124 (2020) 109484.
[47] M.N. Pervez, G.K. Stylios, Y. Liang, F. Ouyang, Y. Cai, Low-temperature synthesis of novel polyvinylalcohol (PVA) nanofibrous membranes for catalytic dye degradation, Journal of Cleaner Production 262 (2020) 121301.
[48] M.H. El-Newehy, M.E. El-Naggar, S. Alotaiby, H. El-Hamshary, M. Moydeen, S. Al-Deyab, Preparation of biocompatible system based on electrospun CMC/PVA nanofibers as controlled release carrier of diclofenac sodium, Journal of Macromolecular Science, Part A 53(9) (2016) 566-573.
[49] S.R. Muppalla, S.R. Kanatt, S.P. Chawla, A. Sharma, Carboxymethyl cellulose–polyvinyl alcohol films with clove oil for active packaging of ground chicken meat, Food Packaging and Shelf Life 2(2) (2014) 51-58.
[50] E.O.M. Osman, Synthesis and Improvement of Degree of Substitution and Characterization of Carboxymethylcellulose from Cotton Fuzz, Sudan University of Science and Technology, 2016.
[51] A. Pettignano, A. Charlot, E. Fleury, Solvent-Free Synthesis of Amidated Carboxymethyl Cellulose Derivatives: Effect on the Thermal Properties, Polymers 11(7) (2019).
[52] M.F.A. Taleb, H.L.A. El-Mohdy, H.A.A. El-Rehim, Radiation preparation of PVA/CMC copolymers and their application in removal of dyes, Journal of Hazardous Materials 168(1) (2009) 68-75.
[53] N.F. Mazuki, A.P.P. Abdul Majeed, Y. Nagao, A.S. Samsudin, Studies on ionics conduction properties of modification CMC-PVA based polymer blend electrolytes via impedance approach, Polymer Testing 81 (2020) 106234.
[54] M.M. Pérez-Madrigal, M.G. Edo, M.G. Saborío, F. Estrany, C. Alemán, Pastes and hydrogels from carboxymethyl cellulose sodium salt as supporting electrolyte of solid electrochemical supercapacitors, Carbohydrate Polymers 200 (2018) 456-467.
[55] D. Duquette, M.-J. Dumont, Comparative studies of chemical crosslinking reactions and applications of bio-based hydrogels, Polymer Bulletin 76(5) (2019) 2683-2710.
[56] K. Suppiah, P.L. Teh, S. Husseinsyah, R. Rahman, Properties and characterization of carboxymethyl cellulose/halloysite nanotube bio-nanocomposite films: Effect of sodium dodecyl sulfate, Polymer Bulletin 76(1) (2019) 365-386.
[57] Y. Zahedi, B. Fathi-Achachlouei, A.R. Yousefi, Physical and mechanical properties of hybrid montmorillonite/zinc oxide reinforced carboxymethyl cellulose nanocomposites, International Journal of Biological Macromolecules 108 (2018) 863-873.
[58] D.G. Prajapati, B. Kandasubramanian, Biodegradable Polymeric Solid Framework-Based Organic Phase-Change Materials for Thermal Energy Storage, Industrial & Engineering Chemistry Research 58(25) (2019) 10652-10677.
[59] N. Hasirci, C. Kilic, A. Kömez, G. Bahcecioglu, V. Hasirci, Hydrogels in Regenerative Medicine, Gels Handbook, WORLD SCIENTIFIC2016, pp. 1-52.
[60] K. Kozłowicz, S. Nazarewicz, D. Góral, A. Krawczuk, M. Domin, Lyophilized Protein Structures as an Alternative Biodegradable Material for Food Packaging, Sustainability 11(24) (2019).
[61] J. Ampaiwong, P. Rattanawaleedirojn, K. Saengkiettiyut, N. Rodthongkum, P. Potiyaraj, N. Soatthiyanon, Reduced Graphene Oxide/Carboxymethyl Cellulose Nanocomposites: Novel Conductive Films, Journal of Nanoscience and Nanotechnology 19(6) (2019) 3544-3550.
[62] C. Xiang, C. Wang, R. Guo, J. Lan, S. Lin, S. Jiang, X. Lai, Y. Zhang, H. Xiao, Synthesis of carboxymethyl cellulose-reduced graphene oxide aerogel for efficient removal of organic liquids and dyes, Journal of Materials Science 54(2) (2019) 1872-1883.
[63] S.C. Daminabo, S. Goel, S.A. Grammatikos, H.Y. Nezhad, V.K. Thakur, Fused deposition modeling-based additive manufacturing (3D printing): techniques for polymer material systems, Materials Today Chemistry 16 (2020) 100248.
[64] H. Dai, Y. Huang, H. Huang, Eco-friendly polyvinyl alcohol/carboxymethyl cellulose hydrogels reinforced with graphene oxide and bentonite for enhanced adsorption of methylene blue, Carbohydrate Polymers 185 (2018) 1-11.
[65] M.A. Saadiah, A.S. Samsudin, Electrical study on Carboxymethyl Cellulose-Polyvinyl alcohol based bio-polymer blend electrolytes, IOP Conference Series: Materials Science and Engineering 342 (2018) 012045.
[66] W.F. Su, Principles of Polymer Design and Synthesis, Springer Berlin Heidelberg2013.
[67] M.T. Taghizadeh, N. Sabouri, B. Ghanbarzadeh, Mechanochemical activation of carboxy methyl cellulose and its thermoplastic polyvinyl alcohol/starch biocomposites with enhanced physicochemical properties, International Journal of Biochemistry and Biophysics 1(1) (2013) 9-15.
[68] J. Miao, R. Zhang, R. Bai, Poly (vinyl alcohol)/carboxymethyl cellulose sodium blend composite nanofiltration membranes developed via interfacial polymerization, Journal of Membrane Science 493 (2015) 654-663.
[69] B. Tajeddin, N. Ramedani, Preparation and Characterization (Mechanical and Water Absorption Properties) of CMC/PVA/Clay Nanocomposite Films, Iranian Journal of Chemistry and Chemical Engineering (IJCCE) 35(3) (2016) 9-15.
[70] J. Zhu, Q. Li, Y. Che, X. Liu, C. Dong, X. Chen, C. Wang, Effect of $Na_2CO_3$ on the Microstructure and Macroscopic Properties and Mechanism Analysis of PVA/CMC Composite Film, Polymers 12(2) (2020) 453.
[71] A. Kazemzadeh, H. Kazemzadeh, L. Bazli, Determination of Hg2+ by Diphenylcarbazone Compound in Polymer Film, Composites and Compounds 1(1) (2019).
[72] L.-Y. Wang, M.-J. Wang, Removal of heavy metal ions by poly (vinyl alcohol) and carboxymethyl cellulose composite hydrogels prepared by a freeze–thaw method, ACS Sustainable Chemistry & Engineering 4(5) (2016) 2830-2837.
[73] M.M. Abutalib, Effect of zinc oxide nanorods on the structural, thermal, dielectric and electrical properties of polyvinyl alcohol/carboxymethyle cellulose composites, Physica B: Condensed Matter 557 (2019) 108-116.
[74] A. Goswami, A.K. Bajpai, J. Bajpai, B.K. Sinha, Designing vanadium pentoxide-carboxymethyl cellulose/polyvinyl alcohol-based bionanocomposite films and study of their structure, topography, mechanical, electrical and optical behavior, Polymer Bulletin 75(2) (2018) 781-807.
[75] S.A. Oleyaei, H. Almasi, B. Ghanbarzadeh, A.A. Moayedi, Synergistic reinforcing effect of $TiO_2$ and montmorillonite on potato starch nanocomposite films: Thermal, mechanical and barrier properties, Carbohydrate Polymers 152 (2016) 253-262.
[76] H. Fasihi, M. Fazilati, M. Hashemi, N. Noshirvani, Novel carboxymethyl cellulose-polyvinyl alcohol blend films stabilized by Pickering emulsion incorporation method, Carbohydrate Polymers 167 (2017) 79-89.
[77] D. Jeong, S.-W. Joo, Y. Hu, V.V. Shinde, E. Cho, S. Jung, Carboxymethyl cellulose-based superabsorbent hydrogels containing carboxymehtyl β-cyclodextrin for enhanced mechanical strength and effective drug delivery, European Polymer Journal 105 (2018) 17-25.
[78] S. Villarruel, L. Giannuzzi, S. Rivero, A. Pinotti, Changes induced by UV radiation in the presence of sodium benzoate in films formulated with polyvinyl alcohol and carboxymethyl cellulose, Materials Science and Engineering: C 56 (2015) 545-554.
[79] E. Asadi, A. Fassadi Chimeh, S. Hosseini, S. Rahimi, B. Sarkhosh, L. Bazli, R. Bashiri, A.H. Vakili Tahmorsati, A Review of Clinical Applications of Graphene Quantum Dot-based Composites, Composites and Compounds 1(1) (2019).
[80] M. Radmansouri, E. Bahmani, E. Sarikhani, K. Rahmani, F. Sharifianjazi, M. Irani, Doxorubicin hydrochloride-Loaded electrospun chitosan/cobalt ferrite/titanium oxide nanofibers for hyperthermic tumor cell treatment and controlled drug release, International journal of biological macromolecules 116 (2018) 378-384.
[81] M.S.N. Shahrbabak, F. Sharifianjazi, D. Rahban, A. Salimi, A comparative investigation on bioactivity and antibacterial properties of sol-gel derived 58S bioactive glass substituted by Ag and Zn, Silicon 11(6) (2019) 2741-2751.
[82] A. Moghanian, A. Ghorbanoghli, M. Kazem-Rostami, A. Pazhouheshgar, E. Salari, M. Saghafi Yazdi, T. Alimardani, H. Jahani, F. Sharifian Jazi, M. Tahriri, Novel antibacterial Cu/Mg-substituted 58S-bioglass: Synthesis, characterization and investigation of in vitro bioactivity, International Journal of Applied Glass Science (2019).
[83] J. Daraei, Production and characterization of PCL (Polycaprolactone) coated TCP/nanoBG composite scaffolds by sponge foam method for orthopedic applications, Journal of Composites and Compounds 1(1) (2020).

[84] P. Abasian, M. Radmansouri, M.H. Jouybari, M.V. Ghasemi, A. Mohammadi, M. Irani, F.S. Jazi, Incorporation of magnetic NaX zeolite/DOX into the PLA/chitosan nanofibers for sustained release of doxorubicin against carcinoma cells death in vitro, International journal of biological macromolecules 121 (2019) 398-406.
[85] H. Won Jang, A. Zareidoost, M. Moradi, A. Abuchenari, A. Bakhtiari, R. Pouriamanesh, B. Malekpouri, A. Jafari Rad, Photosensitive nanocomposites: environmental and biological applications, Journal of Composites and Compounds 1(1) (2020).
[86] V.S. Ghorpade, R.J. Dias, K.K. Mali, S.I. Mulla, Citric acid crosslinked carboxymethylcellulose-polyvinyl alcohol hydrogel films for extended release of water soluble basic drugs, Journal of Drug Delivery Science and Technology 52 (2019) 421-430.
[87] R. Agarwal, M.S. Alam, B. Gupta, Polyvinyl alcohol-polyethylene oxide-carboxymethyl cellulose membranes for drug delivery, Journal of Applied Polymer Science 129(6) (2013) 3728-3736.
[88] R.N. Oliveira, A.P.D. Moreira, R.M.d.S.M. Thiré, B. Quilty, T.M. Passos, P. Simon, M.C. Mancini, G.B. McGuinness, Absorbent polyvinyl alcohol–sodium carboxymethyl cellulose hydrogels for propolis delivery in wound healing applications, Polymer Engineering & Science 57(11) (2017) 1224-1233.
[89] E.A. Kamoun, E.-R.S. Kenawy, X. Chen, A review on polymeric hydrogel membranes for wound dressing applications: PVA-based hydrogel dressings, Journal of Advanced Research 8(3) (2017) 217-233.
[90] İ. Özen, G. Okyay, A. Ulaş, Coating of nonwovens with potassium nitrate containing carboxymethyl cellulose for efficient water and fertilizer management, Cellulose 25(2) (2018) 1527-1538.

Available online at www.jourcc.com

Journal homepage: www.JOURCC.com

Journal of Composites and Compounds

# Production methods of ceramic-reinforced Al-Li matrix composites: A review

***Kaiqiang Zhang[a], Ho Won Jang[b], Quyet Van Le[c]****

[a] *School of Chemistry and Chemical Engineering, Nanjing University, Nanjing 210023, China*
[b] *Department of Materials Science and Engineering, Seoul National University, Seoul, Republic of Korea*
[c] *Institute of Research and Development, Duy Tan University, Da Nang, 550000, Viet Nam*

A B S T R A C T

Recently, the increasing need for good quality, high performance, and low-cost materials has directed research towards composite materials rather than monolithic materials. In the case of metal matrix composites (MMCs), composites based on aluminum matrix have been widely developed for the automobile and aerospace industry as well as structural applications due to having a low cost, high wear resistance, and high strength to weight ratio. Moreover, a facile and economical method for the production of the composites is a very important factor for expanding their application. Ceramic reinforcements such as graphite, silicon carbide, alumina, and fly ash particulates can be introduced in metal matrices. Moreover, there has been considerable interest in developing Al-Li alloys and composites because of having high specific strength and high specific modulus. The present article has focused on the development of aluminum-lithium alloy composites as well as their production methods.



Peer review under responsibility of jourcc

A R T I C L E I N F O R M A T I O N

*Article history:*
Received 11 June 2020
Received in revised form 19 June 2020
Accepted 28 June 2020

*Keywords:*
MMCs
Al-Li alloy
Al-Li matrix composites
Ceramic reinforcement

Table of contents



## 1. Introduction

Composite materials are composed of two or more separate phases that have sufficient bonding together and exhibit their distinctive characteristics [1, 2]. MMCs are composites containing continuous metallic matrices in which one or more reinforcement components with different concentrations are dispersed [3-10]. By decreasing the size of the reinforcement, a given enhancement of composite properties could be achieved with the incorporation of a smaller amount of the reinforcement [11]. MMCs are categorized based on different factors including the matrix (e.g., titanium, copper aluminum), the reinforcement material (e.g. graphite, $Al_2O_3$, SiC), the shape of reinforcement (e.g., whiskers, particles, fibers), and the manufacturing process (e.g., stir casting, infiltration, diffusion bonding, powder metallurgy). Most metals are duc-

* *Corresponding author: Quyet Van Le; E-mail: levanquyet@dtu.edu.vn*
https://doi.org/10.29252/jcc.2.2.3 

tile, exhibit high thermal and electrical conductivity, while ceramics are brittle, conductivity. However, most ceramics exhibit high stiffness and stability even at high temperatures, while most metallic materials have limited service life even at moderate temperatures. At high temperatures, microstructural changes and deterioration of mechanical properties occur in metals. The most common type of MMCs is the incorporation of ceramics in metallic matrices. Ceramic reinforced metal composites are expected to possess distinct benefits over mono-phased metals and their alloys. MMCs benefit from ductility and toughness of metallic matrix and high-temperature stability, stiffness, and low thermal expansion of the ceramic reinforcements to meet the required properties for applications in which both metals and ceramics would fail independently [9, 10, 12-15].

Various metals and metal alloys can be utilized as a matrix for the fabrication of MMCs. The main factor that determines a proper material as the matrix is the requirements of a specific application [16]. Nickel, copper, cobalt, magnesium, titanium, aluminum, silver, and their alloys are among common matrix materials [5, 17, 18]. As a result of improved stiffness, enhanced strength, wear resistance, improved abrasion, and reduced density, aluminum matrix composites (AMCs) are better candidates compared to existing materials employed for functional and structural applications [19, 20]. Recently, Al-Li alloy has attracted the researchers' attention due to its good wettability properties. Because of providing good strength and bonding in MMCs, metal alloys are preferred as the matrix materials instead of metals [21]. Li is a lightweight metal with a density of 0.54 g/cm$^3$, which is highly soluble in aluminum, and by adding 1% of this metal, the density of the aluminum alloy decreases by 3%. Additionally, amongst all soluble metals in Al, the addition of 1% of Li leads to 6% increase in the elastic modulus. The other advantage of Al-Li alloys is that they respond to age hardening [22].

The performance limits of Al-Li alloys, such as Al-8090, are significantly improved by the incorporation of ceramic particles as reinforcements [23]. Aluminum oxide ($Al_2O_3$) and silicon carbide (SiC) are prevalent reinforcements used in these alloys. The addition of SiC as a reinforcement leads to the increase in wear resistance, hardness, the tensile strength, and density of Al and its alloys [24]. Different methods can be used to prepare different types of MMCs including in-situ fabrication techniques, liquid-state methods, solid-state methods, and semisolid-state methods. Fig. 1 illustrates different preparation methods of MMCs [25].

## 2. Aluminum matrix composites

Copper, cobalt, magnesium, titanium, aluminum, and their alloys are common matrix metals in MMCs. Generally, the metal matrices are reinforced by brittle ceramic material, such as SiC, $B_4C$, and more recently, TiC [26-28]. Al matrix composites (AMCs) consist of the pure Al or its alloys reinforced with a non-metallic ceramic material including AlN, $B_4C$, $SiO_2$, SiC, and $Al_2O_3$. Because of good thermal and electrical conductivities, high damping capacity, low density, and good corrosion resistance, Al alloys are more prevalent than the pure metal. AMCs have shown promising properties to be used in various engineering divisions such as structural and functional applications. Depending on the chemical composition of the Al matrix and reinforcement proportion, various mechanical properties could be achieved. Among AMCs, those reinforced by particulates are attracting researchers due to their relatively low cost and isotropic properties [10].

Mazaheri et al. [29] fabricated Al-$B_4C$, Al-TiC-$B_4C$, and Al-TiC hybrid composites and compared their mechanical properties. According to the results, Al/TiC/$B_4C$ composite exhibited the highest hardness, Al-$B_4C$ composite exhibited the highest tensile and yield strength, and maximum elongation was obtained for Al-TiC composite. A359/$Al_2O_3$ composite was developed using the electromagnetic stir casting process by Kumar et al. [30]. They reported an increase in the hardness values from 46 HRC for pure alloy to 72.8 HRC. Additionally, they reported the tensile strength of 103.7 N/mm$^2$ and 148.7 N/mm$^2$ for the pure alloy and the composite, respectively. Akbari et al. [31] reinforced A356 alloy with milled nano $Al_2O_3$ and Al particles and with Cu particles and nano $Al_2O_3$. The results demonstrated that ultimate tensile strength and compressive strength of the prepared composites were superior to the pure alloy. The enhancement of mechanical properties was more significant for the Al/$Al_2O_3$/Cu composite. The mechanical properties of the AL7075-$B_4C$ composite were studied by Baradeswarn et al. [32]. It was shown that the hardness, compressive strength, and ultimate tensile strength of the synthesized composite increased with an increase in a volume percentage of the reinforcement. In other research, Selvam et al. [33] reinforced 6061 aluminum alloy with SiC and Fly Ash by stir casting and evaluated its mechanical properties. With the increase in the proportion of the SiC particles, tensile strength, and macro hardness of the composite were enhanced.

## 3. Aluminum-lithium alloys

Due to excellent characteristics including corrosion resistance, low density, high toughness, and good strength, Al alloys are employed in important applications of aerospace field. The commonly used alloys in these applications are Al-Zn-Mg-Cu and Al-Cu-Mg alloys, which have the capability of precipitation hardening. One of the most important aluminum alloys with precipitation hardening ability is Al-Li alloys. Adding a primary alloying element of Li to Al reduces the density and improves

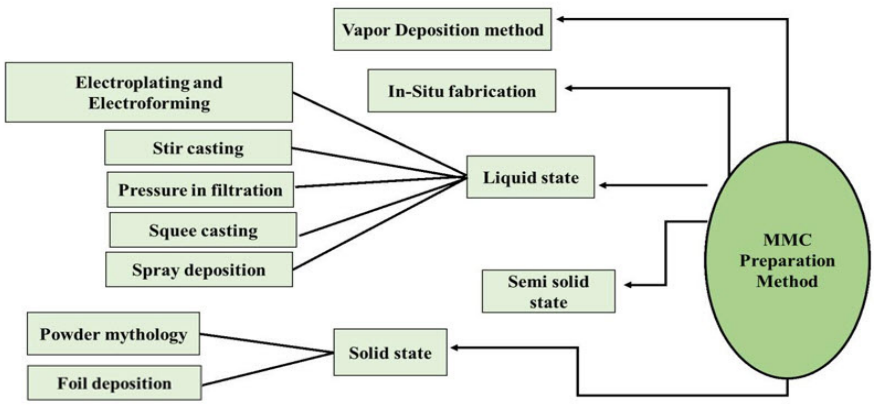


**Fig. 1.** MMCs preparation methods.

the elastic modulus of the alloy. Therefore, the major application of this development has been the aerospace industry. Similar to Al-Zn-Mg-Cu and Al-Cu-Mg alloys, Al-Li alloys have precipitation hardening ability. However, the incorporated precipitation hardening mechanism of these alloys is far more complicated than that of conventional Al alloys [34]. Although Al alloys offer good properties for various applications, improving one property in aluminum alloys usually is at the expense of degrading another property. For instance, the improvement of an alloy strength without a decrease in the toughness is challenging. Due to the possibility of cold work after solutionizing and thermal treatments after cold working, the Al-Li alloys could achieve enhanced combinations of properties [35]. The addition of Li to Al leads to a reduction of density by 3 % per 1 wt% and an increase in the elastic modulus by 6 % per 1 wt%. A combination of characteristics including increased specific stiffness, specific strength, good cryogenic, and fatigue properties provide the possibility for Al-Li alloys to be used in aerospace structural applications such as the external tank of Space Shuttle and fuel tanks of launch vehicles [36-38]. The first attempts to develop Al-Li alloys began in early 1920 [39]. AA2020 with the composition of Al-1.1Li-4.5Cu-0.5Mn-0.2Cd was the first commercial alloy, which was introduced in 1958. AA2020 was utilized for the Northrop RA-5C Vigilante aircraft tails and wing skins, however, it was withdrawn in the 1960s due to concerns about its fracture toughness. During this time, research attempts in the former Soviet Union resulted in the fabrication of the 1420 alloy (Al-2.0Li-5.3 Mg-0.5Mn) and VAD-23 (Al–1.1Li-5.3Cu-0.6Mn-0.17Cd). These three alloys were the first generation of these aluminum-lithium alloys. The concerns about the potential threat arouse from the replacement of Al alloys by composites reinforced with carbon fibers led to research work on novel Al–Li alloys in the 1970s. However, the development of the second generation of aluminum-lithium alloys was unsuccessful due to thermal instability, low short transverse properties, and unacceptable degrees of property anisotropy. Working on the third generation alloys based on aluminum-lithium commenced in the late 1980s, and developments continued. These recently developed Al-Li alloys are promising alloys to replace common Al alloys used in aerospace structures [40]. The most effective way used to reduce the structural weight of aircraft is by decreasing the density of materials. Lithium is one of the handful of elements that is highly soluble in Al with a low density of 0.54 g/cm$^3$. The reduction of density is significant, as adding each 1% of this element leads to the reduction of Al density by 3%. The other superiority of Li over the more soluble alloying elements in Al is that it results in a remarkable enhancement in the elastic modulus. Age hardening response is additional advantage of Al-Li alloys [22]. Yuan et al. [41] investigated the influence of thermomechanical and normal heat treatments on the fracture toughness and mechanical properties of a new generation of aluminum-lithium alloy (2A97). They aimed to enhance the relationships of fracture toughness, ductility, and strength to make them proper candidates for applications in the aeronautical industries.

The primary attempt of the Al-Li 2A97 alloy was to be used for forgings and plates employed as aerospace material. However, this alloy has some problems such as yielding low fracture toughness and ductility in T8 temper while possessing high tensile strength, and yielding a fracture toughness and high ductility in T6 temper while having low strength. Investigations revealed that the fracture toughness and ductility were enhanced in this alloy by 4% deformation after under aging at low temperatures [41].

## 4. Fabrication of ceramic-reinforced Al-Li matrix composites

### *4.1 Liquid-state processes*

There are different methods for the development of MMCs using liquid state processes [25]. Using a liquid route, metals with relatively low melting temperatures, such as Al and its alloys, could be easily incorporated as a matrix material. By processes in the liquid state, including stir casting, and squeeze casting, greater freedom in the design of components and manufacturing can be provided [14].

#### *4.1.1. Liquid infiltration*

In the liquid infiltration process, a fiber bundle is infiltrated by molten metal. Due to difficulties related to the wetting of the ceramic phase by the liquid metal, fabrication of MMCs by simple liquid infiltration is not easy. The significant degradation of fiber properties can occur due to reactions between the molten metal and fiber during the infiltration of a fiber preform. To enhance wetting and control the reactions between the phases, fibers can be coated prior to infiltration. However, exposure of the fiber coatings to air must be prevented before the infiltration process to prevent oxidation of the surface and its negative effects [42]. The Duralcan process is a successful commercial liquid infiltration method for reinforcing with particulates. This process is illustrated schematically in Fig. 2. In this process, ingot-grade aluminum and ceramic particulates are mixed and melted. A proprietary treatment is performed on the ceramic particles. The melt is stirred between 600 ˚C and 700 ˚C, a few degrees higher than its melting temperature. The prepared melt is transformed into a rolling ingot, rolling bloom, foundry ingot, or extrusion blank. The particle size of the reinforcement in the Duralcan process is 8–12 mm and very small particles lead to the formation of a very large interface region and the increase in the viscosity of the melt. SiC and $Al_2O_3$ particles are typically utilized in the wrought aluminum alloys and foundry alloys, respectively [43, 44].

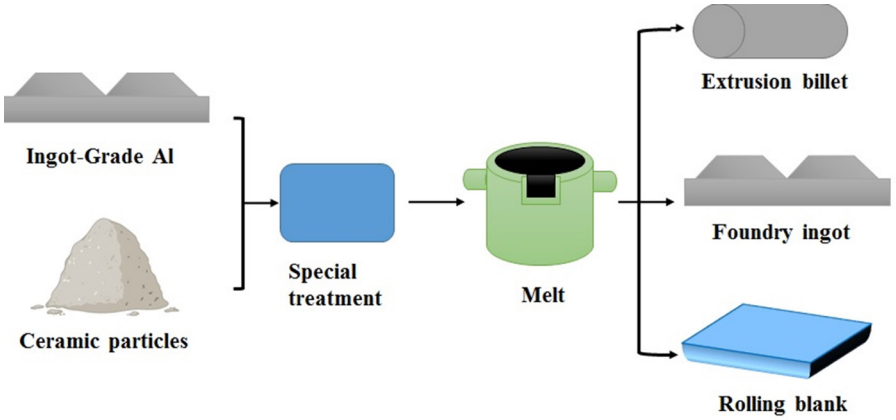


**Fig. 2.** Schematic illustration of Duralcan process.

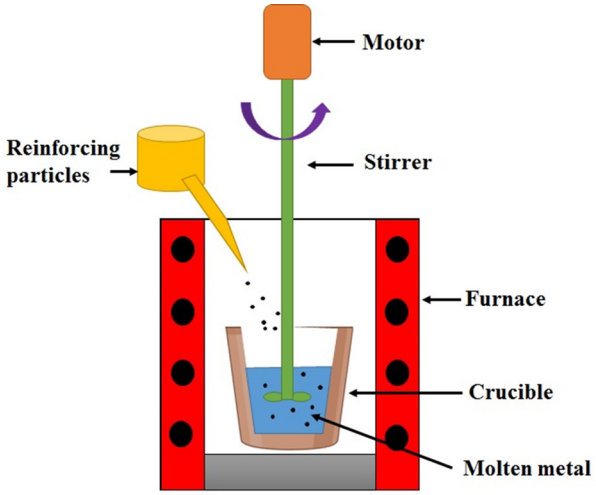


**Fig. 3.** Stir casting process.

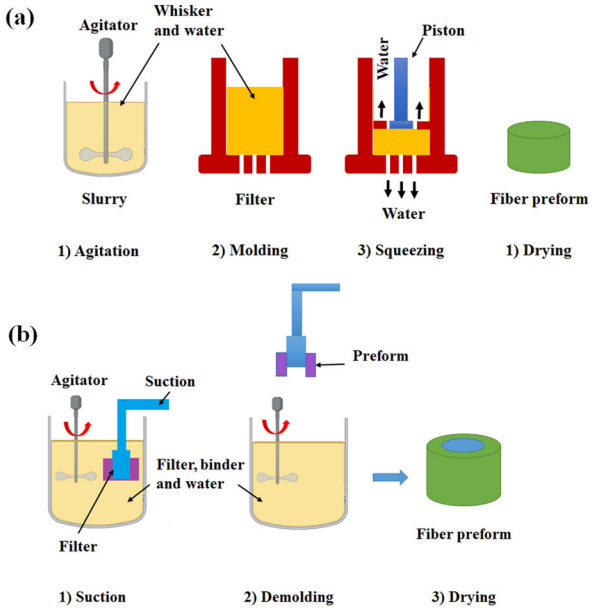


**Fig. 4.** Schematic illustration of fibrous preform fabrication.

*4.1.2. Stir casting*

The stir casting involves the introduction of the reinforcing agent into the molten metal with the help of stirring. Fig. 3 depicts the schematic of the stir casting process. This fabrication method is considered as one of the most cost-effective methods to produce large near-net-shape parts made from MMCs by conventional stirring followed by casting. The most commercially used and the simplest one among other stir casting methods is the vortex technique, in which the pre-treated ceramic particles are introduced in the vortex of molten alloy with the rotating impeller [45, 46].

Bauri et al. [47] fabricated 8090 Al alloy/SiCp composites using the stir casting process. The average size of SiC particles was 40 µm, various contents of SiC were introduced in the composite, and the cast billets were undergone hot extrusion. According to the results, the composites exhibited higher damping capacity compared to the unreinforced alloy. This was reported to be related to the higher interface damping, grain boundary, and dislocation density. Moreover, the moduli of both composites and alloy reduced with the increment of the temperature.

In other research, Bauri et al. [48] prepared Al-Li-$SiC_p$ composites using a modified stir casting technique. The incorporation of the SiC particulates improved the elastic modulus, ultimate tensile strength, hardness, and 0.2% proof stress of the composites with 8% and 12% of SiC. It was proposed that the reduction of the strength of the composite containing 18% of SiC was due to the clustering of the SiC particles.

*4.1.3. Pressure infiltration/squeeze casting*

In the squeeze casting process, which is a pressure infiltration method, the infiltration of a fibrous preform by the molten metal is carried out by applying a force. Fig. 4 depicts two processes used for the fabrication of fibrous preforms. In the press forming method, fibers are well agitated in an aqueous slurry and then poured into a mold followed by squeezing out the water by applied pressure, and finally the preform is dried (Fig. 4 (a)). In the second method, the preform is fabricated by applying suction to an agitated mixture of water, binder, and whisker. The preform then is ejected from the mold and is dried (Fig. 4 (b)) [49]. The squeeze casting technique is schematically presented in Fig. 5. The pressure application continues until the complete solidification of the composite. In this method, good wettability of the preform by the melt is provided using the pressure to force the liquid metal into small pores in the fibrous preform. The advantages of this technique include the absence of prevalent casting defects including shrinkage cavities and porosity and having minimum reaction between the molten metal and reinforcement due to short dwell time at elevated temperature. Squeeze casting as an old method, was developed to produce aluminum alloy components with no pores and fine grains, which have superior properties in comparison with conventional mold casting. This casting method has been employed for the production of aluminum alloys such as silicon-free alloys in pistons of the diesel engine. Obtaining these alloys by conventional methods is difficult [50, 51].

For the fabrication of composites with selective reinforcements, this method of casting has been quite popular. In squeeze casting, a porous fiber preform is firstly located in the die, the melt then is poured into the preheated die. The penetration of molten metal into the preform and bonding with the fibers occur by applying pressure about 70–100 MPa. Another liquid metal infiltration method involves the infiltration of the preform by a pressurized inert gas under the controlled pressure. Complex-shaped structures and higher fractions of fiber volume are achievable by this technique. In this type of molten metal infiltration, the fibrous preform is heated in the die and melting of the matrix alloy is carried out in a crucible in a vacuum. Subsequently, the molten metal, which its temperature is about 100 ˚C higher than its melting temperature, is poured onto the fibrous preform and infiltrates the preform by introducing Ar gas pressure. Generally, some additives are added in the molten metal to assist wetting the fibers [52].

Dong et al. [53] fabricated a composite of $SiC_w$ and Al-Li-Cu-Mg-Zr alloy using the squeeze casting technique and investigated its age-hardening behavior. According to the results, the prepared composite showed an accelerated hardening response in comparison with pure matrix alloy at 130, 160, 190, and 220 °C. The hardening behavior of the composite was greatly influenced by the aging temperature. They exhibited that the incorporation of SiC whiskers to the alloy could accelerate the growth rate of δ´ ($Al_3Li$) phase, which resulted in the nucleation of S´ ($Al_2CuMg$) phase in earlier stages. They proposed that the enhanced age hardening of the composite was due to accelerated precipitation of S´ and δ´.

In other research conducted by Dong et al. [54] incorporated $SiC_w$ in Al-Li and Al-Li-Cu-Mg-Zr alloys by squeeze casting method and studied their tensile deformation microstructure. Based on the results, a considerable suppression of planar slip was observed by the addition of SiC whisker to Al-Li alloys. This is a general phenomenon observed

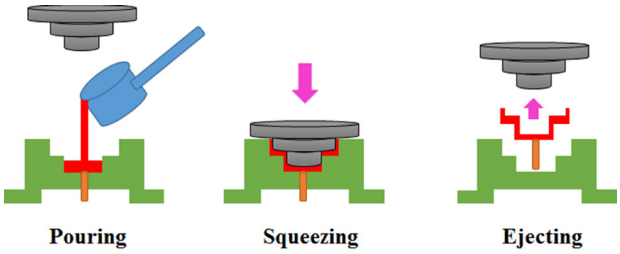


**Fig. 5.** A schematic of squeeze casting process.

in Al-Li based alloys, which happens by the interaction between dislocations and δ phase.

*4.1.4. Spray forming*

Spray methods that have been used for the production of monolithic alloys, can be utilized for spray forming of particulate-reinforced MMCs [55]. In this process, a molten aluminum alloy is atomized by a spray gun and ceramic particulates, such as $SiC_p$, are injected into the atomized alloy stream. The ceramic particulates are usually preheated to remove the moisture. Fig. 6 exhibits a schematic of this technique. For an efficient transfer in this process, the particle should be in the optimum size range. For instance, whiskers are very fine for being transferred. The produced preform in this process has generally a porous structure; therefore, the cosprayed MMCs are subjected to secondary finishing processes to make a wrought material [56]. This process falls under the category of liquid metallurgy processes, is totally controlled by the computer, and is conducted quite fast. Due to the short time of flight, detrimental reaction products are not formed. By this method, the incorporation of $SiC_p$ into Al alloys with volume fractions up to 20% and an aspect ratio between 3 and 4 has been possible. The capability of fabricating different types of composites is a significant advantage of this technique. For instance, selective reinforcement is possible and in situ laminates can be produced by two sprayers. However, the spray forming method is relatively expensive due to the expensive capital equipment [57].

Gomez et al. [58] added 15 vol.% of SiC particles to the 8090 Al alloy using spray codeposition of the $SiC_p$ and matrix on a substrate; then, the composite was extruded into rectangular bars at 420 ˚C. The results revealed that the reinforcement enhanced the wear behavior of the alloy and delayed the transition to higher sliding velocities, temperatures, and normal loads. However, wear rates of the synthesized composite were higher than those of the pure alloy in the mild wear regime. This was proposed to be a result of the abrasive role of $SiC_p$ detached from the composite surface during the wear test.

Gonzalez et al. [59] also developed 8090 Al alloy composite by adding 15 vol.% of $SiC_p$ using spray co-deposition of the particles and the matrix on a substrate and subsequent extrusion at 420 ˚C. Within the whole temperature range, damage in the composite was initiated by the fracture of particles. By increasing the temperature, the mechanisms associated with the final matrix fracture changed from intergranular fracture to ductile void growth. Furthermore, the elongation to failure of the composite was less affected by temperature compared to the alloy. However, the onset of plastic instability dictated the fracture strain of the prepared composites rather than the physical fracture mechanism.

*4.2. Solid-state processes*

Solid-state processing (SSP) is one of the various production techniques for AMCs preparation. In the SSP method, the matrix and the reinforcement are in solid state and are categorized as powder metallurgy (PM) and diffusion bonding processing [60].

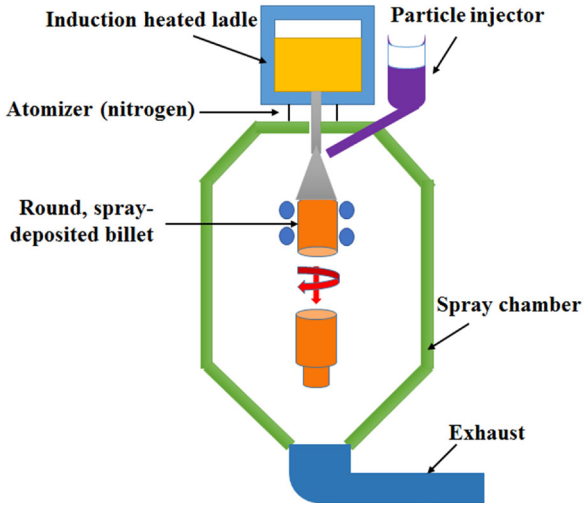


**Fig. 6.** Spray forming process schematic.

*4.2.1. Powder metallurgy*

Powder metallurgy involves mixing of ceramic fibers, platelets, or dispersion powders with matrix powders followed by cold pressing, sintering, and plastic working (extrusion or forging) [61]. Hot plastic working is performed when only a green part is produced by cold pressing and cold plastic working is performed when the green part is preliminary sintered [62]. The schematic illustration of this technique is shown in Fig. 7. Because of simplicity, PM is widely used for producing composite materials based on copper matrices [63, 64], aluminum alloys matrix [65, 66], and magnesium alloys matrix [67].

Nowadays, mechanical alloying has become a widely employed technique for producing particle-reinforced composite materials. In this process, hard dispersion particles are introduced into a metal matrix by a high-energy ball mill [68-70]. The prepared composite powders are then cold-pressed, sintered, and undergone cold plastic working or cold-pressed and undergone hot plastic working such as hot isostatic pressing, forging, or extrusion. The mechanical alloying process is used to produce composite materials, magnetic materials, amorphous materials, and materials with very fine grains [71].

Tan et al. [72] used PM technology to produce MMC materials based on AA2196 (Al-Li Alloy) and $TiB_2$ dispersion particles. They reported a homogeneous dispersion of the reinforcements in the main matrix using the PM process. It was observed that by adding $TiB_2$ reinforcement, the hardness of the composite increased, and with the increment of $TiB_2$ content, more porosities were formed in the composite. $TiB_2$ particles resulted in the formation of porosities in the grains as well as the grain boundaries of the matrix. The coarse particle size of the matrix was affected by sintering parameters, as the sinterability decreased by the increase in grain size.

*4.2.2. Diffusion bonding*

Diffusion bonding method is a solid-state process to weld similar or dissimilar metal pieces together. Welding is the result of atomic interdiffusion from the surfaces of clean metals in contact at high temperatures. The basic diffusion bonding technique has many variants; however, applying high temperature and pressure simultaneously is common among all of them. In this process, monolayer laminae, matrix alloy foil and composite wire, or fiber arrays are stacked in the desired order [73]. In Fig. 8, depicts a diffusion bonding technique schematically, which is also known as the foil-fiber-foil method. In this case, panels and filaments are stacked and hot pressed. For metal matrix composites, vacuum hot pressing should be carefully examined in the diffusion bonding tech-

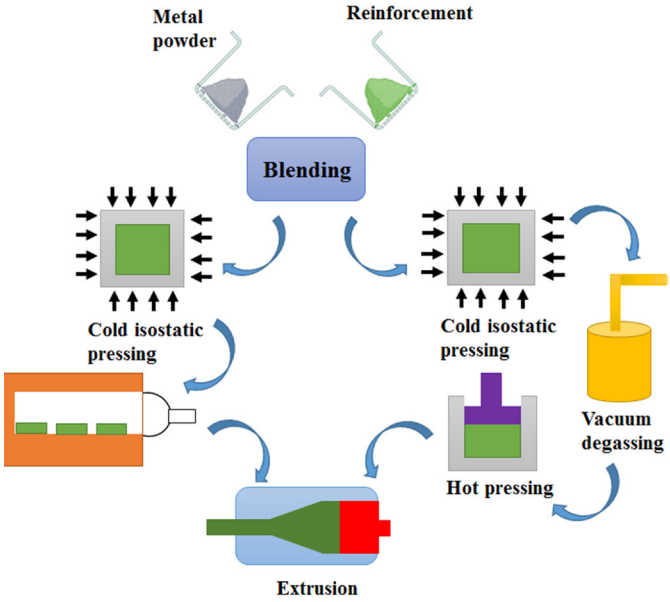


**Fig. 7.** Powder metallurgy process.

niques. The remarkable advantages of the diffusion bonding process include the ability to control fiber volume fraction and orientation as well as the capability of processing various metal matrices [74]. On the other hand, high processing pressures and temperatures and long processing times make this technique quite expensive. Additionally, the produced objects are of limited size. Instead of uniaxial pressing, hot isostatic pressing (HIP) could also be employed, in which the consolidation of the composite is carried out by gas pressure against a die containing the composite. Variable geometries can be obtained by HIP due to the relatively easy application of high pressures at high temperatures [75].

Wang et al. [76] used accumulative roll bonding (ARB) to fabricate Al-Li/$B_4C$ composite at room temperature. The investigations showed that by the increment of the number of cycles, the $B_4C$ agglomerates in the interfaces of Al-Li layers were transformed into the uniform dispersed particles and small clusters in the matrix. After 8 cycles of ARB, a few nano-grains were observed, which indicates that near nanostructure was successfully prepared. It was reported that the simultaneous improvement of ductility and strength was obtained with the increment of ARB cycles. In addition, after 8 cycles, high Young's modulus and excellent mechanical properties were obtained. It was proposed that the high strength of the prepared composite was associated with dislocation strengthening and grain refinement strengthening. Furthermore, good ductility of the Al-Li/$B_4C$ composite after 8 cycles of ARB resulted from proper wide grain size distribution and the uniform dispersion of $B_4C$ particles.

*4.3. In situ processes*

The in situ process involves the in situ formation of the reinforcement phase. In contrast to typical composite processing, the production of composites is carried out in one step out of a suitable starting alloy, in which the difficulties originating from the combination of the separate components are avoided [77, 78]. The controlled unidirectional solidification of eutectic alloys is an example of this technique. Because of unidirectional solidification, one phase is dispersed in fiber or ribbon form in a eutectic alloy. Controlling the solidification rate can lead to the fine distribution of the reinforcement. However, the practical solidification rate is limited because of maintaining a stable growth front. Furthermore, a high temperature gradient is required for the stable growth front. During this process, a precast rod of a eutectic alloy is usually melted in an inert gas atmosphere or vacuum by induction and more thermal gradients could be obtained by cooling the crucible below the induction coil [79, 80].

Another in situ process is the XD™ technique, in which the third phase is obtained by an exothermic reaction between two components. Such processing methods are sometimes considered as the self-propagating high-temperature synthesis (SHS) process and are commonly used to produce ceramic particle reinforced MMCs. Using the reaction synthesis, master alloys with high contents of reinforcement are fabricated. To develop a composite with a desirable volume fraction of particle reinforcement, the master alloy is blended and remelted with the base alloy. Typical reinforcement particles include $TiB_2$, SiC, etc. in Ni, Al, or intermetallic matrix [42, 81, 82].

Wu et al. [83] studied mechanical properties and microstructural evolution of cast Al-Li-Cu/$TiB_2$ composite during heat treatment. In this research, the salt-metal reaction technique was used to synthesize an in-situ Al-Li-Cu/$TiB_2$ composite. The as-cast composite showed clusters of larger reinforcement particulates, mixed with coarse secondary phases along the alloy grain boundaries. It was reported that most of these phases dissolved into the α-aluminum phase by two-stage solution heat treatment. The grain boundaries are pinned by the stable particulates at high temperatures leading to the thermal stability of the composite grain size. Therefore, no remarkable increase was observed after solution treatment. A significant age-hardening response was shown in the composite with the peak-hardness at 175 °C in 160 h.

Zhao et al. [84] fabricated the in-situ Al-Cu-Li/$TiB_2$ composite by hot extrusion and evaluated the influence of nano $TiB_2$ particulates on mechanical properties and microstructural of the composite after T6 heat treatment. The results indicated that the majority of $TiB_2$ particles were aggregated together and particle bands were formed. The matrix developed weak < 113 > and < 111 > textures, while the prepared composite developed the typical fiber textures with < l00 > and < 111 > parallel to extruded direction. It was demonstrated that the addition of $TiB_2$ nanoparticles could increase the volume fraction and intensity of major texture components. S and T1 phases were smaller and possessed higher number density resulted from the incorporation of $TiB_2$ particles. Additionally, the T1 phases could form a continuous network by connecting with each other. In contrast to the matrix alloy, the θ′ phase was rarely appeared in the composite. In comparison with the matrix alloy, the yield and ultimate tensile strength of the composite enhanced by 152 MPa and 248 MPa, respectively.

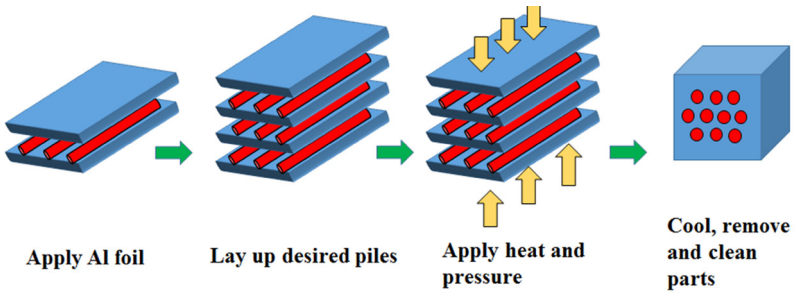


**Fig. 8.** A schematic of diffusion bonding process.

## 5. Conclusions and future insights

In the review of the aluminum-Lithium alloy matrix composite reinforced with ceramics, it was concluded that ceramic-reinforced Al and its alloys show noticeable improvement in their mechanical properties including tensile strength, yield strength, and hardness, at the expense of ductility. The preparation methods could also result in different properties in these composites. It has been revealed that the alloy composition affects the route employed for processing, the corrosion behavior, mechanical properties, and heat-treatment of the composites. Regarding the properties of low-density Al-Li composites, they will be considered as promising materials for aerospace industry applications. It is expected that more research works would be performed on tailoring the microstructure and properties of these alloys by the careful control of the processing parameters and developing new production routes.

REFERENCES

[1] L. Bazli, M. Siavashi, A. Shiravi, A Review of Carbon nanotube/$TiO_2$ Composite prepared via Sol-Gel method, Journal of Composites and Compounds 1(1) (2019) 1-12.
[2] L. Bazli, A. Khavandi, M.A. Boutorabi, M. Karrabi, Morphology and viscoelastic behavior of silicone rubber/EPDM/Cloisite 15A nanocomposites based on Maxwell model, Iranian Polymer Journal 25(11) (2016) 907-918.
[3] E. Omrani, A.D. Moghadam, M. Algazzar, P.L. Menezes, P.K. Rohatgi, Effect of graphite particles on improving tribological properties Al-16Si-5Ni-5Graphite self-lubricating composite under fully flooded and starved lubrication conditions for transportation applications, The International Journal of Advanced Manufacturing Technology 87(1-4) (2016) 929-939.
[4] A.D. Moghadam, E. Omrani, P.L. Menezes, P.K. Rohatgi, Effect of in-situ processing parameters on the mechanical and tribological properties of self-lubricating hybrid aluminum nanocomposites, Tribology Letters 62(2) (2016) 25.
[5] A.D. Moghadam, B.F. Schultz, J. Ferguson, E. Omrani, P.K. Rohatgi, N. Gupta, Functional metal matrix composites: self-lubricating, self-healing, and nanocomposites-an outlook, Jom 66(6) (2014) 872-881.
[6] A.D. Moghadam, E. Omrani, P.L. Menezes, P.K. Rohatgi, Mechanical and tribological properties of self-lubricating metal matrix nanocomposites reinforced by carbon nanotubes (CNTs) and graphene–a review, Composites Part B: Engineering 77 (2015) 402-420.
[7] E. Omrani, A.D. Moghadam, P.L. Menezes, P.K. Rohatgi, Influences of graphite reinforcement on the tribological properties of self-lubricating aluminum matrix composites for green tribology, sustainability, and energy efficiency—a review, The International Journal of Advanced Manufacturing Technology 83(1-4) (2016) 325-346.
[8] M. Tabandeh-Khorshid, E. Omrani, P.L. Menezes, P.K. Rohatgi, Tribological performance of self-lubricating aluminum matrix nanocomposites: role of graphene nanoplatelets, Engineering science and technology, an international journal 19(1) (2016) 463-469.
[9] P.K. Rohatgi, M. Tabandeh-Khorshid, E. Omrani, M.R. Lovell, P.L. Menezes, Tribology of metal matrix composites, Tribology for scientists and engineers, Springer2013, pp. 233-268.
[10] I. Tajzad, E. Ghasali, Production Methods of CNT-reinforced Al Matrix Composites: A Review, Composites and Compounds 1(1) (2020).
[11] L. Bazli, A. Khavandi, M.A. Boutorabi, M. Karrabi, Correlation between viscoelastic behavior and morphology of nanocomposites based on SR/EPDM blends compatibilized by maleic anhydride, Polymer 113 (2017) 156-166.
[12] K.U. Kainer, Basics of metal matrix composites, Wiley Online Library2006.
[13] J. Hooker, P. Doorbar, Metal matrix composites for aeroengines, Materials science and technology 16(7-8) (2000) 725-731.
[14] R. Etemadi, B. Wang, K. Pillai, B. Niroumand, E. Omrani, P. Rohatgi, Pressure infiltration processes to synthesize metal matrix composites–A review of metal matrix composites, the technology and process simulation, Materials and Manufacturing Processes 33(12) (2018) 1261-1290.
[15] P.K. Rohatgi, A. Dorri, B.F. Schultz, J. Ferguson, Synthesis and properties of metal matrix nanocomposites (MMnCs), syntactic foams, self lubricating and self-healing metals, Proceedings of the 8th Pacific Rim International Congress on Advanced Materials and Processing, Springer, 2013, pp. 1515-1524.
[16] A. Masoudian, A. Tahaei, A. Shakiba, F. Sharifianjazi, J.A. Mohandesi, Microstructure and mechanical properties of friction stir weld of dissimilar AZ31-O magnesium alloy to 6061-T6 aluminum alloy, Transactions of nonferrous metals society of China 24(5) (2014) 1317-1322.
[17] A. Dorri Moghadam, J. Ferguson, B.F. Schultz, H. Lopez, P.K. Rohatgi, Direct Synthesis of nanostructured in situ hybrid aluminum matrix nanocomposite, Industrial & Engineering Chemistry Research 55(22) (2016) 6345-6353.
[18] A.D. Moghadam, J. Ferguson, B.F. Schultz, P.K. Rohatgi, In-situ reactions in hybrid aluminum alloy composites during incorporating silica sand in aluminum alloy melts, AIMS Materials Science 3(3) (2016) 954-964.
[19] M. Surappa, Aluminium matrix composites: Challenges and opportunities, Sadhana 28(1-2) (2003) 319-334.
[20] S. Adhikari, P. Mukhopadhyay, Physical metallurgy of beryllium and its alloys, Mineral Processing and Extractive Metullargy Review 14(1) (1995) 253-299.
[21] D. Huda, M. El Baradie, M. Hashmi, Metal-matrix composites: Materials aspects. Part II, Journal of Materials Processing Technology 37(1-4) (1993) 529-541.
[22] I. Polmear, Aluminium Alloys--A Century of Age Hardening, Materials forum, 2004, p. 13.
[23] M. Furukawa, Y. Miura, M. Nemoto, Strengthening mechanisms in Al–Li alloys containing coherent ordered particles, Transactions of the Japan institute of metals 26(4) (1985) 230-235.
[24] S.N. Murty, B.N. Rao, B. Kashyap, On the hot working characteristics of 6061Al–SiC and 6061–$Al_2O_3$ particulate reinforced metal matrix composites, Composites science and technology 63(1) (2003) 119-135.
[25] S. Kumar, R. Singh, M. Hashmi, Metal matrix composite: a methodological review, Advances in Materials and Processing Technologies 6(1) (2020) 13-24.
[26] J.P. Davim, Diamond tool performance in machining metal–matrix composites, Journal of materials processing technology 128(1-3) (2002) 100-105.
[27] R.N. Rai, G. Datta, M. Chakraborty, A. Chattopadhyay, A study on the machinability behaviour of Al–TiC composite prepared by in situ technique, Materials Science and Engineering: A 428(1-2) (2006) 34-40.
[28] J.D. Torralba, C. Da Costa, F. Velasco, P/M aluminum matrix composites: an overview, Journal of Materials Processing Technology 133(1-2) (2003) 203-206.
[29] Y. Mazaheri, M. Meratian, R. Emadi, A. Najarian, Comparison of microstructural and mechanical properties of Al–TiC, Al–$B_4C$ and Al–TiC–B4C composites prepared by casting techniques, Materials Science and Engineering: A 560 (2013) 278-287.
[30] S. Kumar, B. Kumar, A. Baruah, V. Shanker, Synthesis of magnetically separable and recyclable g-$C_3N_4$–$Fe_3O_4$ hybrid nanocomposites with enhanced photocatalytic performance under visible-light irradiation, The Journal of Physical Chemistry C 117(49) (2013) 26135-26143.
[31] M.K. Akbari, H. Baharvandi, O. Mirzaee, Fabrication of nano-sized $Al_2O_3$ reinforced casting aluminum composite focusing on preparation process of reinforcement powders and evaluation of its properties, Composites Part B: Engineering 55 (2013) 426-432.
[32] A. Baradeswaran, A.E. Perumal, Influence of B4C on the tribological and mechanical properties of Al 7075–$B_4C$ composites, Composites Part B: Engineering 54 (2013) 146-152.
[33] J.D.R. Selvam, D.R. Smart, I. Dinaharan, Synthesis and characterization of

Al6061-Fly Ashp-SiCp composites by stir casting and compocasting methods, Energy procedia 34 (2013) 637-646.
[34] K.K. Chawla, Metal matrix composites, Composite Materials, Springer2012, pp. 197-248.
[35] R.G. Kamat, J.M. Newman, R.R. Sawtell, J.C. Lin, Aluminum-lithium alloys, and methods for producing the same, Google Patents, 2012.
[36] N.E. Prasad, A. Gokhale, R. Wanhill, Aluminum-lithium alloys: processing, properties, and applications, Butterworth-Heinemann2013.
[37] J. Ekvall, J. Rhodes, G. Wald, Methodology for evaluating weight savings from basic material properties, Design of Fatigue and Fracture Resistant Structures, ASTM international1982.
[38] C. Peel, B. Evans, C. Baker, D. Bennett, P. Gregson, H. Flower, The development and application of improved aluminium-lithium alloys, Aluminum-lithium alloys II (1984) 363-392.
[39] K.V. Rao, R. Ritchie, Fatigue of aluminium—lithium alloys, International materials reviews 37(1) (1992) 153-186.
[40] N.E. Prasad, A.A. Gokhale, R. Wanhill, Aluminium–lithium alloys, Aerospace Materials and Material Technologies, Springer2017, pp. 53-72.
[41] Z.S. Yuan, Z. Lu, Y.H. Xie, X.L. Wu, S.L. Dai, C.S. Liu, Mechanical properties of a novel high-strength aluminum-lithium alloy, Materials Science Forum, Trans Tech Publ, 2011, pp. 385-389.
[42] K.K. Chawla, Composite materials: science and engineering, Springer Science & Business Media2012.
[43] G. M.-C., W. D.-B., W. J.-J., Y. G.-J., L. C.-G., Microstructure and mechanical properties of cast (Al–Si)/SiCp composites produced by liquid and semisolid double stirring process, Materials science and technology 16(5) (2000) 556-563.
[44] W.H. Hunt Jr, Aluminum metal matrix composites today, Materials science forum, Trans Tech Publ, 2000, pp. 71-84.
[45] A. Contreras, V. Lopez, E. Bedolla, Mg/TiC composites manufactured by pressureless melt infiltration, Scripta materialia 51(3) (2004) 249-253.
[46] H. Su, W. Gao, Z. Feng, Z. Lu, Processing, microstructure and tensile properties of nano-sized $Al_2O_3$ particle reinforced aluminum matrix composites, Materials & Design (1980-2015) 36 (2012) 590-596.
[47] R. Bauri, M. Surappa, Damping behavior of Al-Li-SiC p composites processed by stir casting technique, Metallurgical and Materials Transactions A 36(3) (2005) 667-673.
[48] R. Bauri, M. Surappa, Processing and properties of Al–Li–SiCp composites, Science and Technology of Advanced Materials 8(6) (2007) 494.
[49] D. Wittig, A. Glauche, C. Aneziris, T. Minghetti, C. Schelle, T. Graule, J. Kuebler, Activated pressureless melt infiltration of zirconia-based metal matrix composites, Materials Science and Engineering: A 488(1-2) (2008) 580-585.
[50] P. Garg, A. Jamwal, D. Kumar, K.K. Sadasivuni, C.M. Hussain, P. Gupta, Advance research progresses in aluminium matrix composites: manufacturing & applications, Journal of Materials Research and Technology 8(5) (2019) 4924-4939.
[51] A. Demir, N. Altinkok, Effect of gas pressure infiltration on microstructure and bending strength of porous $Al_2O_3$/SiC-reinforced aluminium matrix composites, Composites Science and Technology 64(13-14) (2004) 2067-2074.
[52] Q. Zhang, G. Chen, G. Wu, Z. Xiu, B. Luan, Property characteristics of a AlNp/Al composite fabricated by squeeze casting technology, Materials Letters 57(8) (2003) 1453-1458.
[53] S. Dong, J. Mao, D. Yang, Y. Cui, L. Jiang, Age-hardening behavior of a SiCw/Al-Li-Cu-Mg-Zr composite, Materials Science and Engineering: A 327(2) (2002) 213-223.
[54] S. Dong, D. Yang, S. Chen, Influence of SiC whisker on planar slip in Al-Li based alloys, Journal of materials science 37(12) (2002) 2527-2534.
[55] T.S. Srivatsan, E. Lavernia, Use of spray techniques to synthesize particulate-reinforced metal-matrix composites, Journal of materials science 27(22) (1992) 5965-5981.
[56] A. Agarwal, T. McKechnie, S. Seal, Net shape nanostructured aluminum oxide structures fabricated by plasma spray forming, Journal of Thermal Spray Technology 12(3) (2003) 350-359.
[57] A. Agarwal, T. McKechnie, S. Seal, The spray forming of nanostructured aluminum oxide, JOM 54(9) (2002) 42-44.
[58] T. Gómez-del Río, A. Rico, M. Garrido, P. Poza, J. Rodríguez, Temperature and velocity transitions in dry sliding wear of Al–Li/SiC composites, Wear 268(5-6) (2010) 700-707.
[59] C. González, A. Martín, J. Llorca, Effect of temperature on the fracture mechanisms of 8090 Al–Li alloy and 8090 Al–Li/SiC composite, Scripta Materialia 51(11) (2004) 1111-1115.
[60] D. Lloyd, Particle reinforced aluminium and magnesium matrix composites, International materials reviews 39(1) (1994) 1-23.
[61] Z.Y. Liu, B.L. Xiao, W.G. Wang, Z.Y. Ma, Singly dispersed carbon nanotube/aluminum composites fabricated by powder metallurgy combined with friction stir processing, Carbon 50(5) (2012) 1843-1852.
[62] K. Padmavathi, R. Ramakrishnan, K. Palanikumar, Aluminium Metal Matrix composite–an insight into solid state and liquid state processes, Applied Mechanics and Materials, Trans Tech Publ, 2015, pp. 234-239.
[63] Y. Wan, Y. Wang, H. Luo, G. Cheng, Effect of interfacial bonding strength on thermal expansion behaviour of PM $Al_2O_3$/copper alloy composites, Powder metallurgy 43(1) (2000) 76-78.
[64] H.-K. Kang, Microstructure and electrical conductivity of high volume $Al_2O_3$-reinforced copper matrix composites produced by plasma spray, Surface and Coatings Technology 190(2-3) (2005) 448-452.
[65] M. Aboraia, H. Wasly, M. Doheim, G. Abdalla, A. Mahmoud, Characterization of Al/(10% $Al_2O_3$-10% $ZrO_2$) nanocomposite powders fabricated by high-energy ball milling, International Journal of Engineering Research and Applications 3 (2013) 474-482.
[66] N. Zhao, P. Nash, X. Yang, The effect of mechanical alloying on SiC distribution and the properties of 6061 aluminum composite, Journal of Materials Processing Technology 170(3) (2005) 586-592.
[67] Y. Xi, D. Chai, W. Zhang, J. Zhou, Titanium alloy reinforced magnesium matrix composite with improved mechanical properties, Scripta Materialia 54(1) (2006) 19-23.
[68] S. Aksöz, B. Bostan, Effects of ageing and cryo-ageing treatments on microstructure and hardness properties of AA2014–SiC MMCs, Transactions of the Indian Institute of Metals 71(8) (2018) 2035-2042.
[69] A. Abuchenari, M. Moradi, The Effect of Cu-Substitution on the Microstructure and Magnetic Properties of Fe-15%Ni alloy Prepared by Mechanical Alloying, Composites and Compounds 1(1) (2019).
[70] M. Alizadeh, F. Sharifianjazi, E. Haghshenasjazi, M. Aghakhani, L. Rajabi, Production of nanosized boron oxide powder by high-energy ball milling, Synthesis and Reactivity in Inorganic, Metal-Organic, and Nano-Metal Chemistry 45(1) (2015) 11-14.
[71] J. Cintas, F. Cuevas, J. Montes, E. Herrera, High-strength PM aluminium by milling in ammonia gas and sintering, Scripta Materialia 53(10) (2005) 1165-1170.
[72] E. Tan, Y. Kaplan, H. Ada, S. Aksöz, Production of the AA2196-$TiB_2$ MMCs via PM Technology, Springer International Publishing, Cham, 2019, pp. 153-157.
[73] R. Casati, M. Vedani, Metal matrix composites reinforced by nano-particles—a review, Metals 4(1) (2014) 65-83.
[74] M. Alizadeh, M. Paydar, F.S. Jazi, Structural evaluation and mechanical properties of nanostructured Al/$B_4C$ composite fabricated by ARB process, Composites Part B: Engineering 44(1) (2013) 339-343.
[75] M. Muratoğlu, O. Yilmaz, M. Aksoy, Investigation on diffusion bonding characteristics of aluminum metal matrix composites (Al/SiCp) with pure aluminum for different heat treatments, Journal of materials processing Technology 178(1-3) (2006) 211-217.
[76] Y. Wang, F. Zhong, R. Wu, H. Wu, N. Turakhodjaev, B. Kudratkhon, J. Sun, L. Hou, J. Zhang, X. Li, M. Zhang, High-strength, ductility and modulus Al–Li/$B_4C$ composite with near nanostructure produced by accumulative roll bonding, Journal of Alloys and Compounds 834 (2020) 155105.
[77] Y. Sahin, M. Acılar, Production and properties of SiCp-reinforced aluminium alloy composites, Composites Part A: Applied Science and Manufacturing 34(8) (2003) 709-718.
[78] E.H. Jazi, R. Esalmi-Farsani, G. Borhani, F.S. Jazi, Synthesis and Characterization of In Situ Al-$Al_{13}Fe_4$-$Al_2O_3$-$TiB_2$ Nanocomposite Powder by Mechanical Alloying and Subsequent Heat Treatment, Synthesis and Reactivity in Inorganic, Metal-Organic, and Nano-Metal Chemistry 44(2) (2014) 177-184.
[79] H. Wang, G. Li, Y. Zhao, G. Chen, In situ fabrication and microstructure of $Al_2O_3$ particles reinforced aluminum matrix composites, Materials Science and Engineering: A 527(12) (2010) 2881-2885.
[80] N. Chawla, K.K. Chawla, Processing, Metal Matrix Composites (2013) 55-97.
[81] A. Masoudian, M. Karbasi, F. SharifianJazi, A. Saidi, Developing $Al_2O_3$-TiC in-situ nanocomposite by SHS and analyzingtheeffects of Al content and mechanical activation on microstructure, Journal of Ceramic Processing Research 14(4) (2013) 486-491.
[82] V. Balouchi, F.S. Jazi, A. Saidi, Developing (W, Ti) C-(Ni, Co) nanocomposite by SHS method, Journal of Ceramic Processing Research 16(5) (2015) 605-608.
[83] L. Wu, C. Zhou, X. Li, N. Ma, H. Wang, Microstructural evolution and mechanical properties of cast high-Li-content $TiB_2$/Al-Li-Cu composite during heat treatment, Journal of Alloys and Compounds 739 (2018) 270-279.
[84] B. Zhao, Q. Yang, L. Wu, X. Li, M. Wang, H. Wang, Effects of nanosized particles on microstructure and mechanical properties of an aged in-situ $TiB_2$/Al-Cu-Li composite, Materials Science and Engineering: A 742 (2019) 573-583.

Available online at www.jourcc.com

Journal homepage: www.JOURCC.com

Journal of Composites and Compounds

# Clay-reinforced nanocomposites for the slow release of chemical fertilizers and water retention

*Aliasghar Abouchenari[a]*, Khatereh Hardani[b], Somayeh Abazari[c], Fahimeh naghdi[d], Mehdy Ahmady Keleshteri[e], Ata Jamavari[f], Amir Modarresi Chahardehi[g]*

[a] *Materials Engineering, Shahid Bahonar University, Kerman, Iran*
[b] *Department of Marine Chemistry, Faculty of Marine Science, Khorramshahr University of Marine Science and Technology, Khorramshahr, Iran*
[c] *Department on Materials and Metallurgical Engineering, Amirkabir University on Technology (Tehran Ploythechnic), Tehran, Iran*
[d] *Department of Materials and Industrial Engineering, Babol Noshirvani University of Technology, Mazandaran, Iran*
[e] *Advanced Materials Research Center, Materials Engineering Department, Najafabad Branch, Islamic Azad University, Najafabad, Isfahan, Iran*
[f] *Department of material science and engineering, Iran University of Science and Technology, Tehran, Iran*
[g] *Integrative Medicine Cluster, Advanced Medical and Dental Institute, Universiti Sains Malaysia, Bertam, 13200, Kepala Batas, Pulau Pinang, Malaysia*

A B S T R A C T

The present study includes an overview of the applications of clay-based nanocomposites from the past decade to date in various fields such as pharmaceuticals, water treatment, food packaging, electricity, automotive, and especially the production of chemical fertilizers with water retention and slow release. In the agricultural area, one of the promising materials that help green chemical engineering and green chemistry is slow-release fertilizer (SRF). Clay minerals and clay nanocomposites provide cost-effective and efficient material for this purpose. In this paper, the research and development of polymer nanocomposites based on clay in recent years with the focus on their application as novel fertilizers have been reviewed. Clay minerals are promising reinforcements to manufacture high-performance, lightweight, and low-cost nanocomposites because of their abundance, layered structure, low cost, and rich intercalation chemistry.



Peer review under responsibility of jourcc

A R T I C L E I N F O R M A T I O N

*Article history:*
Received 4 June 2020
Received in revised form 14 June 2020
Accepted 26 June 2020

*Keywords:*
Clay nanocomposites
Slow release
Controlled release
Fertilizer

Table of contents



## 1. Introduction

The main factor in the agricultural area playing a very important role in plant growth is an appropriate distribution of fertilizer and water. However, around 50–70 % of potassium, 80–90 % of phosphorus, and 40–70 % of nitrogen incorporated in conventional fertilizers are wasted by volatilization or leaching, which leads to release of them into the environment rather than being absorbed by plants [1, 2]. Therefore, there

* *Corresponding author: Aliasghar Abouchenari; E-mail: aliab596@yahoo.com*
*https://doi.org/10.29252/jcc.2.2.4* 

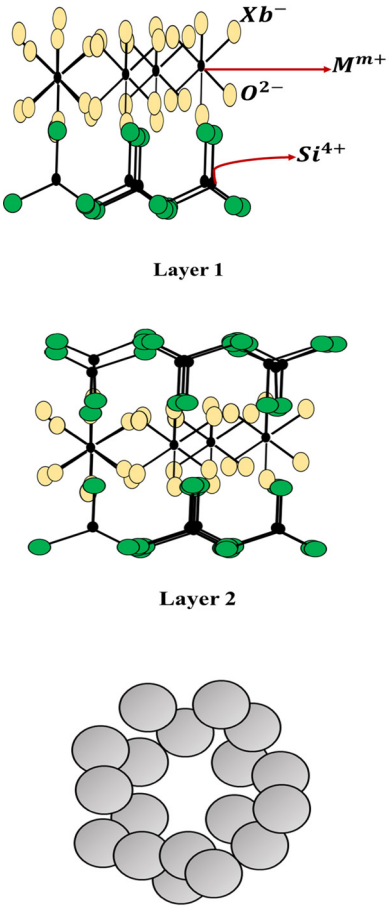


**Fig. 1.** (a) Crystal structure of clay minerals including 1:1 and 2:1-layer type, where M can be Fe, Mg, Al, etc. and X is mostly OH (b) Siloxane cavity in the basal plane of a tetrahedral sheet.

is a need for improvement and management of fertilizer nutrients and water resources utilization. The utilization of controlled- or slow-release fertilizers is one way to improve the fertilizer application. The first major category of this kind of fertilizer is matrix type formulations as a result of their facile fabrication. In this system, the active materials are distributed in the matrix and its diffusion occurs through intergranular (pores) or continuum openings (channels) in the matrix [3, 4]. Moreover, the aim of developing slow-release fertilizers is the gradual secretion of the nutrient to be regulated based on the nutrient requirement of plants. In order to control the release rate, the physical preparation of the fertilizers using engineered matrices could be used [5, 6]. As environmental protection issues are nowadays in the center of attention, the degradability of these systems is desired [7]. Clay-based nanocomposites have significantly attracted attentions among nanocomposites that are utilized in chemical fertilizers. Polymer nanocomposites are composed of a polymeric matrix filled with reinforcements with at least one dimension in the nanometer-scale [8]. One-dimensional nanofillers are in the form of layered minerals such as clay [9-12]. In the following sections, we have briefly mentioned the applications of clay-based nanocomposites, mainly in the field of chemical fertilizers for agricultural applications.

## 2. Clay-reinforced nanocomposite

Polymer nanocomposites have attracted much attention leading to investment in research and development around the world [8]. Clay platelets are one-dimensional disc-like nanoparticles that possess unique structure and characteristics [13]. These minerals are both synthesized clays such as magadiite, laponite, and fluorohectorite, and natural clays viz. saponite, hectorite, and montmorillonite [10]. Nowadays, the use

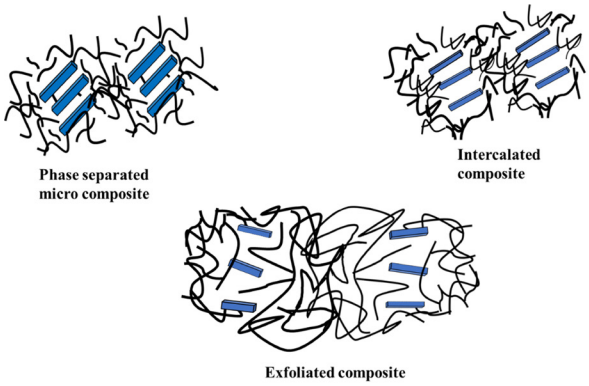


**Fig. 2.** Type of polymer clay nanocomposite.

of polymer/clay nanocomposites (PCNs) is one of the most applied modern technologies, since they can generate new polymer properties [14]. PCNs are widely used in modern technologies due to being able to introduce new properties to polymers [14]. PCNs possess unique characteristics including their capability to confine polymer chains at the nanometer scale and disperse in the matrix [15]. Properties of polymers such as gas barrier properties, toughness, heat distortion temperature, stiffness, modulus, strength, and chemical resistance could be significantly enhanced by adding a low amount of fillers [16-18].

Nanocomposites or conventional composites can be formed under the processing condition, components nature as well as the interfacial interactions of modified or unmodified layered silicates and polymer chains. The type of formed nanocomposites is illustrated in Fig. 2 [19].

## 3. Applications of Clay-reinforced nanocomposite

Clay-based polymer nanocomposites are promising alternatives to conventional micro composites as a result of the ability to disperse clay platelets in nanoscale in the matrix and improve physical, chemical, electrical, optical, thermal, mechanical, and barrier properties [10, 22].

### *3.1. Electro materials*

New organic-inorganic hybrids with excellent electrical properties could be produced based on polymer nanocomposites. Conducting polymers reinforced with clay particles exhibit remarkable electrochemical properties, which have been employed for applications including smart windows, solid-state batteries, modified electrodes biosensors, and other electrochemical devices. PPR nanocomposites, for instance, could be developed to produce modified electrodes that are utilized as devices for electrocatalysis or sensors. Because PEO nanocomposites exhibit single ionic conduction behavior and relatively high conductivity at ambient temperature and they do not have significant dependence on temperature over conventional electrolytes based on $LiBF_4$/PEO, they could be offered as new electrolyte materials. Additionally, these nanocomposites are excellent models for investigation of the interfacial structure and dynamics [10, 23].

### *3.2. Automotive Components*

Today, automotive industries are widely benefiting from polymer composites. Nevertheless, these composites are composed of polymers filled with a great number of microscale particles, flame resistant, chemical resistant, and thermal stabilizer additives. Hence, the enhanced performance often leads to the low fuel efficiency and increment of materials density. On the other hand, by using polymer nanocompos-

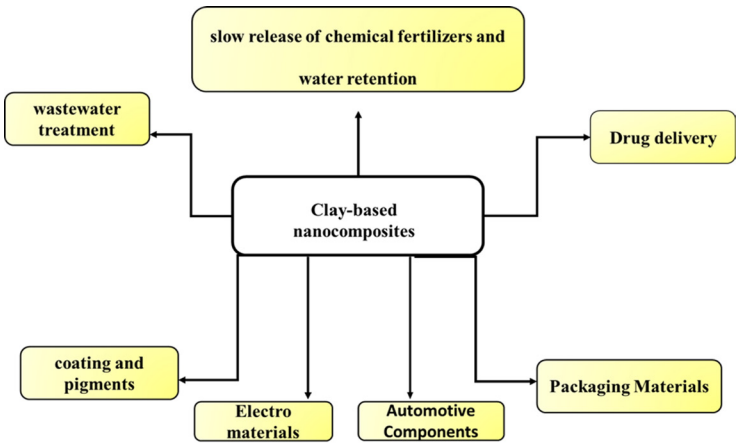


**Fig. 3.** Applications of clay-nanocomposite.

ites, transport industries such as aerospace and automotive can benefit from higher performance with affordable materials, and a significant reduction of weight. The commercial nylon 6/clay nanocomposites were first used by Toyota Motors in the timing-belt cover in the early 1990s. The manufactured timing-belt cover showed excellent thermal stability, enhanced rigidity with no wrap. As a result of the lower amount of clays, the weight also was saved by up to 25%. Besides, due to their remarkable enhancement of mechanical properties, barrier properties, and heat distortion temperature (HDT), nylon 6/clay nanocomposites have also been utilized as fuel hoses, oil reservoir tank, and engine cover in the automotive industry. In 2002, a thermoplastic olefin/clay nanocomposite with 2.5% reinforcement was also used by General Motors for step-assist on Chevrolet and Safari. Today, polymer nanocomposites are believed to have the potential to be used in different internal and external parts of vehicles including under-the-hood parts, door handles, and mirror housings. The polymer nanocomposites weight can benefit material recycling and environmental protection [10, 23]. The fundamental stages of nanocomposites' production for automotive applications are illustrated in Figure 4. In the production of competitive parts for a particular use, there might be some great challenges in each step that must be resolved. There exist different variations in the preparation process for a specific application that must be regulated according to the part specifications as well as the method of processing. Regarding these considerations, critical demands are imposed on the science and technology required for the processing of polymer-based composites [24].

### *3.3. Coating and Pigments*

Nano pigments or PlanoColors® consisting of environment-friendly organic dyes and clays have been offered as potential substitutes for toxic palladium (Pd) and cadmium (Cd) pigments. The Plano Colors are easily dispersed in coatings and bulk polymers in the nanometer scale. By selecting suitable dyes from various organic dyes, different pigment colors are possibly synthesized. Additionally, materials that are dyed with Plano Colors completely keep their transparency due to the smaller size of these pigments in comparison with the light wavelength. Moreover, these nano pigments enhance temperature, ultraviolet (UV), and oxygen stability accompanied by high color efficiency and brilliance which is due to their improved interaction with light by their large surface area [10, 25].

### *3.4. Packaging Materials*

Clay/polymer nanocomposites could exhibit remarkable improvement of shelf-life for various types of packaged food due to their excellent barrier properties. Furthermore, adding clay to polymers maintain the optical transparency of the nanocomposite films, which is not possible to achieve in conventional polymer micro composites. Hence, due to the above-mentioned characteristics, clay/polymer nanocomposites are widely acceptable in packaging industries including beverage containers, wrapping films, packaging of cereals, confectionery, cheese, processed meats, dairy products, fruit juice, and carbonated drinks bottles. Bayer, for example, has recently produced a novel food packaging plastic films made from nylon-6/clay nanocomposites with the exfoliated structure [26].

### *3.5. Drug Delivery*

Recently, polymer/clay nanocomposites have attracted the attention of researchers in the field of controlled drug delivery. The number of published reports on these nanocomposites for drug delivery applica-

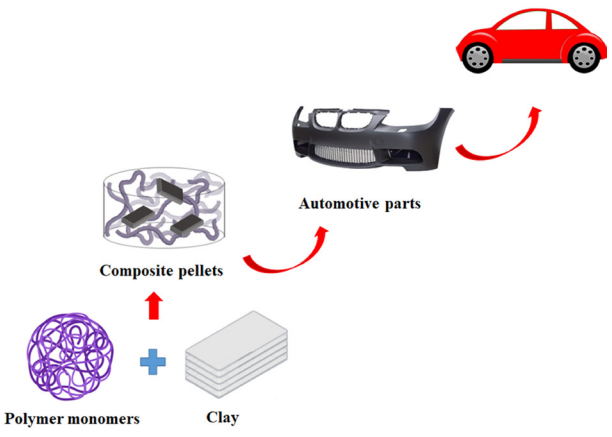


**Fig. 4.** Nanocomposites processing steps for automotive applications.

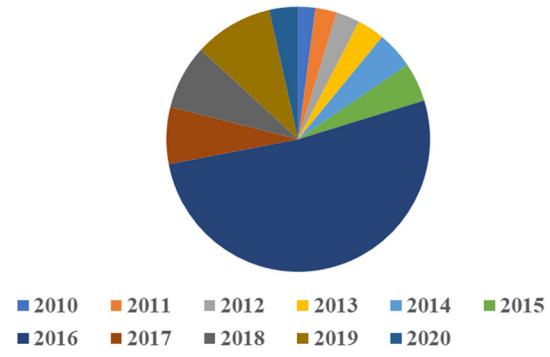


**Fig. 5.** Number of publication reporting clay-based nanocomposite for drug delivery.

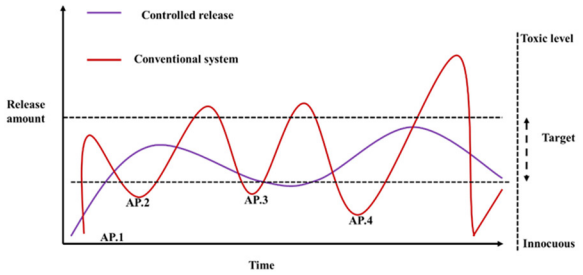


**Fig. 6.** Comparison between the controlled-release system and the conventional systems.

tions is illustrated in Fig. 5 [27, 28]. As a result of specific properties superior to pristine polymers such as increased thixotropy, enhanced mechanical strength, higher heat resistance, increased gaseous permeability, even with the addition of 5% or less content of clay, these nanocomposites have attracted considerable attention [29-34]. Due to the promising characteristics, polymer/clay nanocomposites have been proposed for applications in various fields such as pharmaceutical, biomedical, and biochemical fields [35-37].

### *3.6. Wastewater Treatment*

One of the applications of polymer/clay is in the effective water treatment by adsorbing and flocculating of both organic and inorganic micro-sized pollutants from aqueous solutions. When some of these nanocomposites are modified with biocides, they show the ability of microorganisms removal including Escherichia coli, Staphylococcus aureus, Candida albicans, and Pseudomonas aeruginosa from wastewater. Compared to neat clay, polymer/clay nanocomposites could be easily recovered from aqueous solutions [38]. Furthermore, the treatment times of PCNs are reported to be better than that of either clay or polymer adsorbents. The nanocomposites also possess better life cycles and improved adsorption capacity in comparison with clay alone. Therefore, clay-reinforced nanocomposites exhibit a high potential of efficient wastewater treatment [39, 40].

### *3.7. Controlled- or Slow-Release Systems Applied to Fertilizers*

Smart fertilizers that are fertilizers with controlled- and slow-release, can gradually release the containing nutrient with the possibility to regulate the release according to the nutritional requirements of plants. These systems make the nutrients available for a longer period compared to fertilizers with high solubility, which release their nutrients rapidly [41, 42]. The official distinction between slow-release and controlled-release of fertilizers does not exist. Reduction of environmental contamination, minimizing root damage and soil compaction, saving fuel, reducing the labor, elimination of parcels for covering, and prevention of physical damage to the crop due to application processes are the remarkable benefits of these systems [41]. Figure 6 compares a controlled release and conventional system for a specific active nutrient. Zhao et al. [43] studied the influence of fertilizer with controlled-release on the production, photosynthetic rate, nitrogen use efficiency, and ammonia volatilization in maize cultivation. According to their observation, the use of coated urea with sulfur or resin exhibited improved outcomes in all parameters compared to common fertilizers. Li et al. [44] utilized a slow-release fertilizer system based on treated coal ash for potassium sources. They tested the system directly in the soil and reported that the use of the slow-release system led to a positive effect on the development of crops. A new series of hydrogels consisting of methylcellulose, polyacrylamide, and montmorillonite were synthesized by Bortolin et al. [45]. They reported that the incorporation of clay led to some improvements in the properties of the materials. Adsorption–desorption investigation of urea demonstrated that the hydrogel composite that included montmorillonite released urea in a more controlled rate (around 200 times slower release rate compared to conventional pure urea) in comparison with the neat hydrogel. The results show the excellent potential of clay, especially montmorillonite, to produce novel fertilizers with controlled- or slower release.

## 4. Polymer/Clay Nanocomposites for Fertilizers

Due to being easily obtained, having higher efficiency, and resistance to environmental effects, systems based on polymers are more commonly used for various applications [46]. Besides, polymer-based products are used in different physical states as carriers such as melts, hydrogels, solutions, and powders. As biodegradable polymers can be degraded by microorganisms activity, they have some advantage over conventional polymeric systems leading to having greater control over the release of active component [47].

Nanocomposites based on polymer and low clay loading are new materials for the controlled release of materials [48, 49]. This group of nanocomposites consists of a polymeric matrix in which layered nano-scaled silicate is dispersed. The clay minerals are the general type of 2:1 layer- or phyllo-silicates including synthetic mica, saponite, montmorillonite, etc. In these minerals, silicate layers of 1 nm thickness and 10–2000 nm length are stacked [50-52]. It has been reported that the combination of polymer and clay could demonstrate greater control rate for the release of materials and could provide a firm network through strengthening the lattice structure [53].

### *4.1. Chitosan/Clay Nanocomposites*

By partial deacetylation of chitin (abundantly found in the exoskeleton of water animals such as shrimp, crab, etc.), chitosan polysaccharide is derived [54]. Chitosan is considered as a naturally abundant material due to being naturally regenerating resource; moreover, it is degradable and non-toxic. Owing to the mentioned properties, this polysaccharide has gained considerable attention in various applications such as agricultural applications [54-59]. Chitosan has been used as a coating for compound fertilizers such as potassium, phosphorus, and nitrogen compounds [60]. Incorporation of layered silicates such as montmorillonite in the polymer could improve some properties such as the adsorption capacity for chemical compounds as well as water. Santos et al. [61] developed chitosan and montmorillonite clay microspheres containing potassium using a coagulation route. They reported that the incorporation of montmorillonite into chitosan resulted in enhanced sorption properties compared to the neat chitosan microspheres. Souza et al. [62] monitored the performance of microspheres based on chitosan/clay hybrid for the release of potassium nitrate in lettuce cultivation. Based on the obtained results, soils that were treated with the nanocomposites exhibited higher electrical conductivity and moisture. Additionally, in comparison with conventional fertilization, a gradual and homogenous release was observed. According to the statistical analysis, the nanocomposite microspheres exhibited an efficient, controlled release of nitrogen.

Messa et al. [63] developed microparticles of chitosan and montmorillonite for prolonged potassium nitrate release as an efficient fertilizer. The results indicated that the prepared microparticles could maintain higher potassium content in the soil for up to several weeks. They proposed that the chitosan/clay microparticles are good candidates for agricultural applications due to their release efficiency.

### *4.2. Alginate/Clay Nanocomposites*

Alginate is a linear polysaccharide consisting of β-D mannuronic

acid moieties and 1–4 linked α-L-guluronic in different compositions that is obtained from brown seaweed [64]. By incorporation of $Ca^{2+}$ ions in an aqueous solution, alginate can be ionically crosslinked. As a result of this mild gelation capability, alginate is widely utilized as fertilizing systems with the controlled-release [64, 65]. On the other hand, the sodium alginate matrix is easily destructed by monovalent cations with poor mechanical properties. Moreover, controlled-release behavior is not always observed in sodium alginate hydrogels. A burst release of nutrients at the first stage is exhibited and then the remaining nutrients are released slowly [66]. He et al. [67] used sodium bentonite and alginate composites to encapsulate Raoultella planticola Rs-2 to prepare a slow-release biofertilizer with high efficiency and minimized production costs. After six months of storage, around 88.9% of Rs-2 in dried bentonite/alginate microcapsules survived. The efficient amount of alginate for the production of desirable composite microcapsules was remarkably lower compared to alginate alone. Release rate, biodegradability, and swelling decreased with increasing the content of bentonite and enhanced with the increment of NaAlg content. An initial burst in release curves of bacteria was observed for all the composite microcapsules; then a gradual increase occurred indicating that the release model was the first-order release. Therefore, the low-cost encapsulated microcapsules could be offered as promising slow-release fertilizers in farmlands. In another research, Singh et al. [68] synthesized starch–alginate beads by the incorporation of bentonite and kaolin for modification of the thiram fungicide release as well as minimizing the environmental contamination. Kaolin and bentonite were employed as adsorbent materials in the bead composition. According to the results, the addition of bentonite and kaolin to starch–alginate beads led to the controlled release of thiram. In comparison with the kaolin-based beads, the bentonite-based composition demonstrated a slower release rate.

### *4.3. Cellulose and their derivative*

The most abundantly found biopolymer on earth is cellulose, which is the main constituent of plant-based materials such as hemp, wood, and cotton [69]. This linear polysaccharide is composed of β (1-4) linked D-glucose units (several hundred to thousands). There are multiple hydroxyl groups on the glucose units, which can react with different reagents either fully or partially to form other derivatives including cellulose esters and cellulose ethers [70].

As a result of film-forming ability, biodegradability, and renewability, the application of cellulose and its derivatives as carriers for fertilizing substances has attracted attention [45, 71-74]. The primarily used cellulose derivative for fertilizer coating is ethylene cellulose (EC), which is a biodegradable, hydrophobic, and inert material. Pérez et al. [75] sprayed EC ethanol solution (5%) onto urea-lignin particles in a Wurster fluidized bed at 60 °C. Different coating thicknesses of EC were applied on the particles and the nitrogen-release rates were measured by water leaching experiments. The observations showed that EC coating could inhibit water diffusion and decrease the nitrogen release rate.

Ni et al. [76] developed a slow-release nitrogen fertilizer system based on natural attapulgite clay, EC film, and sodium carboxymethylcellulose/hydroxyethylcellulose hydrogel. They reported that the prepared fertilizer system could effectively decrease the loss of nutrients, enhance the efficiency of water consumption, and increase the time of irrigation cycles in drought-prone environments.

### *4.4. Acrylamide/clay nanocomposites*

Most superabsorbents are produced using synthetic hydrophilic polymers including polyacrylic acid or polyacrylic acid-poly acrylamide copolymer; however, they suffer from poor degradability in soil and accumulation over time [77].

Verma et al. [78] synthesized nanoclay/polymer composite based on in-situ polymerized acrylic acid-acrylamide and modified nanoclay for the availability of phosphorus for wheat as a test crop. They reported that the amount of phosphorus uptake enhanced from 3.32 mg $kg^{-1}$ to 8.71 mg $kg^{-1}$ for the treatment by conventional diammonium phosphate fertilizer and nanoclay/polymer composite treatment in Alfisol, respectively. The amount of increase in the case of Inceptisol was from 4.45 to 9.78 mg $kg^{-1}$. The percentage of soil phosphorus fixation at the flowering stage decreased from 50 to 0 and from 60 to 19 in Inceptisol and Alfisol, respectively. Moreover, fertilizer phosphorus use efficiency improved by loading phosphorus into the nanoclay-polymer composite. Thus, the modified nanoclay/polymer composite exhibited promising properties as a fertilizer carrier to decrease production cost and enhance nutrient use efficiency, particularly for phosphorus because its availability in soil is very low.

Rashidzadeh et al. [79] developed a slow-released system for nitrogen, phosphorus, and potassium (NPK) fertilizer encapsulated in a superabsorbent nanocomposite. NPK was encapsulated by in-situ polymerization of acrylamide, acrylic acid, and sodium alginate in the presence of montmorillonite clay. According to the results, the incorporation of montmorillonite led to the release of the nutrients in a more controlled way compared to neat superabsorbent. Because of good water retention capacity and good slow-release property, this system could be offered as a potential fertilizer carrier for agricultural applications.

## 5. Conclusions and future insights

It can be concluded that a significant part of the growing research fields is focused on polymer/clay nanocomposites for various challenging applications. More importantly, by the continuous increase in population, there is an ever-increasing food demand worldwide; therefore, it is necessary to increase crop productivity is to provide sufficient food for people. On the one hand, crop productivity could be achieved by using fertilizers. On the other hand, overusing fertilizers can cause some damage to environments and human health. Hence, to enhance the efficiency of fertilizing, slow-release fertilizers have attracted much attention. Polymer/clay nanocomposites exhibit promising properties to be used as superabsorbent and slow-release fertilizing systems [80].

In this regard, there will be further growth in the application of clays in different fields, especially in industrial and environmental applications. The significant technological importance of these composites is due to their tailoring characteristics including size, shape, hydrophilicity, and elementary building unit combinations. Various types of these minerals and their composites have not yet been widely investigated to develop new high-performance polymer composites. Therefore, the properties of these composites will be tailored to expand their potential applications.

REFERENCES

[1] B. Ni, M. Liu, S. Lü, Multifunctional slow-release urea fertilizer from ethylcellulose and superabsorbent coated formulations, Chemical Engineering Journal 155(3) (2009) 892-898.

[2] W. Wang, A. Wang, Synthesis, swelling behaviors, and slow-release characteristics of a guar gum-g-poly (sodium acrylate)/sodium humate superabsorbent, Journal of Applied polymer science 112(4) (2009) 2102-2111.

[3] S. Al-Zahrani, Utilization of polyethylene and paraffin waxes as controlled delivery systems for different fertilizers, Industrial & engineering chemistry research 39(2) (2000) 367-371.

[4] R. Parish, Effect of coating thickness on spreader damage to encapsulated controlled-release fertilizer granules, Applied Engineering in Agriculture 17(4) (2001) 459.

[5] A. Pakseresht, A. Javadi, E. Ghasali, A. Shahbazkhan, S. Shakhesi, Evaluation of hot corrosion behavior of plasma sprayed thermal barrier coatings with graded intermediate layer and double ceramic top layer, Surface and Coatings Technology 288 (2016) 36-45.

[6] A. Giroto, S. Fidélis, C. Ribeiro, Controlled release from hydroxyapatite nanoparticles incorporated into biodegradable, soluble host matrixes, Rsc Advances 5(126) (2015) 104179-104186.
[7] U. Shavit, M. Reiss, A. Shaviv, Wetting mechanisms of gel-based controlled-release fertilizers, Journal of Controlled Release 88(1) (2003) 71-83.
[8] S. Saadi, B. Nazari, Submission Title: Recent Developments and Applications of Nanocomposites in Solar Cells: a Review, Composites and Compounds 1(1) (2019).
[9] S.S. Ray, M. Okamoto, New polylactide/layered silicate nanocomposites, 6 melt rheology and foam processing, Macromolecular materials and engineering (288; NUMB 12) (2003) 936-944.
[10] Q. Zeng, A. Yu, G. Lu, D.R. Paul, Clay-based polymer nanocomposites: research and commercial development, Journal of nanoscience and nanotechnology 5(10) (2005) 1574-1592.
[11] P.C. LeBaron, Z. Wang, T.J. Pinnavaia, Polymer-layered silicate nanocomposites: an overview, Applied clay science 15(1-2) (1999) 11-29.
[12] T.J. Pinnavaia, G.W. Beall, Polymer-clay nanocomposites, John Wiley2000.
[13] C. Kannan, R. Ramanujam, Comparative study on the mechanical and microstructural characterisation of AA 7075 nano and hybrid nanocomposites produced by stir and squeeze casting, Journal of advanced research 8(4) (2017) 309-319.
[14] R. Singh, V. Mahto, Synthesis, characterization and evaluation of polyacrylamide graft starch/clay nanocomposite hydrogel system for enhanced oil recovery, Petroleum Science 14(4) (2017) 765-779.
[15] M. Mousa, N.D. Evans, R.O. Oreffo, J.I. Dawson, Clay nanoparticles for regenerative medicine and biomaterial design: a review of clay bioactivity, Biomaterials 159 (2018) 204-214.
[16] S. Wu, A. Cheng, H. Hua, J. Shen, A study on structure and mechanical properties of polyurethane/organic-montmorillonite nanocomposites, Polymer-Plastics Technology and Engineering 45(6) (2006) 685-689.
[17] W. Chow, J. Teoh, L. Lim, Mechanical and hygrothermal aging study on polystyrene/organo-montmorillonite nanocomposites, Polymer-Plastics Technology and Engineering 47(10) (2008) 1040-1045.
[18] S.C. Tjong, Structural and mechanical properties of polymer nanocomposites, Materials Science and Engineering: R: Reports 53(3-4) (2006) 73-197.
[19] S. Pavlidou, C. Papaspyrides, A review on polymer–layered silicate nanocomposites, Progress in polymer science 33(12) (2008) 1119-1198.
[20] G. Sposito, N.T. Skipper, R. Sutton, S.-h. Park, A.K. Soper, J.A. Greathouse, Surface geochemistry of the clay minerals, Proceedings of the National Academy of Sciences 96(7) (1999) 3358-3364.
[21] M. Alexandre, P. Dubois, Polymer-layered silicate nanocomposites: preparation, properties and uses of a new class of materials, Materials Science and Engineering: R: Reports 28(1-2) (2000) 1-63.
[22] L. Bazli, A. Khavandi, M.A. Boutorabi, M. Karrabi, Correlation between viscoelastic behavior and morphology of nanocomposites based on SR/EPDM blends compatibilized by maleic anhydride, Polymer 113 (2017) 156-166.
[23] G. Madhumitha, J. Fowsiya, S. Mohana Roopan, V.K. Thakur, Recent advances in starch–clay nanocomposites, International Journal of Polymer Analysis and Characterization 23(4) (2018) 331-345.
[24] J.M. Garces, D.J. Moll, J. Bicerano, R. Fibiger, D.G. McLeod, Polymeric nanocomposites for automotive applications, Advanced Materials 12(23) (2000) 1835-1839.
[25] A.C. Lima, L.M. Jou, O.E. Barcia, I.C. Margarit-Mattos, Montmorillonite as corrosion protective pigment, Corrosion Science 141 (2018) 182-194.
[26] A.M. Youssef, S.M. El-Sayed, Bionanocomposites materials for food packaging applications: Concepts and future outlook, Carbohydrate polymers 193 (2018) 19-27.
[27] E. Asadi, A. Fassadi Chimeh, S. Hosseini, S. Rahimi, B. Sarkhosh, L. Bazli, R. Bashiri, A.H. Vakili Tahmorsati, A Review of Clinical Applications of Graphene Quantum Dot-based Composites, Composites and Compounds 1(1) (2019).
[28] W. Paul, C.P. Sharma, Inorganic nanoparticles for targeted drug delivery, Biointegration of Medical Implant Materials, Elsevier2020, pp. 333-373.
[29] J.-H. Chang, Y.U. An, D. Cho, E.P. Giannelis, Poly (lactic acid) nanocomposites: comparison of their properties with montmorillonite and synthetic mica (II), Polymer 44(13) (2003) 3715-3720.
[30] S.H. Cypes, W.M. Saltzman, E.P. Giannelis, Organosilicate-polymer drug delivery systems: controlled release and enhanced mechanical properties, Journal of controlled release 90(2) (2003) 163-169.
[31] A. Kiersnowski, J. Pigłowski, Polymer-layered silicate nanocomposites based on poly (ε-caprolactone), European polymer journal 40(6) (2004) 1199-1207.
[32] E. Günister, D. Pestreli, C.H. Ünlü, O. Atıcı, N. Güngör, Synthesis and characterization of chitosan-MMT biocomposite systems, Carbohydrate Polymers 67(3) (2007) 358-365.
[33] C. Pérez, V. Alvarez, A. Vazquez, Creep behaviour of layered silicate/starch–polycaprolactone blends nanocomposites, Materials Science and Engineering: A 480(1-2) (2008) 259-265.
[34] Y. Rao, Gelatin–clay nanocomposites of improved properties, Polymer 48(18) (2007) 5369-5375.
[35] M.-Y. Chang, R.-S. Juang, Stability and catalytic kinetics of acid phosphatase immobilized on composite beads of chitosan and activated clay, Process Biochemistry 39(9) (2004) 1087-1091.
[36] M.-Y. Chang, R.-S. Juang, Use of chitosan–clay composite as immobilization support for improved activity and stability of β-glucosidase, Biochemical Engineering Journal 35(1) (2007) 93-98.
[37] M.-Y. Chang, H.-C. Kao, R.-S. Juang, Thermal inactivation and reactivity of β-glucosidase immobilized on chitosan–clay composite, International journal of biological macromolecules 43(1) (2008) 48-53.
[38] V.B. Yadav, R. Gadi, S. Kalra, Clay based nanocomposites for removal of heavy metals from water: A review, Journal of Environmental Management 232 (2019) 803-817.
[39] E.I. Unuabonah, A. Taubert, Clay–polymer nanocomposites (CPNs): Adsorbents of the future for water treatment, Applied Clay Science 99 (2014) 83-92.
[40] S.A. Hosseini, M. Vossoughi, N.M. Mahmoodi, M. Sadrzadeh, Clay-based electrospun nanofibrous membranes for colored wastewater treatment, Applied Clay Science 168 (2019) 77-86.
[41] M.E. Trenkel, Slow-and controlled-release and stabilized fertilizers: An option for enhancing nutrient use efficiency in agriculture, IFA, International fertilizer industry association2010.
[42] M. Sultan, A. Abdelhakim, M. Nassar, Cellulose-Based Hydrogels as Smart, Green and Controllable Nitrogenous Fertilizers Releasing Agents, Journal of Testing and Evaluation 49(4) (2019).
[43] B. Zhao, S. Dong, J. Zhang, P. Liu, Effects of controlled-release fertiliser on nitrogen use efficiency in summer maize, PloS one 8(8) (2013).
[44] J. Li, X. Zhuang, O. Font, N. Moreno, V.R. Vallejo, X. Querol, A. Tobias, Synthesis of merlinoite from Chinese coal fly ashes and its potential utilization as slow release K-fertilizer, Journal of hazardous materials 265 (2014) 242-252.
[45] A. Bortolin, F.A. Aouada, L.H. Mattoso, C. Ribeiro, Nanocomposite PAAm/methyl cellulose/montmorillonite hydrogel: evidence of synergistic effects for the slow release of fertilizers, Journal of agricultural and food chemistry 61(31) (2013) 7431-7439.
[46] L. Bazli, M.H. Bagherian, M. Karrabi, F. Abbassi-Sourki, H. Azizi, Effect of starch ratio and compatibilization on the viscoelastic behavior of POE/starch blends, Journal of Applied Polymer Science (2019) 48877.
[47] T.S. Daitx, M. Giovanela, L.N. Carli, R.S. Mauler, Biodegradable polymer/clay systems for highly controlled release of NPK fertilizer, Polymers for Advanced Technologies 30(3) (2019) 631-639.
[48] K. Yano, A. Usuki, A. Okada, T. Kurauchi, O. Kamigaito, Polymer Science Part A, Polymer Chemistry 31 (1993) 2493.
[49] R. Bharadwaj, A. Mehrabi, C. Hamilton, C. Trujillo, M. Murga, R. Fan, A. Chavira, A. Thompson, Structure–property relationships in cross-linked polyester–clay nanocomposites, Polymer 43(13) (2002) 3699-3705.
[50] N. Sheng, M.C. Boyce, D.M. Parks, G. Rutledge, J. Abes, R. Cohen, Multiscale micromechanical modeling of polymer/clay nanocomposites and the effective clay particle, Polymer 45(2) (2004) 487-506.
[51] C. Thellen, C. Orroth, D. Froio, D. Ziegler, J. Lucciarini, R. Farrell, N.A. D'Souza, J.A. Ratto, Influence of montmorillonite layered silicate on plasticized poly (l-lactide) blown films, Polymer 46(25) (2005) 11716-11727.
[52] L. Bazli, A. Khavandi, M.A. Boutorabi, M. Karrabi, Morphology and viscoelastic behavior of silicone rubber/EPDM/Cloisite 15A nanocomposites based on Maxwell model, Iranian Polymer Journal 25(11) (2016) 907-918.
[53] N. Xiaoyu, W. Yuejin, W. Zhengyan, W. Lin, Q. Guannan, Y. Lixiang, A novel slow-release urea fertiliser: Physical and chemical analysis of its structure and study of its release mechanism, Biosystems engineering 115(3) (2013) 274-282.
[54] M. Rinaudo, Chitin and chitosan: properties and applications, Progress in polymer science 31(7) (2006) 603-632.
[55] Q. Li, E. Dunn, E. Grandmaison, M.F. Goosen, Applications and properties of chitosan, Journal of Bioactive and Compatible Polymers 7(4) (1992) 370-397.
[56] K. Haraguchi, Nanocomposite hydrogels, Current Opinion in Solid State and Materials Science 11(3-4) (2007) 47-54.
[57] X. Wang, S. Lü, C. Gao, X. Xu, Y. Wei, X. Bai, C. Feng, N. Gao, M. Liu, L. Wu, Biomass-based multifunctional fertilizer system featuring controlled-release nutrient, water-retention and amelioration of soil, RSC advances 4(35) (2014) 18382-18390.
[58] K. Xing, X. Zhu, X. Peng, S. Qin, Chitosan antimicrobial and eliciting properties for pest control in agriculture: a review, Agronomy for Sustainable Develop-

ment 35(2) (2015) 569-588.
[59] J.J. Perez, N.J. Francois, Chitosan-starch beads prepared by ionotropic gelation as potential matrices for controlled release of fertilizers, Carbohydrate polymers 148 (2016) 134-142.
[60] D.Y. Wu, S. Meure, D. Solomon, Self-healing polymeric materials: a review of recent developments, Progress in polymer science 33(5) (2008) 479-522.
[61] B.R. dos Santos, F.B. Bacalhau, T. dos Santos Pereira, C.F. Souza, R. Faez, Chitosan-montmorillonite microspheres: a sustainable fertilizer delivery system, Carbohydrate polymers 127 (2015) 340-346.
[62] C.F. Souza, R. Faez, F.B. Bacalhau, M.F. Bacarin, T.S. Pereira, In situ monitoring of a controlled release of fertilizers in lettuce crop, Engenharia Agrícola 37(4) (2017) 656-664.
[63] L.L. Messa, C.F. Souza, R. Faez, Spray-dried potassium nitrate-containing chitosan/montmorillonite microparticles as potential enhanced efficiency fertilizer, Polymer Testing 81 (2020) 106196.
[64] M. George, T.E. Abraham, Polyionic hydrocolloids for the intestinal delivery of protein drugs: alginate and chitosan—a review, Journal of controlled release 114(1) (2006) 1-14.
[65] Z. Wu, Y. Zhao, I. Kaleem, C. Li, Preparation of calcium–alginate microcapsuled microbial fertilizer coating Klebsiella oxytoca Rs-5 and its performance under salinity stress, European journal of soil biology 47(2) (2011) 152-159.
[66] A.L. Córdoba, L. Deladino, M. Martino, Effect of starch filler on calcium-alginate hydrogels loaded with yerba mate antioxidants, Carbohydrate polymers 95(1) (2013) 315-323.
[67] Y. He, Z. Wu, L. Tu, Y. Han, G. Zhang, C. Li, Encapsulation and characterization of slow-release microbial fertilizer from the composites of bentonite and alginate, Applied Clay Science 109 (2015) 68-75.
[68] B. Singh, D. Sharma, R. Kumar, A. Gupta, Controlled release of the fungicide thiram from starch–alginate–clay based formulation, Applied Clay Science 45(1-2) (2009) 76-82.
[69] D. Klemm, B. Heublein, H.P. Fink, A. Bohn, Cellulose: fascinating biopolymer and sustainable raw material, Angewandte chemie international edition 44(22) (2005) 3358-3393.
[70] I. Siró, D. Plackett, Microfibrillated cellulose and new nanocomposite materials: a review, Cellulose 17(3) (2010) 459-494.
[71] D. Davidson, F.X. Gu, Materials for sustained and controlled release of nutrients and molecules to support plant growth, Journal of agricultural and food chemistry 60(4) (2012) 870-876.
[72] S. Bajpai, M. Swarnkar, S. Ahuja, On-demand release of urea from a cellulosic hydrogel using a sprinkler based irrigation (SBI) model, Journal of Macromolecular Science, Part A 52(10) (2015) 779-785.
[73] H. Li, Y. Zhou, W. Tu, J. Ye, Z. Zou, State-of-the-art progress in diverse heterostructured photocatalysts toward promoting photocatalytic performance, Advanced Functional Materials 25(7) (2015) 998-1013.
[74] H.A. Essawy, M.B. Ghazy, F.A. El-Hai, M.F. Mohamed, Superabsorbent hydrogels via graft polymerization of acrylic acid from chitosan-cellulose hybrid and their potential in controlled release of soil nutrients, International journal of biological macromolecules 89 (2016) 144-151.
[75] M. Fernández-Pérez, F. Garrido-Herrera, E. González-Pradas, M. Villafranca-Sánchez, F. Flores-Céspedes, Lignin and ethylcellulose as polymers in controlled release formulations of urea, Journal of applied polymer science 108(6) (2008) 3796-3803.
[76] B. Ni, M. Liu, S. Lu, L. Xie, Y. Wang, Environmentally friendly slow-release nitrogen fertilizer, Journal of agricultural and food chemistry 59(18) (2011) 10169-10175.
[77] B. Ni, M. Liu, S. Lü, L. Xie, Y. Wang, Multifunctional slow-release organic–inorganic compound fertilizer, Journal of agricultural and food chemistry 58(23) (2010) 12373-12378.
[78] Y. Verma, S. Datta, I.K. Mandal, D. Sarkar, Effect of phosphorus loaded organically modified nanoclay-polymer composite on release and fixation of phosphorus and its uptake by wheat (Triticum aestivum L.), Journal of Pure and Applied Microbiology 10(3) (2016) 2299-2306.
[79] A. Rashidzadeh, A. Olad, Slow-released NPK fertilizer encapsulated by NaAlg-g-poly (AA-co-AAm)/MMT superabsorbent nanocomposite, Carbohydrate polymers 114 (2014) 269-278.
[80] Y.D. Noh, S. Komarneni, M. Park, Mineral-based slow release fertilizers: a review, Korean Journal of Soil Science and Fertilizer 48(1) (2015) 1-7.

Available online at www.jourcc.com

Journal homepage: www.JOURCC.com

Journal of Composites and Compounds

# Self-expanding stents based on shape memory alloys and shape memory polymers

*Samira Orouji Omid[a]*, Zahra Goudarzi[b], Leila Momeni Kangarshahi[c], Ali Mokhtarzade[d], Fateme Bahrami[e]*

[a] *Nursing Care Research Center, Iran University of Medical Sciences, Tehran, Iran*
[b] *Department of Mining and Metallurgical Engineering, Amirkabir University of Technology, Tehran, Iran*
[c] *Department of Materials and Metallurgical Engineering, Ferdowsi University of Mashhad, Mashhad, Iran*
[d] *Department of biomedical engineering, Amirkabir University of Technology, Tehran, Iran*
[e] *Department of Physics, Amirkabir University of Technology, Tehran, Iran*

A B S T R A C T

A stenotic vessel can be opened using net-shape tubes called "stents" leading to the restoration of the bloodstream. Compared to the commonly used stainless steel stent, self-expandable stents have some advantages. They do not suffer from the risks of damage to the vascular tissue due to the balloon expansion. Moreover, overexpansion for compensating the elastic recoil is not needed, and there is no constant force applied on the artery until the occlusion of the device by the artery stops. However, the stent cannot restore the original dimensions of the vessel in the case of calcified plaques. Self-expandable stents can be utilized for the treatment of atherosclerotic lesions in the carotid, coronary, and peripheral arteries. Shape memory alloys (SMAs), mainly NiTi (nitinol), are employed for self-expandable vascular stent applications. Nitinol is widely applied for medical devices and implants due to its excellent fatigue performance, mechanical properties, and biocompatibility, which make this alloy suitable for long-term installations. Other materials used for self-expandable cardiovascular stents are shape memory polymers (SMPs). Shape memory effect is triggered by the hydration of polymers or temperature change preventing the collapse of small blood vessels. This review has focused on the mechanisms and properties of SMAs and SMPs as promising materials for stent application.



Peer review under responsibility of jourcc

A R T I C L E I N F O R M A T I O N

*Article history:*
Received 2 June 2020
Received in revised form 12 June 2020
Accepted 29 June 2020

*Keywords:*
Self-expanding stents
Shape memory alloys
Shape memory polymers
Nitinol

Table of contents



## 1. Introduction

The development of SMPs is the result of scientists' desire for the production of next-generation functional materials exhibiting interesting characteristics. As a result of various potential applications as well as facile manufacturing, blend and composite polymers, especially SMPs, have greatly desirable among researchers [1-4]. This technology provides the possibility to produce desired polymer architectures that can be tailored by the conditions of thermo-mechanical programming to fabricate high-performance polymers with sophisticated characteristics required for special applications [5-7]. Upon an external stimulus exposure, SMPs are able to transform their temporary shape to their original shape, which is known as the shape memory effect (SME). Due to the dual- or multi-shape capability, these promising materials can be used in different applications such as drug carriers, self-deployable space structures, intelligent medical devices, stents, self-assembling mobile phones, smart fabrics, etc. The external stimulus for SME includes light, direct or indirect heating, solvent exposure, or changes in pH. Using a combination of careful thermo-mechanical programming and polymer

* *Corresponding author: Samira Orouji Omid; E-mail: samira.oroujiomid85@gmail.com*
https://doi.org/10.29252/jcc.2.2.5 

morphology, SME is achieved [8, 9].

A gold-cadmium alloy was the first material whose shape memory effect was discovered by Chang and Read in 1951 [10]. Before them, Vernon reported a type of SME in a dental material based on methacrylic acid resin in 1941 [11]. An equimolar alloy of Ni and Ti, called nitinol, with shape memory properties was reported first by Buehler et al. [12] in 1963. Ti and its alloys have been considered as proper materials for implants due to their good performance in body [13-15]. In continuation of materials with the SME, a number of ceramics and metallic alloys were found by researchers to have the SME behavior [16-18]. The SME in shape memory alloys is based on the reversible thermal transitions between the martensitic phase formed at low temperature and the austenitic phase formed at high temperature [18]. NiTi, CuAlNi, and CuZnAl are the most popular SMAs among all shape memory alloys due to their performance indexes [19].

SMPs exhibit better properties compared to SMAs in many respects. For example, their recoverable strain is greater, they can be processed easily, and they are lighter and cost-effective. Furthermore, they have easily tuned properties and they are responsive to various stimuli [8]. A heat-shrinkable polymer based on covalently cross-linked polyethylene (PE) was developed in the 1980s, exhibiting SME properties. In this polymer, the permanent shape is because of covalent cross-links, and the switching process results from the melting of PE crystallites [20]. Later on, various SMPs based on polynorbornene [21, 22], poly(vinyl alcohol) [23, 24], and polyurethanes [25, 26] were developed.

SMAs have the capability to recover up to 10% of apparent permanent deformations as well as the typical peculiarities related to metals such as workability, stiffness, resistance, and so on. In the common mechanical world, health was the first field where SMAs were utilized extensively since some SMAs have been found to be almost perfectly biocompatible. The most evident examples of SMAs potentials are orthodontic wires and aortic stents, which are part of everyday life [27]. This article summarizes the mechanisms, properties, and application of SMAs and SMPs as stents and most important steps in their development are studied.

## 2. The shape memory cycle in SMPs

Generally, the shape memory cycle involves four stages. First, the material is deformed then is cooled (stage 1-2). The stages 3 and 4 are fixing and recovery [28]. At the first stage, the deformation of the sample to a predetermined strain or stress is done at its deformation temperature ($T_d$). Due to heating above $T_d$, which is above the switching or transition temperature of $T_{trans}$, molecular switches are opened and the shape deformation can occur. Thereafter, the sample is cooled from $T_d$ to a set temperature of $T_s$ under pre-strain constraint. $T_s$ is below the $T_{trans}$, and the deformation history (strain) is stored during the cooling stage. At this stage, the switches become closed and a temporary shape is fixed. At the third stage, a stress-free condition is obtained due to the release of the initial deformation constraint at $T_s$. At the last stage, the opening of the molecular switches occurs by heating again above $T_{trans}$. This stage is the unconstrained recovery under stress-free condition, and the sample achieves its initial permanent shape again. Experimental conditions, geometric considerations, and material properties can affect the whole SM cycle time [29, 30].

## 3. Mechanism of shape memory effect in polymers

SMPs are elastic networks possessing suitable molecular switches responding to stimuli and can form physical cross-links when the temperature is below a critical temperature leading to the temporary shape fixing. Their permanent shape is determined by linking chain segments

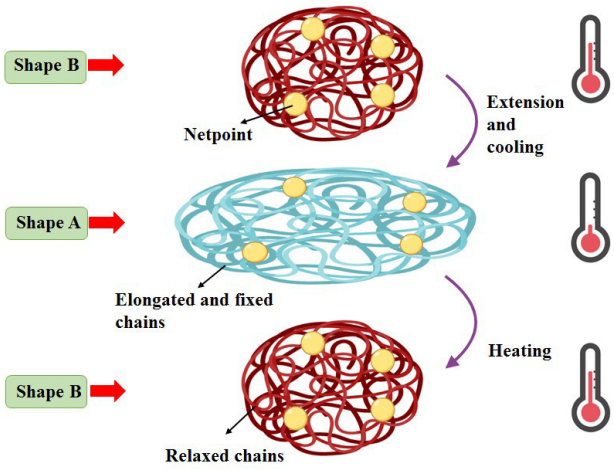


**Fig. 1.** Shape memory effect in polymers.

by net points of either covalent bonds or physical nature such as crystallites. The SME is considered as an entropic phenomenon [31]. In the permanent macroscopic shapes, the molecular chains are thermodynamically stable and their entropy has the highest value. A less stable state with lower entropic is obtained when a macroscopic deformation is applied due to the changes in molecular chain conformation. This entropic state is kinetically trapped while the material undergoes cooling below $T_{trans}$ because the molecular chains freeze and the new conformation of the chains is fixed. Heating above the $T_{trans}$ increases the mobility of molecules resulting in the release of strain energy and getting back to the original shape with the highest entropy and lowest energy (Fig. 1) [30]. Therefore, switch segments fix the temporary shape in SMPs. It should be mentioned that the SME could not be achieved by segmental switching alone. A precondition required for an ideal process of shape recovery is the inhibition of long-range slippage of chains leading to the macroscopic deformation. Thus, the net points should have sufficient stability to resist the thermo-mechanical conditions in order to experience complete recovery. These net points might be either chemical crosslinks by covalent bonds or physical interactions such as chain entanglements, ionic clusters, hydrogen bonding, glassy hard domains, or crystallites. While net points with physical interactions provide reprocessability, a complete recovery is not offered due to weak interactions. On the other hand, an almost complete recovery is achieved by strong chemical crosslinks, but reprocessability is not obtained [28].

## 4. Mechanism of shape memory effect in alloys

Shape memory alloys possess two stable phases that have various crystal structures and characteristics. The phase formed at high temperature is austenite (parent phase) with the crystal structure of body centered cubic. The phase formed at low temperature is martensite that has a lower symmetry crystallized in monoclinic, orthorhombic, or tetragonal structure. Twinned and de-twinned forms are two forms that the martensite assembly can appear.

The reversible transformation of SMAs from the austenite phase to the martensite phase is the base of their functional properties. When there is no loading, austenitic phase transforms into different martensite variants (up to 24 for nitinol) upon cooling, which results in twinned martensite. This transition between the two phases is time-independent and does not proceed by the diffusion of atoms, because atoms need small movements in the crystal lattice for the transition. The transformation occurs over a specific temperature range related to the type of the alloy system [27, 32]. Fig. 2 shows the transformation cycle and name of each point. Stress and/or temperature hysteresis is observed in the austenite to martensite phase transformation. $M_s$ and $M_f$ during heating

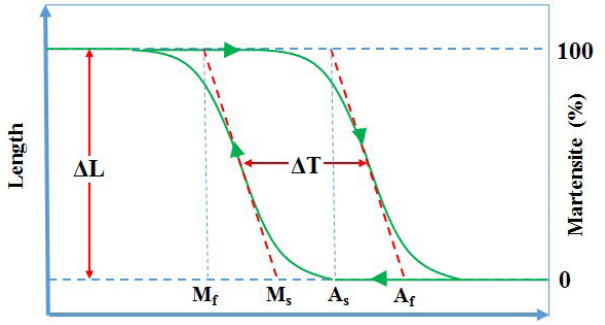


**Fig. 2.** Thermal hysteresis in SMAs.

represent the starting and finishing temperatures of the transformation, whereas $A_s$ and $A_f$ during cooling indicate the beginning and finishing temperatures of the reverse transformation, respectively.

In some NiTi alloys, the phase transition occurs in two steps upon cooling. In these alloys, austenite first transforms into a trigonal structure called the R-phase, and then by the reduction of the temperature, it changes into martensite. Three ways exist for achieving the sequential transformation of austenite-R-martensite: addition of a third element such as Fe, aging of the alloys with a higher Ni content and cold work [33].

Since the 1970s, the intermediate transformation of austenite-R has gained the physicists' attention and material scientists. The σ-ε-T responses show a narrow hysteresis as a result of the austenite-R transformation, and a noticeable change with cycling is not seen through the transformation range. Due to small transformation strains exhibited by austenite-R, excellent fatigue properties are obtained. Considering this property, these alloys are very attractive for being used in actuator applications.

Stress-induced phase transitions can also occur in SMAs besides the transformations by changing temperatures. The transformation to martensite can be achieved by applying a strain to the sample at temperatures above the $A_f$. When the applied stress reached a critical value of $\sigma^{Ms}$, the transformation to martensite is started. In this case, the austenite phase transformation to the de-twinned martensite results in a macroscopic deformation. By applying the load, twinned martensite can be de-twinned, martensite can be reoriented or the de-twinned martensite orientation can be changed with the change in the applied load direction.

The SME is observed in SMAs when they are deformed at low temperatures while retaining the apparent plastic deformation during the unloading step. The original shape is recovered by heating above $A_f$ due to transforming in austenitic [34]. Fig. 3 schematically demonstrates the SME in shape memory alloys showing the stress-strain-temperature diagram. The starting point is from the reference configuration at zero stress and a given temperature. Slope 1-2 shows linear elastic behavior of the material when the stress is increased, then at plateau 2-3, plastic deformations develop at constant stress. However, after the deformation reaches a saturation value, SMA demonstrates a new linear elastic branch with a further increase of the load unlike the typical plastic deformation (slope 3-4). At point 5, a residual strain exists after unloading. This residual deformation can be recovered by the increment of the temperature to a characteristic temperature without applying a load, which is presented in points 6-7. Finally, the complete recovery of the initial material state is possible if the temperature is reduced to the initial temperature [35, 36].

## 5. Shape memory alloys for vascular stents

The stent implantation during transluminal coronary angioplasty can treat coronary arterial stenosis. In 1994, the Food and Drug Administration (FDA) approved the application of coronary stents expanding by balloons. However, a metallic stent was the first clinically applied in 1986. Thereafter, many investigations have been carried out to develop stents with enhanced materials and design. Schematic illustration of vascular stents performance is shown is Fig. 4.

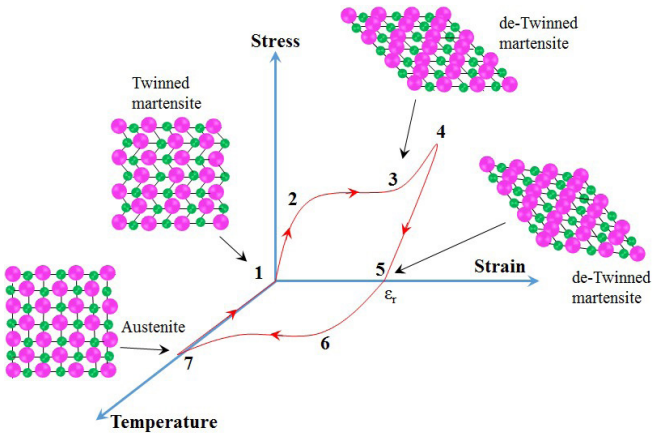


**Fig. 3.** Shape memory effect in SMAs.

As a result of excellent fatigue performance, mechanical characteristics, and biocompatibility, NiTi is widely utilized as materials for medical devices and implants requiring long-term installations [37]. The NiTi-based stent was introduced in 2003, which was perhaps the most famous application of this alloy in medical devices, using the super-elastic behavior of the alloy [38]. The stent is a miniaturized cylindrical elastic device used for the support of diseased arteries. Nitinol is utilized in about 25% of all the stents implanted in arteries. The diameter of self-expanding shape memory alloy stents is larger than that of target arteries. In order for the device to work easily under standard environmental conditions, $A_f$ is set to a small value below the body temperature. The stent is constrained to a rig to inhibit the premature release, and after the installation, it is removed. After a short time of installation, the stent attains its final configuration [39, 40].

An essential property for any biomaterial is biocompatibility, particularly for NiTi, which has the possibility of Ni release. Ni has been proved to have immune-sensitizing, carcinogenic, and toxic effects. However, NiTi is extremely stable and shows very different biocompatibility properties in comparison with Ni alone. In general, some studies have shown that the NiTi alloys exhibit even more biocompatibility than stainless steel [41]. Its good biocompatibility is originated from the more-rapidly oxidized Ti resulting in the formation of protective $TiO_2$ film on the surface, which prevents the release od Ni-ion and provides corrosion resistance [42]. However, the body fluid is highly corrosive and the corrosion resistance is not provided by just the $TiO_2$ layer. Therefore, it is required to modify the surface of NiTi devices to improve surface corrosion resistance and develop implant-safe conditions [43, 44].

Compared to common engineering metals, NiTi alloys show non-standard fatigue and fracture responses due to microstructural evolutions resulting from stress and/or heat and the complex various phases [45]. Consequently, well-known standard fatigue testing procedures and theoretical models cannot be applied, and there is still a lack of universal description for the fatigue behavior of NiTi [45, 46]. In order for nitinol to be more fracture-resistant, recent studies focused on optimizing the applied geometry [47, 48].

For the improvement of the biocompatibility of anodized NiTi, Mohammadi et al. [49] coated the alloy with chitosan-heparin nanoparticles. The results show that the chitosan-heparin coating had the ability

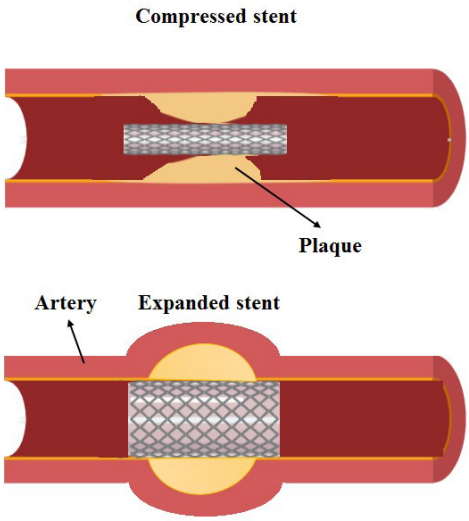


**Fig. 4.** Schematic illustration of vascular stents performance.

to prevent the nickel ion release, while the ion release was observed in the anodized sample without coating. Furthermore, heparin was released in a controlled manner from the coating, resulting in the remarkable enhancement of blood compatibility. The cell compatibility of the coated specimens was confirmed by the attachment and proliferation of HUVECs.

Lotkove et al. [50] used plasma immersion ions to dope Si into intravascular NiTi stent. According to the results, the stress required for the stress-induced martensite formation under loading was reduced by surface modification. The hysteresis was also increased upon unloading. It could be concluded that the Si-doped self-expanding stents are a promising material for peripheral vascular treatment. Park et al. [51] also reported that Ta-coated NiTi stent developed by ion-induced plasma sputtering showed enhanced biocompatibility and radiopacity. The improved radiopacity was stated to be due to the large thickness and the large X-ray absorption coefficient of the Ta coating layer. Additionally, Ta coating was believed to improve the attachment and proliferation of endothelial cells.

Park et al. [52] investigated the influence of the TiN on endothelial cell function on the NiTi alloy and its corrosion resistance. In contrast to bare NiTi, TiN-coated samples showed effective prevention of the Ni ions release, promotion of focal adhesion formation, actin cytoskeleton, and amino acid metabolism, improved inflammation regulation, and enhanced energy metabolism.

Witkowska et al. [53] coated composite surface layers (a-C(Ag)+-$TiO_2$) on NiTi using ion beam assisted deposition. It was found that the produced hybrid surface exhibited improved corrosion resistance, surface roughness, altered surface free energy, and wettability, as well as decreased platelet activation, aggregation, and adhesion compared to the uncoated alloy in the initial state. Therefore, these properties offer great benefits for cardiac applications.

Bakhshi et al. [54] developed a polymeric coating based on poly(carbonate-urea) urethane (PCU) and polyhedral oligomeric silsesquioxanes (POSS) for being applied on the nitinol stent using electrohydrodynamic spraying. According to the results, the POSS–PCU coating on the stent surface could improve biocompatibility and enhance surface resistance. Moreover, the peel strength was improved by surface modification before and after degradation.

## 6. Shape memory polymers for vascular stents

SMPs are used in various possible applications due to having great functionality in SME. The most important applications include engineering, textile, medical, and spacecraft applications. In medical applications, SMP is used as actuation, fixation, and deployment such as cardiovascular stents [55]. Small blood vessels can be protected from collapse, owing to the shape memory effect triggered by hydration of polymers or the temperature change [56, 57].

There is the possibility of artery re-narrowing and occlusion after 6 months using metal stents. These stents must overcome some limitations including thrombogenicity, compliance mismatches, low stiffness, and low flexibility. These devices have been investigated in terms of materials improvement, and the most attractive candidates are biodegradable SMPs [58-61]. Igaki-Tamai stent was one of the first biodegradable shape memory polymer stents. This SMP stent is consisted of poly-l-lactic acid (PLLA), which can recover its shape in 20 min at 37 °C [62]. A bi-layered device composed of PLLA and polyglycolic acid (PLGA) is another example of the biodegradable shape memory stent, which fully degrades at biological environments [63].

Drug delivery systems are gaining increasing significance for the treatment of human diseases [64, 65]. For the prevention of in-stent restenosis, drug-eluting stents (DESs) have been developed recently. It has been found that the restenosis rate can be reduced by local drug delivery. The used drugs in these stents are mainly antibacterial and antiplatelet drugs [66-68].

Yakacki et al. [55] prepared a shape memory polymer using photopolymerization of poly(ethylene glycol) dimethacrylate and tert-butyl acrylate for cardiovascular applications. It was found that crosslink density and $T_g$ highly affected the storage of the stent at room temperature. It was also demonstrated that the crosslink density influenced the stent pressurized response. The prepared SMP showed extensive thermomechanical and shape memory responses to meet the special requirements of cardiovascular devices with minimal invasion.

Biswas et al. [69] developed a biodegradable polyurethane/ two-dimensional platelets nanohybrid SMP for smart biomedical applications such as self-expanding stents. They found that the overall crystallinity in the nanohybrid SMP decreased due to the strong dipolar interaction between polymer chains and nanoclay resulting in remarkable enhancement of flexibility and toughness required for most implants. In addition, the nanohybrid thermal stability improved by the barrier created by the silicate layers of the nanoclay. Therefore, the developed shape memory nanohybrid demonstrated good shape memory property at physiological temperature favored for biomedical applications.

Small et al. [70] presented a novel prototype device comprised of a polyurethane-based SMP stent and a shape memory polymer embolic foam that was attached to the outside of the stent for fusiform aneurysms endovascular embolization. The stent had the role of maintaining an open lumen in the artery and the aneurysm lumen is filled with the embolic foam. An expansion of the foam at body temperature was accompanied by the controlled expansion of the stent in the suitable orientation/location by laser heating. Additionally, for the provision of the control over actuation, a stent with higher elastic modulus and $T_g$ could construct a more rigid structure for supporting the embolic foam. They reported that the laser heating possibly affects the prepheral arterial tissue adversely by direct heating or heat transfer from the device to the blood cells or surrounding tissue. The blood flow convective cooling was stated to be able to alleviate the adverse thermal effects. However, in localized areas, the blood flow is decreased by the device. By optimization of the device, the laser power amount required for expansion, and the consequent adverse effects can be minimized.

The thermo/moisture response of a polyurethane-based SMP was investigated by Sun et al. [71] for possible surgery inside living cells. Polyurethane SMP has been traditionally recognized for its thermo-responsive behavior. Recently, it has been found that moisture can influence its glass transition temperature, enabling us to understand the shape recovery after a pre-determined sequence and the water-driven shape

recovery. These characteristics are in favor of delivering tiny micro/nano devices for surgery in living cells through a hole with a very small size.

Xue et al. [72] developed biodegradable block co-polymers SMPs based on poly(ε-caprolactone) (PCL) and Poly(3-hydroxybutyrate-co-3-hydroxyvalerate) (PHBV) for fast self-expanding stents. They found that the stent containing 25 wt% PHBV exhibited complete self-expansion within 25 s at 37 °C. This performance is much better for the best developed biodegradable stents. Thus, the non-cytotoxic, biodegradable SMP containing 25 wt% PHBV exhibited great thermal expansion property at body temperature proper for fast self-expandable stents.

Baer et al. [73] investigated the expansion, collapse pressure, and thermomechanical properties of neurovascular stent prototypes based on MM7520 polyurethane SMP. According to the results, with the increment of temperature from 32˚C to 47 ˚C, the collapse pressures of the stents decreased. At temperatures higher than 47 ˚C, collapse pressures reached a plateau. At body temperature, the stents showed full collapse pressures values larger than 4.7 psi. After crimping, full recovery was obtained by the stents. Their axial shortening and radial expansion ratio were 1.1% and 2.7, respectively. This investigation revealed the promising application of this SMP as neurovascular stents.

The expansion of an SMP stent was simulated and modeled by Liu et al. [74]. The results showed that the shape memory polymer stent could exhibit a stable and soft expansion in the body. Moreover, by applying a higher recovery temperature and a lower heating rate, higher expansion can be achieved. It was shown that the result of the recovery radius fitting function could well describe the performance of the SMP stent according to the recovery temperature and characteristic recovery ratio. The model was proposed to be proper for assisting the design of SMP stent.

Ansari et al. [75] developed PCL/PU SMP and studied its properties in combined torsion-tension loading for the cardiovascular stent application. They found that the stress-strain behavior of the SMP was significantly affected by the increment of the temperature. In the combined loading, normal strain recovery and angle recovery were influenced by high pre-torsion loading and high pre-stretch, respectively. Minimum elastic recovery was achieved at pre-torsion and pre-stretch of 25% and 720°, respectively. The reduction of recovery finished temperature (RFT) was mostly affected by the heating rate among other parameters. In the combined torsion-tension loading condition, these findings can help to develop novel shape memory polymer structures with enhanced performance in biomedical applications.

Jia et al. [76] developed biodegradable self-expanding vascular stents based on PLA using 3D printing. The prepared stent was able to obtain a temporary compressed shape easy for implantation. The stent could keep the temporary compressed shape at ambient temperature, which makes their storage possible. The stent had also excellent shape fixity. The compressed printed stent could expand to its initial shape by heating after implantation. By taking advantage of both self-expansion of biodegradable PLA and tailored design of 3D printing, cardiovascular disease can be effectively treated by the vascular stent.

Lin et al. [77] developed vascular stents based on PLA by the 4D printing technique with negative Poisson's ratio structure. It was shown that shape recovery of the stents was as high as 98% and they had the ability to expand narrow blood vessels within 5 seconds. However, some limitations were observed in the shape memory stents such as the high $T_g$ value of the shape memory PLA although serious vessel injury has not been observed.

## 7. Conclusion and future insights

SMAs have attracted the attention of many scientists due to their fascinating properties providing their infinite applications. However, a few devices made of SMA have found a place in the market and their commercial use is limited for very precise aims. Currently, the most important applications of these type of materials are in medicine such as stents and orthodontics appliances, micromanipulators, and robotic actuators. Although the application of such compounds in the medical field is continuously growing and has become almost a standard, the certification for biocompatibility is a major issue for biomedical implants. Thus, the development of more biocompatible materials has found a ground to be investigated. Ongoing research on more functional materials ensures the continuity of SMAs for medical issues.

Biodegradable SMPs can be adapted to the various requirements for biomedical applications. Furthermore, some of their properties, such as biodegradability, flexibility, biocompatibility, chemical stability, and their potential for drug delivery, will encourage the research on the development of SMPs. Various applications including tissue engineering, scaffolds for aesthetic or reconstructive surgery, and biomaterial-assisted therapies require such a combination of biodegradability, functions, drug delivery capability, and shape memory. Presently-used multimaterial systems in these fields are not able to fulfill the needs; therefore, materials that possess all these functions will be of great interest.

REFERENCES

[1] W. Huang, Z. Ding, C. Wang, J. Wei, Y. Zhao, H. Purnawali, Shape memory materials, Materials today 13(7-8) (2010) 54-61.
[2] A. Lendlein, R. Langer, Biodegradable, elastic shape-memory polymers for potential biomedical applications, Science 296(5573) (2002) 1673-1676.
[3] H. Won Jang, A. Zareidoost, M. Moradi, A. Abuchenari, A. Bakhtiari, R. Pouriamanesh, B. Malekpouri, A. Jafari Rad, Photosensitive nanocomposites: environmental and biological applications, Journal of Composites and Compounds 1(1) (2020).
[4] L. Bazli, M.H. Bagherian, M. Karrabi, F. Abbassi-Sourki, H. Azizi, Effect of starch ratio and compatibilization on the viscoelastic behavior of POE/starch blends, Journal of Applied Polymer Science 137(29) (2020) 48877.
[5] Q. Meng, J. Hu, A review of shape memory polymer composites and blends, Composites Part A: Applied Science and Manufacturing 40(11) (2009) 1661-1672.
[6] T. Pretsch, Review on the functional determinants and durability of shape memory polymers, Polymers 2(3) (2010) 120-158.
[7] L. Bazli, A. Khavandi, M.A. Boutorabi, M. Karrabi, Morphology and viscoelastic behavior of silicone rubber/EPDM/Cloisite 15A nanocomposites based on Maxwell model, Iranian Polymer Journal 25(11) (2016) 907-918.
[8] J. Parameswaranpillai, S. Siengchin, J.J. George, S. Jose, Shape Memory Polymers, Blends and Composites: Advances and Applications, Springer Singapore2019.
[9] M.C. Serrano, G.A. Ameer, Recent insights into the biomedical applications of shape-memory polymers, Macromolecular bioscience 12(9) (2012) 1156-1171.
[10] L. Chang, T. Read, Plastic deformation and diffusionless phase changes in metals—The gold-cadmium beta phase, JOM 3(1) (1951) 47-52.
[11] L.B. Vernon, H.M. Vernon, Process of manufacturing articles of thermoplastic synthetic resins, Google Patents, 1941.
[12] W.J. Buehler, J. Gilfrich, R. Wiley, Effect of low-temperature phase changes on the mechanical properties of alloys near composition TiNi, Journal of applied physics 34(5) (1963) 1475-1477.
[13] E. Sharifi Sedeh, S. Mirdamadi, F. Sharifianjazi, M. Tahriri, Synthesis and evaluation of mechanical and biological properties of scaffold prepared from Ti and Mg with different volume percent, Synthesis and Reactivity in Inorganic, Metal-Organic, and Nano-Metal Chemistry 45(7) (2015) 1087-1091.
[14] E. Asadi, A. Fassadi Chimeh, S. Hosseini, S. Rahimi, B. Sarkhosh, L. Bazli, R. Bashiri, A.H. Vakili Tahmorsati, A Review of Clinical Applications of Graphene Quantum Dot-based Composites, Composites and Compounds 1(1) (2019).
[15] S. Nasibi, K. Alimohammadi, L. Bazli, S. Eskandarinezhad, A. Mohammadi, N. Sheysi, TZNT alloy for surgical implant applications: A Systematic Review, Composites and Compounds 2(2) (2020).
[16] T. Duerig, D. Richter, J. Albrecht, Shape memory in Ti-10V-2Fe-3Al, Scripta Metallurgica 16(8) (1982) 957-961.
[17] M. Swain, Shape memory behaviour in partially stabilized zirconia ceramics, Nature 322(6076) (1986) 234-236.
[18] T.W. Duerig, J. Albrecht, G.H. Gessinger, A shape-memory alloy for high-temperature applications, JOM 34(12) (1982) 14-20.
[19] W. Huang, On the selection of shape memory alloys for actuators, Materials

& design 23(1) (2002) 11-19.
[20] S. Ota, Current status of irradiated heat-shrinkable tubing in Japan, Radiation Physics and Chemistry (1977) 18(1-2) (1981) 81-87.
[21] D. Ratna, J. Karger-Kocsis, Recent advances in shape memory polymers and composites: a review, Journal of Materials Science 43(1) (2008) 254-269.
[22] J. Parameswaranpillai, S. Siengchin, Shape Memory Polymers, Applied Science and Engineering Progress 10(2) (2017).
[23] T. Hirai, H. Maruyama, T. Suzuki, S. Hayashi, Shape memorizing properties of a hydrogel of poly (vinyl alcohol), Journal of applied polymer science 45(10) (1992) 1849-1855.
[24] T. Hirai, H. Maruyama, T. Suzuki, S. Hayashi, Effect of chemical cross-linking under elongation on shape restoring of poly (vinyl alcohol) hydrogel, Journal of applied polymer science 46(8) (1992) 1449-1451.
[25] B.K. Kim, S.Y. Lee, M. Xu, Polyurethanes having shape memory effects, Polymer-Letchworth 37(26) (1996) 5781-5794.
[26] F. Li, X. Zhang, J. Hou, M. Xu, X. Luo, D. Ma, B.K. Kim, Studies on thermally stimulated shape memory effect of segmented polyurethanes, Journal of Applied Polymer Science 64(8) (1997) 1511-1516.
[27] L. Lecce, A. Concilio, Shape Memory Alloy Engineering: For Aerospace, Structural and Biomedical Applications, Elsevier Science2014.
[28] J. Parameswaranpillai, S.P. Ramanan, J.J. George, S. Jose, A.K. Zachariah, S. Siengchin, K. Yorseng, A. Janke, J.r. Pionteck, PEG-ran-PPG modified epoxy thermosets: a simple approach to develop tough shape memory polymers, Industrial & Engineering Chemistry Research 57(10) (2018) 3583-3590.
[29] Y. Liu, K. Gall, M.L. Dunn, A.R. Greenberg, J. Diani, Thermomechanics of shape memory polymers: uniaxial experiments and constitutive modeling, International Journal of Plasticity 22(2) (2006) 279-313.
[30] J. Parameswaranpillai, S.P. Ramanan, S. Jose, S. Siengchin, A. Magueresse, A. Janke, J.r. Pionteck, Shape memory properties of Epoxy/PPO–PEO–PPO triblock copolymer blends with tunable thermal transitions and mechanical characteristics, Industrial & Engineering Chemistry Research 56(47) (2017) 14069-14077.
[31] M. Behl, J. Zotzmann, A. Lendlein, Shape-memory polymers and shape-changing polymers, Shape-Memory Polymers, Springer2009, pp. 1-40.
[32] E. Oliver, T. Mori, M. Daymond, P. Withers, Neutron diffraction study of stress-induced martensitic transformation and variant change in Fe–Pd, Acta materialia 51(20) (2003) 6453-6464.
[33] E. Gautier, E. Patoor, Experimental observations for shape memory alloys and transformation induced plasticity phenomena, Mechanics of Solids with Phase Changes, Springer1997, pp. 69-103.
[34] E. Patoor, D.C. Lagoudas, P.B. Entchev, L.C. Brinson, X. Gao, Shape memory alloys, Part I: General properties and modeling of single crystals, Mechanics of materials 38(5-6) (2006) 391-429.
[35] C. WYAMAN, Shape memory and related phenomena, Progress in materials Science 36 (1992) 203-224.
[36] D. Mantovani, Shape memory alloys: Properties and biomedical applications, Jom 52(10) (2000) 36-44.
[37] S.A. Shabalovskaya, Surface, corrosion and biocompatibility aspects of Nitinol as an implant material, Bio-medical materials and engineering 12(1) (2002) 69-109.
[38] S.W. Bokhari, O. Vahdat, R.J. Winters, The first clinical experience with a peripheral, self-expanding nitinol stent in the treatment of saphenous vein graft disease: angiographic evidence of late expansion, The Journal of invasive cardiology 15(7) (2003) 418-422.
[39] D. Stoeckel, A. Pelton, T. Duerig, Self-expanding nitinol stents: material and design considerations, European radiology 14(2) (2004) 292-301.
[40] A. Bezrouk, J. Hanus, J. Záhora, Temperature characteristics of nitinol spiral stents, Scripta Med (Brno) 78 (2005) 219-226.
[41] M. Mikulewicz, K. Chojnacka, Release of metal ions from orthodontic appliances by in vitro studies: a systematic literature review, Biological trace element research 139(3) (2011) 241-256.
[42] M. Es-Souni, M. Es-Souni, H. Fischer-Brandies, Assessing the biocompatibility of NiTi shape memory alloys used for medical applications, Analytical and bioanalytical chemistry 381(3) (2005) 557-567.
[43] A.M. Barcelos, A.S. Luna, N.d.A. Ferreira, A.V.C. Braga, D.C.B.d. Lago, L.F.d. Senna, Corrosion evaluation of orthodontic wires in artificial saliva solutions by using response surface methodology, Materials Research 16(1) (2013) 50-64.
[44] S. Shabalovskaya, J. Anderegg, J. Van Humbeeck, Critical overview of Nitinol surfaces and their modifications for medical applications, Acta biomaterialia 4(3) (2008) 447-467.
[45] S. Robertson, A. Pelton, R. Ritchie, Mechanical fatigue and fracture of Nitinol, International Materials Reviews 57(1) (2012) 1-37.
[46] A. Pelton, Nitinol fatigue: a review of microstructures and mechanisms, Journal of Materials Engineering and Performance 20(4-5) (2011) 613-617.
[47] Y. Shen, W. Qian, H. Abtin, Y. Gao, M. Haapasalo, Fatigue testing of controlled memory wire nickel-titanium rotary instruments, Journal of endodontics 37(7) (2011) 997-1001.
[48] A. Pelton, J. Fino-Decker, L. Vien, C. Bonsignore, P. Saffari, M. Launey, M. Mitchell, Rotary-bending fatigue characteristics of medical-grade Nitinol wire, Journal of the mechanical behavior of biomedical materials 27 (2013) 19-32.
[49] F. Mohammadi, N. Golafshan, M. Kharaziha, A. Ashrafi, Chitosan-heparin nanoparticle coating on anodized NiTi for improvement of blood compatibility and biocompatibility, Int J Biol Macromol 127 (2019) 159-168.
[50] A.I. Lotkov, O.A. Kashin, A.N. Kudryashov, K.V. Krukovsky, Structure and properties of self-expanding intravascular NiTi stents doped with Si ions, Materials Today: Proceedings 4(3) (2017) 4647-4651.
[51] C. Park, S. Kim, H.-E. Kim, T.-S. Jang, Mechanically stable tantalum coating on a nano-roughened NiTi stent for enhanced radiopacity and biocompatibility, Surface and Coatings Technology 305 (2016) 139-145.
[52] D. Yang, X. Lu, Y. Hong, T. Xi, D. Zhang, The molecular mechanism for effects of TiN coating on NiTi alloy on endothelial cell function, Biomaterials 35(24) (2014) 6195-205.
[53] J. Witkowska, A. Sowinska, E. Czarnowska, T. Plocinski, B. Rajchel, M. Tarnowski, T. Wierzchon, Structure and properties of composite surface layers produced on NiTi shape memory alloy by a hybrid method, J Mater Sci Mater Med 29(8) (2018) 110.
[54] R. Bakhshi, A. Darbyshire, J.E. Evans, Z. You, J. Lu, A.M. Seifalian, Polymeric coating of surface modified nitinol stent with POSS-nanocomposite polymer, Colloids and Surfaces B: Biointerfaces 86(1) (2011) 93-105.
[55] C.M. Yakacki, R. Shandas, C. Lanning, B. Rech, A. Eckstein, K. Gall, Unconstrained recovery characterization of shape-memory polymer networks for cardiovascular applications, Biomaterials 28(14) (2007) 2255-63.
[56] G.M. Baer, T.S. Wilson, W. Small IV, J. Hartman, W.J. Benett, D.L. Matthews, D.J. Maitland, Thermomechanical properties, collapse pressure, and expansion of shape memory polymer neurovascular stent prototypes, Journal of Biomedical Materials Research Part B: Applied Biomaterials 90(1) (2009) 421-429.
[57] H. Wache, D. Tartakowska, A. Hentrich, M. Wagner, Development of a polymer stent with shape memory effect as a drug delivery system, Journal of Materials Science: Materials in Medicine 14(2) (2003) 109-112.
[58] P.W. Serruys, M.J. Kutryk, A.T. Ong, Coronary-artery stents, New England Journal of Medicine 354(5) (2006) 483-495.
[59] J.C. Palmaz, Intravascular stents in the last and the next 10 years, Journal of endovascular therapy 11(6_suppl) (2004) II-200-II-206.
[60] T. Hu, C. Yang, S. Lin, Q. Yu, G. Wang, Biodegradable stents for coronary artery disease treatment: Recent advances and future perspectives, Materials Science and Engineering: C 91 (2018) 163-178.
[61] J. Daraei, Production and characterization of PCL (Polycaprolactone) coated TCP/nanoBG composite scaffolds by sponge foam method for orthopedic applications, Journal of Composites and Compounds 1(1) (2020).
[62] H. Tamai, K. Igaki, E. Kyo, K. Kosuga, A. Kawashima, S. Matsui, H. Komori, T. Tsuji, S. Motohara, H. Uehata, Initial and 6-month results of biodegradable poly-l-lactic acid coronary stents in humans, Circulation 102(4) (2000) 399-404.
[63] S.S. Venkatraman, L.P. Tan, J.F.D. Joso, Y.C.F. Boey, X. Wang, Biodegradable stents with elastic memory, Biomaterials 27(8) (2006) 1573-1578.
[64] M. Radmansouri, E. Bahmani, E. Sarikhani, K. Rahmani, F. Sharifianjazi, M. Irani, Doxorubicin hydrochloride-Loaded electrospun chitosan/cobalt ferrite/titanium oxide nanofibers for hyperthermic tumor cell treatment and controlled drug release, International journal of biological macromolecules 116 (2018) 378-384.
[65] P. Abasian, M. Radmansouri, M.H. Jouybari, M.V. Ghasemi, A. Mohammadi, M. Irani, F.S. Jazi, Incorporation of magnetic NaX zeolite/DOX into the PLA/chitosan nanofibers for sustained release of doxorubicin against carcinoma cells death in vitro, International journal of biological macromolecules 121 (2019) 398-406.
[66] A. Kraitzer, Y. Kloog, M. Zilberman, Approaches for prevention of restenosis, Journal of Biomedical Materials Research Part B: Applied Biomaterials: An Official Journal of The Society for Biomaterials, The Japanese Society for Biomaterials, and The Australian Society for Biomaterials and the Korean Society for Biomaterials 85(2) (2008) 583-603.
[67] H.S. Jang, H.Y. Nam, J.M. Kim, D.H. Hahm, S.H. Nam, K.L. Kim, J.R. Joo, W. Suh, J.S. Park, D.K. Kim, Effects of curcumin for preventing restenosis in a hypercholesterolemic rabbit iliac artery stent model, Catheterization and Cardiovascular Interventions 74(6) (2009) 881-888.
[68] G. Nakazawa, A.V. Finn, F.D. Kolodgie, R. Virmani, A review of current devices and a look at new technology: drug-eluting stents, Expert review of medical devices 6(1) (2009) 33-42.

[69] A. Biswas, A.P. Singh, D. Rana, V.K. Aswal, P. Maiti, Biodegradable toughened nanohybrid shape memory polymer for smart biomedical applications, Nanoscale 10(21) (2018) 9917-9934.
[70] W. Small, P.R. Buckley, T.S. Wilson, W.J. Benett, J. Hartman, D. Saloner, D.J. Maitland, Shape memory polymer stent with expandable foam: a new concept for endovascular embolization of fusiform aneurysms, IEEE Trans Biomed Eng 54(6 Pt 2) (2007) 1157-60.
[71] L. Sun, W.M. Huang, Thermo/moisture responsive shape-memory polymer for possible surgery/operation inside living cells in future, Materials & Design (1980-2015) 31(5) (2010) 2684-2689.
[72] L. Xue, S. Dai, Z. Li, Biodegradable shape-memory block co-polymers for fast self-expandable stents, Biomaterials 31(32) (2010) 8132-40.
[73] G.M. Baer, T.S. Wilson, W.t. Small, J. Hartman, W.J. Benett, D.L. Matthews, D.J. Maitland, Thermomechanical properties, collapse pressure, and expansion of shape memory polymer neurovascular stent prototypes, J Biomed Mater Res B Appl Biomater 90(1) (2009) 421-9.
[74] R. Liu, S. McGinty, F. Cui, X. Luo, Z. Liu, Modelling and simulation of the expansion of a shape memory polymer stent, Engineering Computations 36(8) (2019) 2726-2746.
[75] M. Ansari, M. Golzar, M. Baghani, M. Soleimani, Shape memory characterization of poly(ε-caprolactone) (PCL)/polyurethane (PU) in combined torsion-tension loading with potential applications in cardiovascular stent, Polymer Testing 68 (2018) 424-432.
[76] H. Jia, S.-Y. Gu, K. Chang, 3D printed self-expandable vascular stents from biodegradable shape memory polymer, Advances in Polymer Technology 37(8) (2018) 3222-3228.
[77] C. Lin, L. Zhang, Y. Liu, L. Liu, J. Leng, 4D printing of personalized shape memory polymer vascular stents with negative Poisson's ratio structure: A preliminary study, Science China Technological Sciences 63(4) (2020) 578-588.

Available online at www.jourcc.com

Journal homepage: www.JOURCC.com

Journal of Composites and Compounds

# Synthesis of copper oxide nanoparticles on activated carbon for pollutant removal in tartrazine structure

*Azadeh Jafari Rad*[a]*

[a] *Department of Chemistry Omidiyeh Branch, Islamic Azad University, Omidiyeh, Iran*

A B S T R A C T

In this study, activated carbon particles were modified by copper oxide to remove the anionic Tartrazine dye from aqueous solutions. Adsorption studies were performed as batch studies and the influences of pH, initial dye concentrations, and contact times were evaluated. Maximum removal percentage was obtained for the initial concentration of 30 mg/L and the equilibrium of the adsorption was achieved within 60 minutes of contact time. The Langmuir and Freundlich kinetic models were used for analyzing the equilibrium data. It was shown that better fitting was observed by the Langmuir model. Pseudo-first-order and Pseudo-second-order kinetic models were also applied to understand the kinetics of the adsorption processes. It was found that the Tartrazine adsorption followed the pseudo-second-order kinetic model.



Peer review under responsibility of jourcc

A R T I C L E I N F O R M A T I O N

*Article history:*
Received 20 May 2020
Received in revised form 5 June 2020
Accepted 27 June 2020

*Keywords:*
Tartrazine
Activated carbon
Copper oxide
Removal efficiency

## 1. Introduction

The major environmental pollution source is the discharge of dye-containing wastewater from cosmetics, textiles, food, plastic, and paper industries [1–5]. These residual dyes present in the wastewater endanger the life of fish as well as other organisms. Moreover, these substances absorb sunshine resulting in photosynthesis prevention and an adverse impact on the natural aquatic ecosystem. As a result of their complex structure and high molecular weight, the degradation of organic dyes is usually difficult [1-3]. Different approaches, such as membrane separation, oxidation, flocculation, coagulation, and adsorption, have been proposed for the removal of these dyes [4-6].

Recently, nanoparticles have been widely investigated because of their potential applications such as information storage devices, optoelectronics [7], nanoelectronics [8], nanosensors [9-11], catalysts, microelectronics, and magnetic recording media [12]. Factors such as size distribution and morphology of the nanoparticles can affect their properties and applications [13-15]. The physical and chemical properties of copper oxide nanoparticles make them promising for applications such as solar energy conversion, gas sensors, batteries, catalysis, high-temperature superconductors, and antibacterial agents with low toxicity and low cost [16, 17].

In wastewater treatment, various adsorbents have been investigated for pollutant removal. Among them, activated carbon (AC) is the most extensively utilized adsorbent because of having various structural forms, chemical stability, low density, and large specific surface area [4]. This carbonaceous material with high porosity is widely utilized in water treatment processes to remove organic/inorganic pollutants [18-20] because of its tunable chemical and physical characteristics [21, 22] including modifiable surface, high surface reactivity, large surface area, and highly porosity with controllability [23]. Currently, activated carbons are mostly considered as a catalyst and mild reducing agent with a low cost. Thus, the development of low-cost effective carbons and other efficient material for contaminants removal from wastewater is necessary [24].

The effect of different parameters such as the CuO/AC ratio, pH, temperature, shaking rate, and contact time on the adsorption performance of this system has been studied in various scenarios. Tartrazine or trisodium (IUPAC name) is known as a typical synthetic, anionic dye with water solubility [25, 26]. Tartrazine causes intolerance and allergic reactions, especially for those with aspirin intolerance and asthmatics. Therefore, it is required to treat the wastewater containing various concentrations of tartrazine prior to discharge [4, 27].

Tartrazine is an anionic, synthetic, water-soluble azo dye with yellow color, which consists of one carboxylic functional group, one azo (N=N), and two sulphonic groups. Tartrazine is widely utilized in pharmaceuticals (gels, pills, and capsules), cosmetics, and different food products (jellies, chewing gum, chips, alcoholic beverages, sodas, and cakes). Several side effects have been appeared to be caused by Tartrazine including allergic reactions, attention deficit disorder, hyperactivity in children, damage to DNA, and lethal asthma [28, 29].

Most studies have concentrated on removing one or two of these contaminants, while several contamination forms usually exist in drinking water. Therefore, the development of materials with the potential to remove several pollutants is extremely valuable, as it could suggest

* *Corresponding author: Azadeh Jafari Rad; E-mail: jafarirad.azadeh@gmail.com*
*https://doi.org/10.29252/jcc.2.2.6* 

simpler and more cost-effective processes.

This research aimed to synthesize copper oxide nanoparticles on activated carbon and study its potential for the Tartrazine removal. The effect of contact time, pH and buffer type and size, adsorption value, time, and electrolyte concentration on color removal percentage was studied.

## 2. Materials and Methods

### *2.1. Materials*

Tartrazine (Trisodium (4E)-5-oxo-1-(4-sulfonatophenyl)-4-[(4- sulfonatophenyl)hydrazono]-3-pyrazolecarboxylate; C.I., 19,140; with a molar mass of 543.40 g mol $L^{-1}$ and chemical formula of $C_{16}H_9N_4Na_3O_9S_2$ was selected as an adsorbate. Fig.1 shows the molecular structure of Tartrazine. Highly pure materials with the analytical grade were used that were obtained from Merck, Iran. The dye concentration was measured at 427 nm. UV–Vis spectrophotometer was used to study the absorption performance. A pH meter was utilized to measure the pH value of the solution.

### *2.2. Sample preparation*

1 g of active carbon and 0.024 g of Cu $(NO_3)_2.3H_2O$ was added to distilled water (100 mL) followed by stirring for 30 min. 1.85 g of $NaBH_4$ was dissolved in distilled water (50 mL), and then 10 mL of this solution was added dropwise to the copper nitrate solution and stirred for 2 h at room temperature. The sediments were filtered, washed with distilled water, and dried at 80 ˚C for 10 h followed by grinding. To study the adsorption performance of CuO-modified AC, 10 mL Tartrazine solution and 2 mL of phosphoric acid buffer solution (pH=7) were dissolved in 100 mL of distilled water. 0.05 g of the adsorbent particles was added to the prepared solution and stirring was applied for 30 min. 10 mL of the solution was centrifuged in determined intervals to measure the adsorption by a UV–vis spectrophotometer at 423 nm indicating the dye concentrations.

### *2.3. Determination of PZC point*

For determination of zero charge point ($pH_{pzc}$), solutions of the absorbent with the ratio of 1 to 1000 (w/v) with different initial pH values ($pH_i$) were prepared using 0.01 M HCl or NaOH. The dispersed solutions were stirred at ambient temperature for 24 h and the pH values of the final solutions ($pH_f$) were then measured. The ΔpH values that are the differences between the initial and final values of pH were plotted vs. $pH_i$, and the point at which the pH change was zero was reported as $pH_{pzc}$.

### *2.4. Kinetic models*

During the physicochemical process of adsorption, the mass transfer of a solute occurs from the aqueous phase to the surface of an adsorbent. In this research, pseudo-first-order and pseudo-second-order kinetic models were used to study the Tartrazine adsorption mechanism onto copper oxide-modified AC. Equation 1 represents the Lagergren-first-order kinetic model [30]:

$$Ln(q_1 - q_t) = Lnq_1 - k_1 t \quad (1)$$

where $q_1$ denotes the Tartrazine amounts adsorbed at equilibrium (mg/g), $q_t$ represents the Tartrazine amounts adsorbed at time t (min), and the rate constant ($min^{-1}$) was represented by $k_1$. The $k_1$ value was obtained using the curve of $\ln(q_1 - q_t)$ vs. time. The following linear pseudo-second-order model [30] was also used for kinetic studies.

$$t/q_t = 1/k_2 q_2^2 + t/q_2 \quad (2)$$

In this equation, the rate constant of the pseudo-second-order kinetic adsorption model is denoted by $k_2$. The slope of the linear plots presenting the change of $t/q_t$ with time is $1/q_2$ and the intercept value gives $1/k_2 q_2^2$.

### *2.5. Adsorption isotherms*

The interaction between the adsorbents and adsorbates can be described in the equilibrium state. To fit the adsorption isotherm data, the Langmuir and Freundlich models were used. Selecting the best-fit model was done based on the linear regression correlation coefficient values ($R^2$). The assumptions of the Langmuir model are the adsorption in a monolayer and the absence of interaction between the molecules of the adsorbate. Equation 3 is the linear equation of Langmuir isotherm.

$$C_e/q_e = (1/q_m)\, K_L + C_e/q_m \quad (3)$$

where $q_e$ represent the equilibrium adsorption amount (mg/g) and $C_e$ denotes the equilibrium concentration (mg $L^{-1}$). The Langmuir constant and the theoretical maximum adsorption capacity are denoted by $K_L$ and $q_m$, respectively. There exists another model that describes the solutes adsorption from a liquid to the solid surface, which is known as the Freundlich model. In this model, it is assumed that different adsorption energies in several sites are involved. The Freundlich model follows the presented equation of:

$$Lnq_e = LnK_F + (1/n)\, LnC_e \quad (4)$$

In this equation, $C_e$ and $q_e$ are the equilibrium concentration of Tartrazine (mg $L^{-1}$) and the adsorbed dye at equilibrium, respectively (mg/g). The adsorbate amount that is adsorbed on the surface for a unit equilibrium concentration is defined by the Freundlich constant of $K_F$, which is a distribution or adsorption coefficient. The Freundlich constant of n reveals how favorable the adsorption process is. All experiments were performed on the batch.

Mass balance equation determines the adsorption capacity in the adsorbents equilibrium. The equation is based on the assumption that the dye amount adsorbed on the adsorbent surface is equal to the amount of the removed adsorbate from the solution:

$$q_e = V(C_0 - C_e)/m \quad (5)$$

where $C_0$, m, and V denote initial adsorbate concentration (mg $L^{-1}$), adsorbent weight (g), and volume of aqueous solution (L), respectively.

For evaluation of the removal efficiency, samples were studied after the flocculation/coagulation and sedimentation. In this regard, the apparent color and the concentration parameters of the yellow dye were characterized. All analyses were carried out based on standard methods and repeated three times for each sample. Equation 6 was employed to

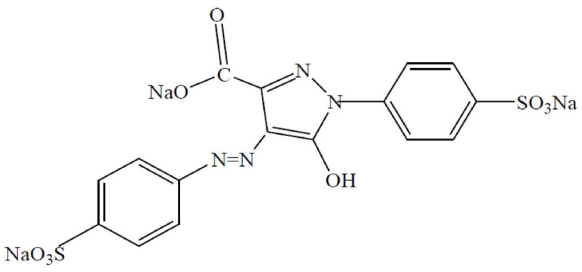


**Fig. 1.** Molecular structure of Tartrazine.

calculate the removal efficiency for each analyzed parameter.

$$Removal\ efficiency\ \% = ((C_i - C_f)/C_i) \times 100 \quad (6)$$

In this equation, $C_i$ is the initial value of each parameter and $C_f$ is its final value.

## 3. Results and discussion

### 3.1. Determination of PZC point

One of the important properties for the surface of solids containing hydroxyl groups is the determination of the PZC point. PZC point is the pH of the surrounding liquid medium, at which the sum of the positive surface charges is in balance with the total negative surface charges and the surface charge density is zero. Determining the PZC point for nanoscale structures is more important because of the increase in surface-to-mass ratio in these particles; subsequently, their surface charge increases. The pH change vs. $pH_i$ is shown in Fig. 2. It is observed that at pH = 7.1, the pH change is zero, indicating that the adsorbent charge at this point is zero.

### 3.2. PH effect

To investigate whether the pH changes influence the contaminant removal and apparent color, the adsorption percentage was measured in different pH of the solution. The adsorption percentages were measured by a UV-Vis spectrometer based on a plotted calibration curve with dye concentrations between 1 to 3 mg $L^{-1}$. In Fig. 3, the effect of pH on the percentage removal of Tartrazine is illustrated. The results showed that the pH value does not significantly affect the dye removal, therefore pH=7 was selected as optimal pH value.

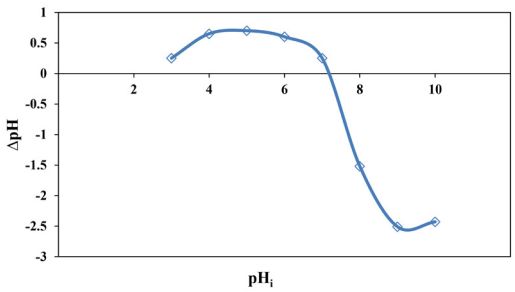


**Fig. 2.** PH changes vs. the initial pH.

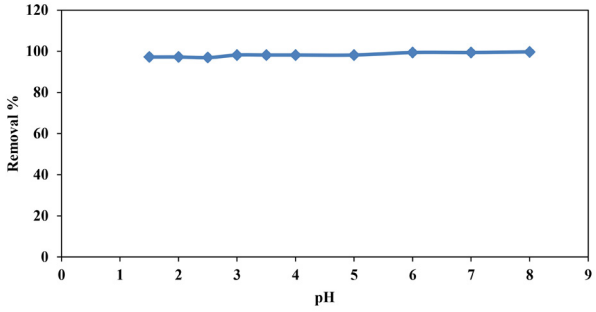


**Fig. 3.** Effect of pH on the Tartrazine removal.

### 3.3. Effect of the adsorbent amount

Modification of activated carbon with copper oxide nanoparticles affects its textural features including the decrease in diameter, pore volume, and surface area. To evaluate the influence of the absorbent amount on the removal efficiency, the adsorption was measured in solutions with different amounts of the adsorbent particles ranging from 0.001 to 0.15 g. According to the observations, with an increase in the adsorbent amount, the amount of surface adsorption enhanced (Table 1). The dye removal reached the highest value in 0.05 g of adsorbent and the further increase in the dye concentration did not show significant changes in the adsorption. This might be due to the interaction of dye molecules with each other or other molecules in the solution preventing the complete removal of the contaminants. Fig.4 shows the removal percentage vs. Tartrazine concentration.

### 3.4. Effect of contact time and initial adsorbate concentration

The influences of the initial adsorbate concentration of Tartrazine dye as well as contact time on the dye removal from the aqueous solu-

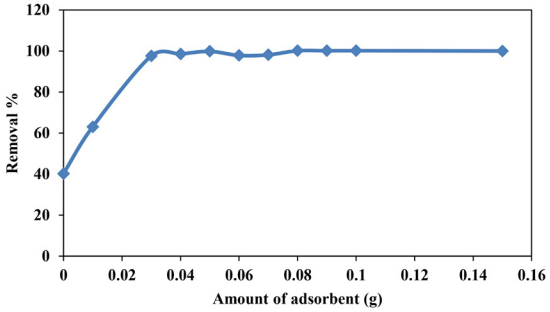


**Fig. 4.** Effect of pH on the Tartrazine removal.

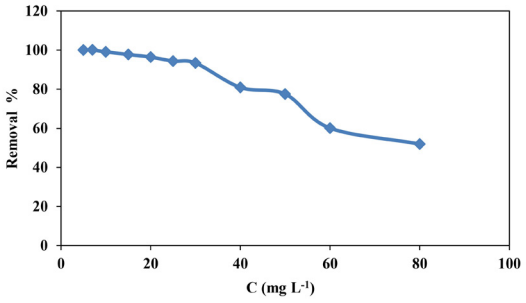


**Fig. 5.** Effect of the initial concentration of Tartrazine.

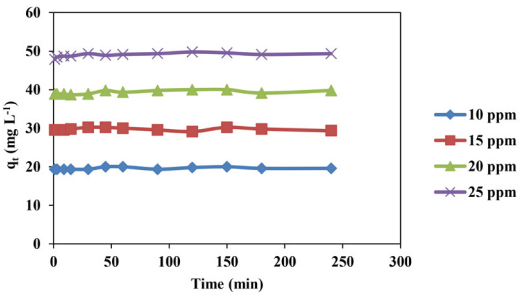


**Fig. 6.** Effect of initial Tartrazine contact time.

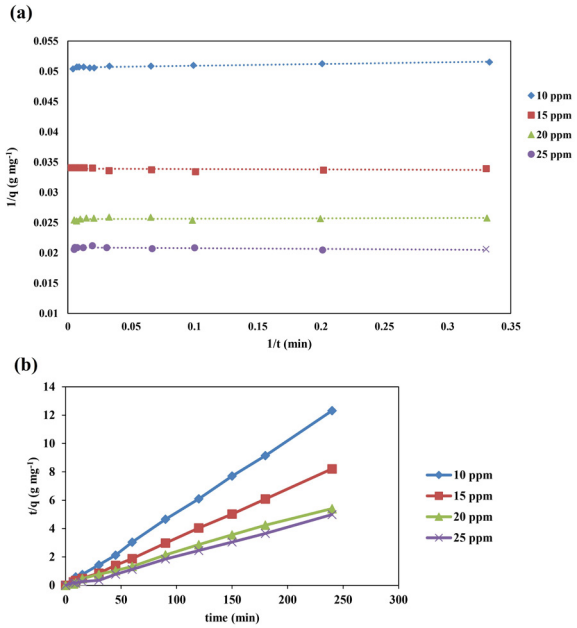


**Fig. 7.** Kinetic plots of adsorption: (a) pseudo-first-order and (b) pseudo-second-order.

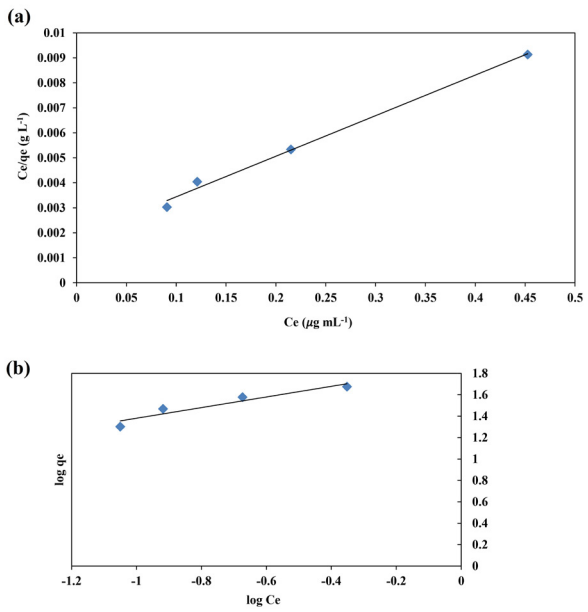


**Fig. 8.** Langumir (a) and Freundlich (b) isotherms of tartrazine adsorption.

tion were investigated. The results of these factors are presented in Fig. 5 and Fig. 6, respectively. According to Fig. 4, the increment of the initial concentration of the dye led to the reduction of Tartrazine removal. Principally, the initial concentration of Tartrazine can provide the driving force necessary for overcoming the resistance to the dye mass transfer between the solid surface of AC and aqueous phase. On the other hand, the interaction between the molecules of Tartrazine increases leading to the reduction of removal percentages. As seen in Fig. 6, the adsorption of the dye onto the modified AC was a relatively rapid process, revealing a high affinity between the surface of the absorbent particles and Tartrazine molecules. The accessibility of adsorption sites on the adsorbent surface was indicated by the high adsorption efficiency at an initial stage. The contact time does not significantly affect the dye removal. The required time for reaching an equilibrium was found to be 60 min. Therefore, all subsequent experiments were conducted at the contact equilibrium time of 60 min.

### *3.5. Study of adsorption kinetics*

The kinetics of the Tartrazine adsorption onto copper oxide-modified AC surface was studied using the adsorption data for different initial dye concentrations. The adsorption kinetic curves are illustrated in Fig. 7 and Table 2 lists the parameters. According to the calculated data, $R^2$ values of the pseudo-second-order model are close to 1, revealing that the adsorption follows this model. Thus, this kinetic model can be used for the prediction of the dye uptake amount at various contact times and at equilibrium.

### *3.6. Adsorption isotherms*

Considering the values of $C_t$, $C_0$, solution volume of 0.1 L, and the adsorbent weight of 0.05 g, the values of $q_e$ for the dye concentrations of 15, 25, 35, and 40 mg $L^{-1}$ were obtained at the equilibrium time of 60 min. The results are shown in Table 3. The $C_e/q_e$ diagram was then plotted against $C_e$ to obtain the parameters of the two equations, which are listed in Table 4. To show the degree of adsorption tendency to the adsorbent, a non-dimensional parameter called $R_L$ is used, which is calculated by Equation 7 obtained from the Langmuir equation.

$$R_L = 1/(1 + K_L C) \quad (7)$$

where C denotes the initial concentration of the dye (mg $L^{-1}$). If the $R_L$

**Table 1.**
Adsorbent value for different amounts of the adsorbent

| **The amount of adsorbent (g)** | 0.001 | 0.010 | 0.030 | 0.040 | 0.050 | 0.060 | 0.070 | 0.080 | 0.090 | 0.100 | 0.150 |
|---|---|---|---|---|---|---|---|---|---|---|---|
| **Removal Percentage** | 40.01 | 63.16 | 96.71 | 97.49 | 99.05 | 98.44 | 97.59 | 99.13 | 99.28 | 99.30 | 96.69 |

**Table 2.**
Kinetic parameters of adsorption

| **Models** | **Parameters** | **Initial concentration** | | | |
|---|---|---|---|---|---|
| | | **10** | **15** | **20** | **25** |
| Pseudo-first-order | $k_1$ (×$10^3$) | 5.8 | 8.6 | 52.3 | 98.5 |
| | $q_1$ | 15.98 | 22.70 | 35.23 | 42.36 |
| | $R^2$ | 0.908 | 0.711 | 0.687 | 0.678 |
| Pseudo-second-order | $k_2$ (×$10^3$) | 61.7 | 88.5 | 214 | 310 |
| | $q_2$ | 19.88 | 29.76 | 42.91 | 49.50 |
| | $R^2$ | 0.999 | 0.999 | 0.997 | 0.999 |

**Table 3.**
The data calculated from Freundlich and Langmuir models from the adsorption isotherms

| $C_0$(mg $L^{-1}$) | $C_e$(mg $L^{-1}$) | $q_e$(mg $g^{-1}$) | $C_e/q_e$(g $L^{-1}$) | log $C_e$ | log $q_e$ |
|---|---|---|---|---|---|
| 10 | 0.0903 | 19.81 | 0.0030 | -1.0443 | 1.2968 |
| 15 | 0.1216 | 29.75 | 0.0040 | -0.9150 | 1.4735 |
| 20 | 0.2122 | 39.57 | 0.0053 | -0.6732 | 1.5973 |
| 25 | 0.4496 | 49.10 | 0.0091 | -0.3471 | 1.6910 |

**Table 4.**
The calculated parameters of the adsorption isotherms

| | | | |
|---|---|---|---|
| **Langmuir** | $q_m$(mg $g^{-1}$) | $K_L$(L $mg^{-1}$) | $R^2$ |
| | 60.975 | 0.0018 | 0.9943 |
| **Freundlich** | $K_F$ (L $g^{-1}$) | n | $R^2$ |
| | 80.612 | 1.9011 | 0.8957 |

**Table 5.**
$R_L$ values for different initial concentrations of Tartrazine

| $C_0$ | 10 | 15 | 20 | 25 |
|---|---|---|---|---|
| $R_L$ | 0.9823 | 0.9737 | 0.9652 | 0.9569 |

value is greater than 1, it reveals that surface adsorption has occurred under undesirable conditions. If $R_L = 1$, it will indicate that the adsorption is linear. When the $R_L$ value is less than 1 and greater than zero, surface adsorption will occur under favorable conditions, and if the $R_L$ equals to 0, the adsorption will be irreversible. The values of $R_L$ for the different initial concentrations are shown in Table 5. Based on the obtained $R_L$ values, surface adsorption has occurred under favorable conditions.

The linear form of Langmuir and Freundlich models was utilized to fit the adsorption isotherms (Fig. 8). The correlation coefficient of $R^2$ indicates whether the isotherm equations are applicable for the description of the adsorption process. The higher linearity and $R^2$ in the $C_e/q_e$ vs. $C_e$ curve (Fig. 8a) indicated that the Langmuir equation could be applied for fitting the experimental data and interpret the dye adsorption onto copper oxide-modified AC particles. It is worth noting that the theoretical value of $q_m$ was obtained close to the maximum adsorption capacities ($q_e$) obtained from the experimental studies. Moreover, it is interesting to understand whether the adsorption of the dye is favorable or not. In the Freundlich model, when the n values are in the range of 2–10, the adsorption is good, while the values less than 1 show poor adsorption behavior. The values between 1 to 2 indicate moderately difficult adsorption characteristics. Based on the obtained values, the studied material is a good adsorbent for tartrazine. Surface heterogeneity or adsorption intensity is measured by the slope of 1/n in the range of 0 to 1. A straight line with slope 1/n is obtained from the curve of ln $q_e$ vs. ln $C_e$ (Fig. 8b). If the value gets closer to 0, it indicates a more heterogeneous surface.

## 4. Conclusions

In this research, activated carbon was modified with copper oxide to absorb the Tartrazine dye from wastewater and the contributed mechanisms in the adsorption process were investigated. AC particles modified with copper oxide were found to be very efficient in the removal of Tartrazine dye. According to the batch experiments, the adsorption process was conducted rapidly, as maximum removal percentage of the dye obtained within 60 minutes of contact time for the initial dye concentration of 30 $mg/L^{-1}$. Based on the equilibrium data related to the Freundlich and Langmuir models, the Langmuir isotherm appeared to be more concise for the description of the Tartrazine adsorption. The adsorption kinetics followed closely the pseudo-second-order kinetic model. Finally, the removal efficiency was found to be more than 98%. Therefore, the modified AC particles can be a good candidate for the removal of Tartrazine from aqueous solutions.

REFERENCES

[1] D. Wang, N. Zhao, T. Wang, C. Zhuang, Y. Wang, B. Yang, Crystal Structure, Spectroscopy and Photocatalytic Properties of a Co(II) Complex Based on 5-(1,2,4-triazol-1-yl)pyridine-3-carboxylic Acid, Crystals 10(2) (2020).

[2] M. Golmohammadi, M. Honarmand, S. Ghanbari, A green approach to synthesis of ZnO nanoparticles using jujube fruit extract and their application in photocatalytic degradation of organic dyes, Spectrochimica Acta Part A: Molecular and Biomolecular Spectroscopy 229 (2020) 117961.

[3] A. Tkaczyk, K. Mitrowska, A. Posyniak, Synthetic organic dyes as contaminants of the aquatic environment and their implications for ecosystems: A review, Science of The Total Environment 717 (2020) 137222.

[4] J. Goscianska, R. Pietrzak, Removal of tartrazine from aqueous solution by carbon nanotubes decorated with silver nanoparticles, Catalysis Today 249 (2015) 259-264.

[5] A. Kazemzadeh, H. Kazemzadeh, L. Bazli, Determination of $Hg^{2+}$ by Diphenylcarbazone Compound in Polymer Film, Composites and Compounds 1(1) (2019).

[6] H. Won Jang, A. Zareidoost, M. Moradi, A. Abuchenari, A. Bakhtiari, R. Pouriamanesh, B. Malekpouri, A. Jafari Rad, Photosensitive nanocomposites: environmental and biological applications, Journal of Composites and Compounds 1(1) (2020).

[7] S. Saadi, B. Nazari, Submission Title: Recent Developments and Applications of Nanocomposites in Solar Cells: a Review, Composites and Compounds 1(1) (2019).

[8] A. Kazemzadeh, M.A. Meshkat, H. Kazemzadeh, M. Moradi, R. Bahrami, R. Pouriamanesh, Submission Title: Preparation of Graphene Nanolayers through Surfactant-assisted Pure Shear Milling Method, Composites and Compounds 1(1) (2019).

[9] L. Bazli, M. Siavashi, A. Shiravi, A Review of Carbon Nanotube/$TiO_2$ Composite Prepared via Sol-Gel Method, Composites and Compounds 1(1) (2019).

[10] E. Asadi, A. Fassadi Chimeh, S. Hosseini, S. Rahimi, B. Sarkhosh, L. Bazli, R. Bashiri, A.H. Vakili Tahmorsati, A Review of Clinical Applications of Graphene Quantum Dot-based Composites, Composites and Compounds 1(1) (2019).

[11] V.S. Rizi, F. Sharifianjazi, H. Jafarikhorami, N. Parvin, L.S. Fard, M. Irani, A. Esmaeilkhanian, Sol–gel derived $SnO_2$/$Ag_2O$ ceramic nanocomposite for $H_2$ gas sensing applications, Materials Research Express 6(11) (2019) 1150g2.

[12] F. Sharifianjazi, M. Moradi, N. Parvin, A. Nemati, A.J. Rad, N. Sheysi, A. Abouchenari, A. Mohammadi, S. Karbasi, Z. Ahmadi, Magnetic $CoFe_2O_4$ nanoparticles doped with metal ions: a review, Ceramics International (2020).

[13] S. Muthukrishnan, A. Eswaran, Phytochemical and antimicrobial profile of nanobased liv-pro-09 polyherbal formulation.

[14] F.S. Jazi, N. Parvin, M. Rabiei, M. Tahriri, Z.M. Shabestari, A.R. Azadmehr, Effect of the synthesis route on the grain size and morphology of ZnO/Ag nanocomposite, Journal of Ceramic Processing Research 13(5) (2012) 523-526.

[15] F.S. Jazi, N. Parvin, M. Tahriri, M. Alizadeh, S. Abedini, M. Alizadeh, The relationship between the synthesis and morphology of $SnO_2$-$Ag_2O$ nanocomposite, Synthesis and Reactivity in Inorganic, Metal-Organic, and Nano-Metal Chemistry 44(5) (2014) 759-764.

[16] J. Peternela, M.F. Silva, M.F. Vieira, R. Bergamasco, A.M.S. Vieira, Synthesis and Impregnation of Copper Oxide Nanoparticles on Activated Carbon through Green Synthesis for Water Pollutant Removal, Materials Research 21 (2018).

[17] A. Moghanian, F. Sharifianjazi, P. Abachi, E. Sadeghi, H. Jafarikhorami, A. Sedghi, Production and properties of Cu/$TiO_2$ nano-composites, Journal of Alloys and Compounds 698 (2017) 518-524.

[18] S. Periyasamy, I.A. Kumar, N. Viswanathan, Activated Carbon from Different Waste Materials for the Removal of Toxic Metals, in: M. Naushad, E. Lichtfouse (Eds.), Green Materials for Wastewater Treatment, Springer International Publishing, Cham, 2020, pp. 47-68.

[19] P.P. Bhave, D. Yeleswarapu, Removal of Indoor Air Pollutants Using Activated Carbon—A Review, in: V. Sivasubramanian, S. Subramanian (Eds.) Global Challenges in Energy and Environment, Springer Singapore, Singapore, 2020, pp. 65-75.

[20] Z. Heidarinejad, M.H. Dehghani, M. Heidari, G. Javedan, I. Ali, M. Sillanpää, Methods for preparation and activation of activated carbon: a review, Environmental Chemistry Letters 18(2) (2020) 393-415.

[21] K. Gong, X. Li, H. Liu, X. Cheng, D. Sun, Q. Shao, M. Dong, C. Liu, S. Wu, T. Ding, B. Qiu, Z. Guo, Residue metals and intrinsic moisture in excess sludge improve pore formation during its carbonization process, Carbon 156 (2020) 320-328.

[22] C.H. Nguyen, H.N. Tran, C.-C. Fu, Y.-T. Lu, R.-S. Juang, Roles of adsorption and photocatalysis in removing organic pollutants from water by activated carbon–supported titania composites: Kinetic aspects, Journal of the Taiwan Institute of Chemical Engineers 109 (2020) 51-61.

[23] F.S. Arakawa, Q.L. Shimabuku-Biadola, M. Fernandes Silva, R. Bergamasco, Development of a new vacuum impregnation method at room atmosphere to produce silver–copper oxide nanoparticles on activated carbon for antibacterial applications, Environmental Technology (2019) 1-12.

[24] M. Ghaedi, A.M. Ghaedi, M. Hossainpour, A. Ansari, M.H. Habibi, A.R. Asghari, Least square-support vector (LS-SVM) method for modeling of methylene blue dye adsorption using copper oxide loaded on activated carbon: Kinetic

and isotherm study, Journal of Industrial and Engineering Chemistry 20(4) (2014) 1641-1649.
[25] M.K.T. Al-Zain, Removal of Toxic Organic Compounds and Dyes from Water by Magnesium Oxide Nanostructure, Al-Azhar University-Gaza, 2019.
[26] K. Rovina, S. Siddiquee, S. Md Shaarani, An electrochemical sensor for the determination of tartrazine based on CHIT/GO/MWCNTs/AuNPs composite film modified glassy carbon electrode, Drug and Chemical Toxicology (2019) 1-11.
[27] K.G. Pavithra, S.K. P, J. V, S.R. P, Removal of colorants from wastewater: A review on sources and treatment strategies, Journal of Industrial and Engineering Chemistry 75 (2019) 1-19.
[28] N.A. Al-Shabib, J.M. Khan, M.S. Khan, M.S. Ali, A.M. Al-Senaidy, M.A. Alsenaidy, F.M. Husain, H.A. Al-Lohedan, Synthetic food additive dye "Tartrazine" triggers amorphous aggregation in cationic myoglobin, International Journal of Biological Macromolecules 98 (2017) 277-286.
[29] G.A.P. Mateus, T.R.T. dos Santos, I.S. Sanches, M.F. Silva, M.B. de Andrade, M.P. Paludo, R.G. Gomes, R. Bergamasco, Evaluation of a magnetic coagulant based on $Fe_3O_4$ nanoparticles and Moringa oleifera extract on tartrazine removal: coagulation-adsorption and kinetics studies, Environmental Technology (2018) 1-16.
[30] S. Sahnoun, M. Boutahala, C. Tiar, A. Kahoul, Adsorption of tartrazine from an aqueous solution by octadecyltrimethylammonium bromide-modified bentonite: Kinetics and isotherm modeling, Comptes Rendus Chimie 21(3-4) (2018) 391-398.

Journal of Composites and Compounds 2 (2020) 105-109

Available online at www.jourcc.com

Journal homepage: www.JOURCC.com

Journal of Composites and Compounds

# Sr-doped bioactive glasses for biological applications

*Zahra Goudarzi[a], Amir Ijadi[a], Ameneh Bakhriari[b]*, Sara Eskandarinezhad[c], Negar Azizabadi[d]*, Mohammadreza Asgari Jazi[e]*

[a] *Department of Mining and Metallurgical Engineering, Amirkabir University of Technology, Tehran, Iran*
[b] *Department of Biology, Shahid Chamran University, Ahvaz, Iran*
[c] *Department of Mining and Metallurgical Engineering, Yazd University, Yazd, Iran*
[d] *Department of Chemistry, Science and Research Branch, IAU, Tehran, Iran*
[e] *Department of dentistry , Isfahan (khorasgan) Branch , Islamic Azad University*

A B S T R A C T

In this work, sol–gel derived bioactive glasses (BGs) system of 60% SiO2-(36-x) CaO-4$P_2O_5$-x SrO (where x = 2, 4, 6 and 8 mol%) were obtained. The bioactivity and proliferation of G292 cells was investigated for Sr-containing BGs. X-ray diffraction analysis (XRD), Scanning electron microscopy (SEM) and Fourier transform infrared spectroscopy (FTIR) were utilized to study the obtained phases, hydroxyapatite (HA) morphology, and its functional groups, respectively. The XRD and FTIR tests showed that the rate of hydroxyapatite formation on sample 2S was higher than that of other samples. Also 3-(4,5 dimethylthiazol-2-yl)-2,5-diphenyltetrazolium bromide (MTT) assay performed after one day revealed that the sample containing 6 mol% of Sr (6S) showed higher viability. However, the sample with 8 mol% Sr (8S) showed a decrease in bioactivity in osteoblast G292 cells proliferation. According to the results, 6S BG specimen with 6 mol% SrO exhibited appropriate bioactivity and cell proliferation. This finding showed that the obtained BGs could be potentially used for drug delivery systems as well as dental and orthopedic applications.



Peer review under responsibility of jourcc

A R T I C L E I N F O R M A T I O N

*Article history:*
Received 6 June 2020
Received in revised form 17 June 2020
Accepted 29 June 2020

*Keywords:*
Bioactive glass
Implant
Strontium
Drug delivery

## 1. Introduction

From the beginning, in medicine and surgery, bone problems have been important issues up to recent years. For this purpose, the first generation of biomaterials (*i.e.* metals and alloys) was introduced and made available to surgeons [1-3]. Nevertheless, implanting metal and alloys in the body can be inefficient and hurmful [3].

On the other hand, many problems can emerge with some bonds, such as autophagy, allograft, xenograft. Thus scientists have focused on designing advanced materials to make appropriate alternatives. Due to the above-mentioned problems, as well as the use of repeated and relatively unsuccessful surgeries in this field, the academic focus turned to the production and replacement of materials with compounds that do not harm healthy tissue. For the first time, Hench [4] developed a combination of bioactive glass that was compatible with the environment and was gradually attached to bone tissue. After that, new compounds with different properties were produced and expanded [1, 5-7].

After his great discovery, the progress and development of glass was categorized in four era: The era of Discovery (1969 to 1979), Era of Clinical Application (1980 to 1995), Era of Tissue Regeneration (1995 to 2005), and Era of Innovation (2005 to 2025). After that Wilson et al. [8], announced that they had found a glass that not only bonds to hard tissues, but also could bond to soft tissue. This was a new feature that led to widespread “clinical use” of glasses, such as middle ear replacement prostheses (MEP) and endosseous ridge maintenance implants (ERMI). They reported that for a range of glass particle sizes, there is an optimum for bone regeneration rate. Also, the rate of new bone formation is so high that the encapsulation of the site would be prevented by epithelial tissues [9]. Until 1992, the glass was often produced by melting, and most research was done on bioactive glass 45s5. In the melting method, a combination of oxides and additives is melted by increasing the temperature and after cooling, they are crushed and used as particles.

The problem with the melting method is high-temperature work and evaporation (volatile component) at this temperature. In this regard, in recent years, extensive research has been done on the sol-gel route as an alternative to the melting method [10, 11].

The sol-gel method can make very homogeneous composites with very high purity. It is also able to produce ceramic and metallic nanomaterials at much lower temperatures than conventional methods that have very high-temperature ranges. Due to the above-mentioned advantages, it can be considered as a suitable method for producing the compounds especially nanomaterials [12].

* *Corresponding authors: Negar Azizabadid; E-mail: Negarazizabadi@gmail.com, Ameneh Bakhriari E-mail: bakhtiariaa@yahoo.com*
*https://doi.org/10.29252/jcc.2.2.7* 

**Table 1.**
Studies worked on Sr-containing BGs.

| BG system | Synthesis route | Time of HA formation after soaking in SBF solution | Ref. |
|---|---|---|---|
| Sr-BGs (0, 5, 10) | Sol-gel process | all samples after 3 days | [31] |
| Sr-BGs (0, 2, 5, 8 and 10) | Sol-gel method | 7 days (for 5% Sr-BGs) | [28] |

Currently, many glasses are made on the basis of the main ingredients of $SiO_2$, $P_2O_5$, CaO [13-17]. $SiO_2$ acts as a network former in the structure of glass, and its release into the environment can positively affect the cell activity and proliferation [18-24]. Ca and P are also useful as factors in the nucleation of calcium phosphate phases such and hydroxyapatite (HA) [15, 25]. Other elements (viz. Mg, Zn Ag, etc.) are added to the glass structure to enhance other properties such as antibacterial, cell proliferation and other biological properties [7, 26-30]. Meanwhile, Sr as a promising element for cell proliferation has been doped into the BGs. Table 1 shows two important works about Sr-doped BGs.

Table 1.

Therefore, since there are insufficient research about doping of Sr in the BGs, in this study, we used different amounts of Sr (2, 4, 6, and 8 mol.%) to investigate the biocompatibility of the BGs. It is reported that the BGs can be potentially applied for implant and orthopedic applications [32].

## 2. Materials and methods

### *2.1. Materials and regents*

Table 2 lists the details about the chemical composition of the synthesized BGs. Tetraethylorthosilicate (TEOS: $Si(OC_2H_5)_4$), calcium nitrate $Ca(NO_3)_2$,$4H_2O$, triethyl phosphate (TEP: $PO(OC_2H_5)_3$), and strontium nitrate $Sr(NO_3)_2$ were used as the source of silicon, calcium, phosphorus, and strontium, respectively (bought from the Merck Company, Germany).

Table 2.

### *2.2. Synthesis of BGs*

The BGs in the $SiO_2$–CaO–$P_2O_5$–SrO system were obtained using the sol-gel route. A 0.1 M nitric acid solution was provided and TEOS was added into the solution and stirring was applied for 45 minutes at 25 °C for hydrolysis of the acid. TEP, strontium nitrate, and calcium nitrate were poured into the TEOS solution, and each reagent was maintained for 30 min to complete the hydrolysis process. In the following, the mixture was further stirred for 50 minutes to let the reactions be completed, so that a sol was obtained. The sol was sealed for 3 days at 37 °C and dried for 1 day at 75 °C to obtain a dried gel. In order to calcine the dried gel, it was maintained in a furnace at 800 °C for 3 h so that the organic substances and nitrates are eliminated. In the next step, a planetary ball mill was utilized to grind the prepared product into a fine powder so that their size become below 50 μm and pressed into disks (weight of 0.5 g, height of 2 mm and diameter of 17 mm) under 10 MPa by ACM device. Finally, the samples were prepared to be evaluated *in-vitro*.

**Table 2.**
Chemical composition and sample coding of all BGs

| Bioglass code | $SiO_2$ (mol.%) | $P_2O_5$ (mol.%) | CaO (mol.%) | SrO (mol.%) |
|---|---|---|---|---|
| S2 | 60 | 4 | 34 | 2 |
| S4 | 60 | 4 | 32 | 4 |
| S6 | 60 | 4 | 30 | 6 |
| S8 | 60 | 4 | 28 | 8 |

### *2.3. Simulated body fluid (SBF) preparation*

The SBF solution is similar to the inorganic part of human plasma that was prepared based on the procedure explained by Kokubo [33]. All chemical reagents were bought from Merck Company, Germany. NaOH, KCl, $NaHCO_3$ $MgCl_2 \cdot 6H_2O$, $CaCl_2$ and $KH_2PO_4$ were used as reagents and dissolved in deionized water. A buffered solution was prepared with the mentioned solution and tris(hydroxymethyl) aminomethane, $(HOCH_2)_3CNH_2$. Next, the pH was adjusted to 7.4 by HCl.

### *2.4 Bioactive glass characterization*

#### *2.4.1. Thermal analysis*

In order to predict the thermal behavior of the samples as a function of temperature, the dried gel of 4S sample was applied for DTA test. During the test, a reference sample was placed in the device along with the samples to determine the temperature of the sample change phase. The obvious feature of the reference sample is that it does not show any phase change during temperature rise. For this purpose, alumina is commonly used in most devices. The tests were performed via Simultaneous Thermal Analysis (STA) (PL-STA 1640), in the range of 30–800 °C under normal atmosphere, along with an increasing temperature rate of 5 °C per min.

#### *2.4.2. X-ray diffraction (XRD) test*

In order to evaluate the phases formed on the glass surface and to ensure the presence of hydroxyapatite, the surfaces of samples were studied by XRD (INEL-Equinox-3000) with the Cu Kα radiation with wavelength of 1.540510 Å by voltage and current of 40 kV and 30 mA. The patterns were recorded in the 2θ range of 20° to 90° via a scanning speed of 2 °/min.

#### *2.4.3. Fourier-transform infrared spectroscopy analysis*

After soaking of the samples in SBF, their surfaces were characterized by FTIR (Bomem MB 100 instrument). In this regard, the glass powders and potassium bromide were mixed with 1:100 ratio. The transmittance mode of spectra was obtained in the range of 400–4000 $cm^{-1}$ by the resolution of 4 $cm^{-1}$.

#### *2.4.4. PH measurement*

On different days of immersion, the pH change was measured via pH meter (Corning pH meter 340).

#### *2.4.5. SEM analysis*

The morphology of the formed hydroxyapatite was examined using SEM analysis (SEM, Philips XL30, Netherlands) with a voltage of 20 kV.

### *2.5. MTT assay*

Cell proliferation was measured using the MTT (Sigma, USA) assay after treating for 1, 3 and 7 days. MTT solution (20 μL) was added to wells. Cells lines of G292 osteoblast were bought from the National Cell Bank of Iran (Pasteur Institute, Iran). The cells were cultured and incubated for 1 day under conditions of 90% humidity and 37 °C, followed by seeding in small plates (with density of $6\times10^4$ cells/well). The wavelength absorbance of the well-plates during the reactions, were elucidated via EL 312e Biokinetics reader, Biotek Instruments. Each measurement was performed in triplicates.

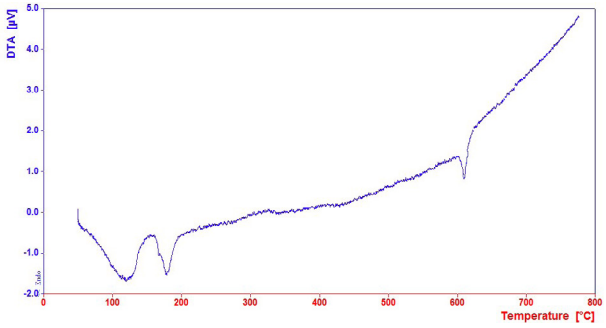


**Fig. 1.** DTA curve of synthesized 4S sample.

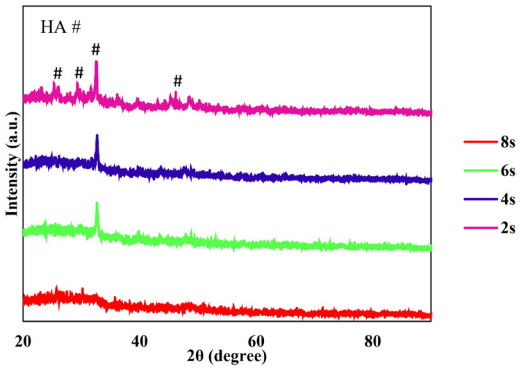


**Fig. 2.** XRD spectra of the BGs after soaking in SBF solution for 3 days.

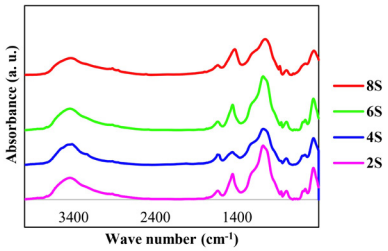


**Fig. 3.** The FTIR spectra of the BG samples after immersing in SBF solution for 3 days.

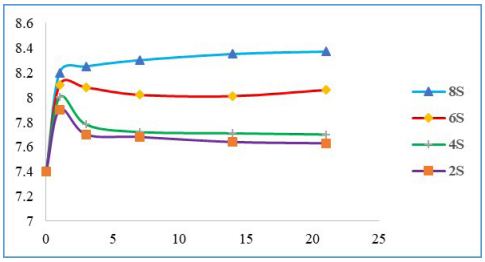


**Fig. 4.** Changes in pH of SBF solution over time in glasses containing strontium oxide.

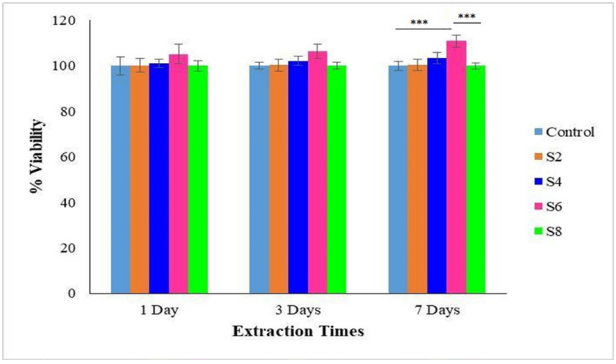


**Fig. 5.** Cytotoxicity of BG samples after exposure to osteoblastic G292 cells after 1, 3, and 7 days.

## 3. Results and discussion

### *3.1. Thermal analysis*

The DTA curve of 4S bioactive glass is shown in Fig. 1. Accordingly, the endothermic peak is observable at 114 °C, in which the physically adsorbed water is removed. The next endothermic peak occurs at 220 °C, which is related to the removal of the sample chemical absorbance of water. The peak for silane and nitrate removal is observable at 600 °C. The results showed that all residuals were removed at 600 °C. This suggested that 700 °C was appropriate for BGs stabilization.

### *3.2. Phase analysis*

Fig. 2 shows XRD patterns of the BGs after 3 days of immersion. It is obvious that, except 8S sample, the peaks related to hydroxyapatite were obvious. Therefore, by increasing the amount of strontium, the tendency to form crystalline apatite has decreased. Also, the peaks observed in the XRD spectra of samples S2, S4 and S6 at 2θ= 31.8° (attributed to the (211) plane) confirmed the crystalline hydroxyapatite formation (JCPDS 09-432). Besides, the intensity of the peak at 2 theta of 31.9° in the XRD spectrum of 2S sample is higher than other samples, which is due to the greater tendency of the sample to form hydroxyapatite on its surface.

### *3.3. FTIR*

The FTIR spectra of the BG samples are presented in Fig. 3. According to the Fig. 3, after 3 days of immersion, two peaks about 1455 and 870 $cm^{-1}$ emerged in the XRD patterns of all samples that are attributed to carbonate (C–O stretching) groups. The presence of hydroxyapatite was confirmed by existence of three peaks at 566, 603, and 1087 $cm^{-1}$. Besides, stretching and bending vibrations of Si–O–Si were also observed in the FTIR spectra of samples (i.e. 430 $cm^{-1}$) [34]. Meanwhile, the intensity of mentioned peaks was higher for 2S sample than that of other samples. Finally, FTIR results depicted that Sr retarded the formation of HA phase.

### *3.4. Measurement of pH*

Fig. 4 shows the pH changes. The pH changes of the SBF solution were measured after 1, 3, 7, 14, and 21 days of immersion. Studies have shown that Ca and Sr exchange ions with $H^+$, so the presence of these two cations in the composition is expected to make the pH of the solution increase at the time of immersion. Exchange of $Ca^{2+}$ glass with soluble $H_3O^+$ results in the formation of OH-Si bands on the glass surface, encourages the formation of apatite, and creates a suitable environment for apatite crystallization. After a time, the rate of increase in pH decreases, which means that silica-rich layers are created, and the cation exchange and release of calcium is prevented. The highest pH is related

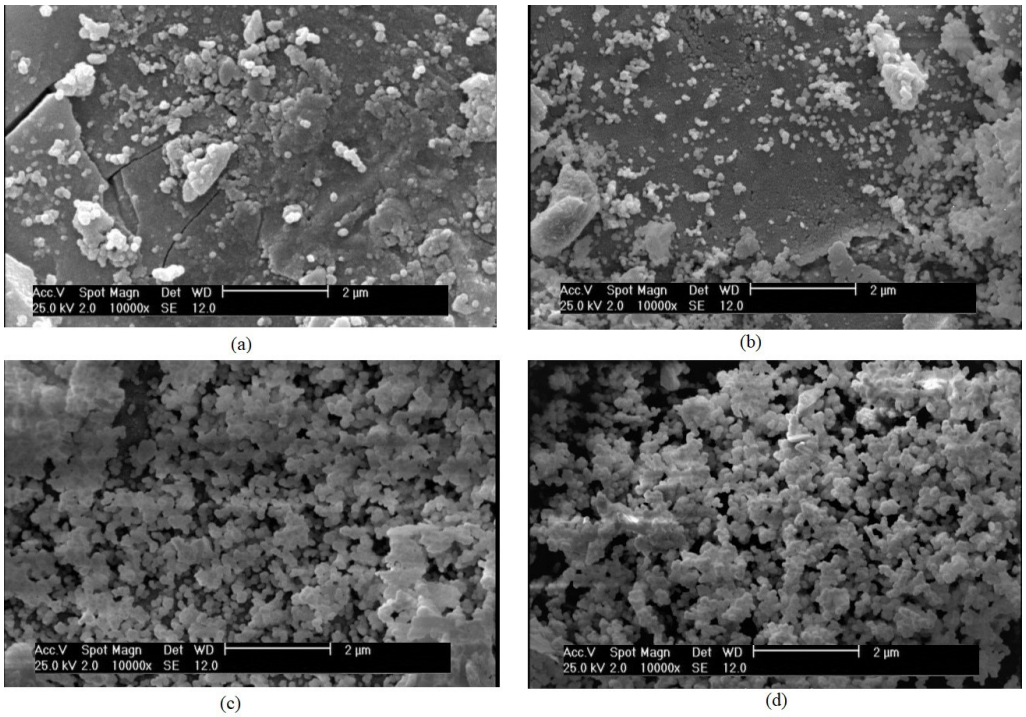


**Fig. 6.** SEM micrographs of S6 BG sample after soaking in the SBF solution for (a) 3, (b) 7, (c) 14 and (d) 21 days.

to the 8S sample due to the high Sr level.

*3.5 Cell proliferation*

Fig. 5 depicts the MTT results of cultured osteoblast G292 cells that contain samples of control, S2, S4, S6, and S8 incubated for 1, 3 and, 7 days. It can be seen that viability of S6 increased by an increment in the soaking time up to 7$^{th}$ day (***P < 0.001). Thus, they led to an increment in cell differentiation and proliferation. The cell viability of S2 and S4 samples, on the other hand, was not significantly different. Also, significantly lower cell proliferation was illustrated by the S8 sample in comparison to S6 (***P<0.001). Thus, the obtained MTT results suggested that the incorporation of 6% Sr in BG composition would significantly improve the cell proliferation, while 8% Sr showed no significant positive effect. Thus, based on the data, S6 was selected as the best BG sample.

*3.6. SEM*

Fig. 6 shows the process of hydroxyapatite formation after different days of immersion on the S6 sample (with the optimum sample composition). It is obvious that some parts of the surface is covered by small spherical particles of apatite after 3 days of soaking (Fig. 6(a)). As the immersion time in solution increases, the density of HA particles also increase (Fig. 6(b), (c), and 6(d)). It is obvious that on 21st day of soaking, the surface of BG is completely covered with hydroxyapatite.

## 4. Conclusions

The $SiO_2$–$P_2O_5$–CaO–SrO BG system was fabricated through sol-gel method. The results of this study are as follows:

- XRD and FTIR analyses confirmed that after 3 days in all samples, except 8S, the peaks related to hydroxyapatite emerged.
- MTT in-vitro test showed that after 7 days of incubation, S6 sample showed a statistically significant increase in viability of osteoblast G292 cells.
- The presence of Sr in BG composition increases the pH of simulated body fluid.
- SEM results showed that the apatite morphology was spherical on the S6 BG sample surface. It was also found that as the immersion time in the SBF increases, the density of HA particles increases.
- According to the results, the sample S6 was selected as the optimum sample in terms of bioactivity and cell proliferation that can be potentially used for drug delivery systems as well as orthopedic and dental applications.

REFERENCES

[1] L.L. Hench, The story of Bioglass®, Journal of Materials Science: Materials in Medicine 17(11) (2006) 967-978.
[2] J.R. Jones, New trends in bioactive scaffolds: The importance of nanostructure, Journal of the European Ceramic Society 29(7) (2009) 1275-1281.
[3] E. Rezabeigi, P.M. Wood-Adams, R.A. Drew, Synthesis of 45S5 Bioglass® via a straightforward organic, nitrate-free sol–gel process, Materials Science and Engineering: C 40 (2014) 248-252.
[4] L.L. Hench, The theory of bioactive bonding, Mat. Clin. Appl (1995) 331-342.
[5] Q. Nawaz, M.A. Ur Rehman, J.A. Roether, L. Yufei, A. Grünewald, R. Detsch, A.R. Boccaccini, Bioactive glass based scaffolds incorporating gelatin/manganese doped mesoporous bioactive glass nanoparticle coating, Ceramics International 45(12) (2019) 14608-14613.
[6] F. Baino, E. Fiume, M. Miola, F. Leone, B. Onida, E. Verné, Fe-doped bioactive glass-derived scaffolds produced by sol-gel foaming, Materials Letters 235 (2019) 207-211.
[7] N. Pajares-Chamorro, J. Shook, N.D. Hammer, X. Chatzistavrou, Resurrection of antibiotics that methicillin-resistant Staphylococcus aureus resists by silver-doped bioactive glass-ceramic microparticles, Acta Biomaterialia 96 (2019) 537-546.
[8] L. Hench, J. Wilson, Bioactive materials, MRS Online Proceedings Library Archive 55 (1985).
[9] L.L. Hench, J.R. Jones, Bioactive glasses: frontiers and challenges, Frontiers in bioengineering and biotechnology 3 (2015) 194.
[10] F. Sharifianjazi, N. Parvin, M. Tahriri, Synthesis and characteristics of sol-gel bioactive $SiO_2$-$P_2O_5$-CaO-$Ag_2O$ glasses, Journal of Non-Crystalline Solids 476 (2017) 108-113.
[11] F. Sharifianjazi, N. Parvin, M. Tahriri, Formation of apatite nano-needles on novel gel derived $SiO_2$-$P_2O_5$-CaO-SrO-$Ag_2O$ bioactive glasses, Ceramics International 43(17) (2017) 15214-15220.
[12] L.L. Hench, J.K. West, The sol-gel process, Chemical reviews 90(1) (1990) 33-72.
[13] R. Orifice, L. Hench, A. Clark, A. Brennan, Novel sol-gel bioactive fibres, J Biomed Mater Res 55 (2001) 460-467.

[14] A. Salinas, A. Martin, M. Vallet-Regí, Bioactivity of three CaO–$P_2O_5$–$SiO_2$ sol-gel glasses, Journal of Biomedical Materials Research: An Official Journal of The Society for Biomaterials, The Japanese Society for Biomaterials, and The Australian Society for Biomaterials and the Korean Society for Biomaterials 61(4) (2002) 524-532.

[15] P. Saravanapavan, J.R. Jones, R.S. Pryce, L.L. Hench, Bioactivity of gel–glass powders in the CaO-$SiO_2$ system: A comparison with ternary (CaO-$P_2P_5$-$SiO_2$) and quaternary glasses ($SiO_2$-CaO-$P_2O_5$-$Na_2O$), Journal of Biomedical Materials Research Part A: An Official Journal of The Society for Biomaterials, The Japanese Society for Biomaterials, and The Australian Society for Biomaterials and the Korean Society for Biomaterials 66(1) (2003) 110-119.

[16] A. Moghanian, A. Ghorbanoghli, M. Kazem-Rostami, A. Pazhouheshgar, E. Salari, M. Saghafi Yazdi, T. Alimardani, H. Jahani, F. Sharifian Jazi, M. Tahriri, Novel antibacterial Cu/Mg-substituted 58S-bioglass: Synthesis, characterization and investigation of in vitro bioactivity, International Journal of Applied Glass Science n/a(n/a) (2019).

[17] M.S.N. Shahrbabak, F. Sharifianjazi, D. Rahban, A. Salimi, A Comparative Investigation on Bioactivity and Antibacterial Properties of Sol-Gel Derived 58S Bioactive Glass Substituted by Ag and Zn, Silicon 11(6) (2019) 2741-2751.

[18] P.V. Phan, M. Grzanna, J. Chu, A. Polotsky, A. El-Ghannam, D. Van Heerden, D.S. Hungerford, C.G. Frondoza, The effect of silica-containing calcium-phosphate particles on human osteoblasts in vitro, Journal of Biomedical Materials Research Part A: An Official Journal of The Society for Biomaterials, The Japanese Society for Biomaterials, and The Australian Society for Biomaterials and the Korean Society for Biomaterials 67(3) (2003) 1001-1008.

[19] L.L. Hench, An introduction to bioceramics, World scientific1993.

[20] T. Kokubo, H. Kushitani, S. Sakka, T. Kitsugi, T. Yamamuro, Solutions able to reproduce in vivo surface-structure changes in bioactive glass-ceramic A-W3, Journal of biomedical materials research 24(6) (1990) 721-734.

[21] A.M. Pietak, J.W. Reid, M.J. Stott, M. Sayer, Silicon substitution in the calcium phosphate bioceramics, Biomaterials 28(28) (2007) 4023-4032.

[22] M. Barekat, R.S. Razavi, F. Sharifianjazi, Synthesis and the surface resistivity of carbon black pigment on black silicone thermal control coating, Synthesis and Reactivity in Inorganic, Metal-Organic, and Nano-Metal Chemistry 45(4) (2015) 502-506.

[23] E. Ghasali, A. Bordbar-Khiabani, M. Alizadeh, M. Mozafari, M. Niazmand, H. Kazemzadeh, T. Ebadzadeh, Corrosion behavior and in-vitro bioactivity of porous Mg/$Al_2O_3$ and Mg/$Si_3N_4$ metal matrix composites fabricated using microwave sintering process, Materials Chemistry and Physics 225 (2019) 331-339.

[24] S. Rahimi, F. SharifianJazi, A. Esmaeilkhanian, M. Moradi, A.H. Safi Samghabadi, Effect of $SiO_2$ content on Y-TZP/$Al_2O_3$ ceramic-nanocomposite properties as potential dental applications, Ceramics International 46(8, Part A) (2020) 10910-10916.

[25] A. Esmaeilkhanian, F. Sharifianjazi, A. Abouchenari, A. Rouhani, N. Parvin, M. Irani, Synthesis and Characterization of Natural Nano-hydroxyapatite Derived from Turkey Femur-Bone Waste, Applied Biochemistry and Biotechnology 189(3) (2019) 919-932.

[26] A. Balamurugan, G. Balossier, J. Michel, S. Kannan, H. Benhayoune, A. Rebelo, J. Ferreira, Sol gel derived $SiO_2$-CaO-MgO-$P_2O_5$ bioglass system—Preparation and in vitro characterization, Journal of Biomedical Materials Research Part B: Applied Biomaterials: An Official Journal of The Society for Biomaterials, The Japanese Society for Biomaterials, and The Australian Society for Biomaterials and the Korean Society for Biomaterials 83(2) (2007) 546-553.

[27] Z. Goudarzi, N. Parvin, F. Sharifianjazi, Formation of hydroxyapatite on surface of $SiO_2$–$P_2O_5$–CaO–SrO–ZnO bioactive glass synthesized through sol-gel route, Ceramics International 45(15) (2019) 19323-19330.

[28] S. Hesaraki, M. Gholami, S. Vazehrad, S. Shahrabi, The effect of Sr concentration on bioactivity and biocompatibility of sol–gel derived glasses based on CaO–SrO–$SiO_2$–$P_2O_5$ quaternary system, Materials Science and Engineering: C 30(3) (2010) 383-390.

[29] A. Oki, B. Parveen, S. Hossain, S. Adeniji, H. Donahue, Preparation and in vitro bioactivity of zinc containing sol-gel–derived bioglass materials, Journal of Biomedical Materials Research Part A: An Official Journal of The Society for Biomaterials, The Japanese Society for Biomaterials, and The Australian Society for Biomaterials and the Korean Society for Biomaterials 69(2) (2004) 216-221.

[30] F. Sharifianjazi, M. Moradi, A. Abouchenari, A.H. Pakseresht, A. Esmaeilkhanian, M. Shokouhimehr, M.S. Asl, Effects of Sr and Mg dopants on biological and mechanical properties of $SiO_2$–CaO–$P_2O_5$ bioactive glass, Ceramics International (2020).

[31] A.H. Taghvaei, F. Danaeifar, C. Gammer, J. Eckert, S. Khosravimelal, M. Gholipourmalekabadi, Synthesis and characterization of novel mesoporous strontium-modified bioactive glass nanospheres for bone tissue engineering applications, Microporous and Mesoporous Materials 294 (2020) 109889.

[32] F. Sharifianjazi, A.H. Pakseresht, M. Shahedi Asl, A. Esmaeilkhanian, H. Nargesi khoramabadi, H.W. Jang, M. Shokouhimehr, Hydroxyapatite Consolidated by Zirconia: Applications for Dental Implant, Composites and Compounds 2(1) (2020).

[33] T. Kokubo, H. Takadama, How useful is SBF in predicting in vivo bone bioactivity?, Biomaterials 27(15) (2006) 2907-2915.

[34] A. Moghanian, S. Firoozi, M. Tahriri, Characterization, in vitro bioactivity and biological studies of sol-gel synthesized SrO substituted 58S bioactive glass, Ceramics International 43(17) (2017) 14880-14890.